

Electrochemical Impedance Spectroscopy and its Applications

Andrzej Lasia

**Département de chimie, Université de Sherbrooke, Sherbrooke
Québec, J1K 2R1**

alasia@courrier.usherb.ca

A. Lasia, Electrochemical Impedance Spectroscopy and Its Applications, Modern Aspects of Electrochemistry, B. E. Conway, J. Bockris, and R.E. White, Edts., Kluwer Academic/Plenum Publishers, New York, 1999, Vol. 32, p. 143-248.

Table of content

I. Introduction.....	4
1. Response of Electrical Circuits.....	4
(i) Arbitrary Input Signal.....	4
(ii) Alternating Voltage (av) Input Signal.....	6
2. Impedance of Electrical Circuits.....	7
(i) Series R-C Circuit.....	8
(ii) Parallel R-C Circuit.....	8
(iii) Series: R_s + Parallel R-C Circuit.....	9
3. Interpretation of the Complex Plane and Bode Plots.....	9
II. Impedance measurements.....	10
1. Ac Bridges.....	10
2. Lissajous Curves.....	11
3. Phase Sensitive Detection (PSD).....	11
4. Frequency Response Analyzers.....	12
5. Fast Fourier Transform (FFT).....	13
(i) Pulse Perturbation.....	14
(ii) Noise Perturbation.....	14
(iii) Sum of Sine Waves.....	14
III. Impedance of faradaic reactions in the presence of diffusion.....	15
1. The Ideally Polarizable Electrode.....	15
2. Semi-Infinite Linear Diffusion.....	15
3. Spherical Diffusion.....	20
4. Cylindrical Electrodes.....	22
5. Disk Electrodes.....	23
6. Finite-Length Diffusion.....	23
(i) Transmissive Boundary.....	24
(ii) Reflective Boundary.....	25
7. Analysis of Impedance Data in the Case of Semi-Infinite Diffusion: Determination of the Kinetic Parameters.....	26
(i) Randles' Analysis ^{64,65,67}	26
(ii) De Levie-Husovsky Analysis.....	27
(iii) Analysis of $\cot \varphi$	27
(iv) Sluyter's Analysis.....	28
IV. Impedance of A faradaic reaction involving adsorption of reacting species.....	29
1. Faradaic Reaction Involving One Adsorbed Species.....	29
2. Impedance Plots in the Case of One Adsorbed Species.....	31
3. Faradaic Impedance in the Case Involving Two Adsorbed Species.....	34
4. Impedance Plots in the Case of Two Adsorbed Species.....	36
5. Faradaic Impedance for the Process Involving Three or More Adsorbed Species.....	36
V. Impedance of solid electrodes.....	37

1.	Frequency Dispersion and Electrode Roughness.....	37
2.	Constant Phase Element.....	37
3.	Fractal Model.....	40
4.	Porous Electrode Model.....	42
(i)	Porous Electrodes in the Absence of Internal Diffusion.....	42
(a)	De Levie's treatment.....	43
(b)	Rigorous treatment.....	45
(ii)	Porous Electrodes in the Presence of Axial Diffusion.....	46
(iii)	Other Pore Geometries.....	49
5.	Generalized Warburg Element.....	49
VI.	Conditions for "good" impedances	50
1.	Linearity, Causality, Stability, Finiteness.....	50
2.	Kramers-Kronig Transforms.....	51
3.	Non-Stationary Impedances.....	53
VII.	Modeling of experimental data	54
1.	Selection of the Model.....	54
2.	CNLS Approximations	56
(i)	CNLS Method.....	56
(ii)	Statistical Weights	57
(iii)	AC Modeling Programs	58
VIII.	Instrumental limitations	58
IX.	Conclusion	60

I. INTRODUCTION

Electrochemical Impedance Spectroscopy (EIS) or ac impedance methods have seen tremendous increase in popularity in recent years. Initially applied to the determination of the double-layer capacitance¹⁻⁴ and in ac polarography,⁵⁻⁷ they are now applied to the characterization of electrode processes and complex interfaces. EIS studies the system response to the application of a periodic small amplitude ac signal. These measurements are carried out at different ac frequencies and, thus, the name impedance spectroscopy was later adopted. Analysis of the system response contains information about the interface, its structure and reactions taking place there. EIS is now described in the general books on electrochemistry,⁸⁻¹⁷ specific books^{18,19} on EIS, and there are also numerous articles and reviews.^{6,20-31} It became very popular in the research and applied chemistry. The Chemical Abstract database shows ~1,500 citations per year of the term "impedance" since 1993 and ~1,200 in earlier years and ~500 citations per year of "electrochemical impedance". Although the term "impedance" may include also non-electrochemical measurements and "electrochemical impedance" may not include all the electrochemical studies, the popularity of this technique cannot be denied.

However, EIS is a very sensitive technique and it must be used with great care. Besides, it is not always well understood. This may be connected with the fact that existing reviews on EIS are very often difficult to understand by non-specialists and, frequently, they do not show the complete mathematical developments of equations connecting the impedance with the physico-chemical parameters. It should be stressed that EIS cannot give all the answers. It is a complementary technique and other methods must also be used to elucidate the interfacial processes.

The purpose of this review is to fill this gap by presenting a modern and relatively complete review of the subject of electrochemical impedance spectroscopy, containing mathematical development of the fundamental equations.

1. Response of Electrical Circuits

(i) *Arbitrary Input Signal*

Application of an electrical perturbation (current, potential) to an electrical circuit causes the appearance of a response. In this chapter, the system response to an arbitrary perturbation and, later, to an ac signal, will be presented. Knowledge of the Laplace transform technique is assumed, but the reader may consult numerous books on the subject.

First, let us consider application of an arbitrary (but known) potential $E(t)$ to a resistance R . The current $i(t)$ is given as: $i(t) = E(t)/R$. When the same potential is applied to the series connection of the resistance R and capacitance C , the total potential difference is a sum of potential drops on each element. Taking into account that for a capacitance $E(t) = Q(t)/C$, where Q is the charge stored in a capacitor, the following equation is obtained:

$$E(t) = i(t)R + \frac{Q(t)}{C} = i(t)R + \frac{1}{C} \int_0^t i(t)dt \quad (1)$$

This equation may be solved using either Laplace transform or differentiation techniques.³²⁻³⁴ Differentiation gives:

$$\frac{di(t)}{dt} + \frac{i(t)}{RC} = \frac{1}{R} \frac{dE(t)}{dt} \quad (2)$$

which may be solved for known $E(t)$ using standard methods for differential equations.

The Laplace transform is an integral transform in which a function of time $f(t)$ is transformed into a new function of a parameter s called frequency, $\bar{f}(s)$ or $F(s)$, according to:

$$\mathcal{L}[f(t)] = \bar{f}(s) = F(s) = \int_0^{\infty} f(t) \exp(-st) dt \quad (3)$$

The Laplace transform is often used in solution of differential and integral equations. In general, the parameter s may be complex, $s = v + j\omega$, where $j = \sqrt{-1}$, but in this chapter only the real transform will be considered, *i.e.* $s = v$. Direct application of the Laplace transform to eqn. (1), taking into account that $\mathcal{L}\left(\int_0^t i(t) dt\right) = i(s)/s$, gives:

$$E(s) = i(s)R + \frac{i(s)}{sC} \quad (4)$$

which leads to:

$$i(s) = E(s) / \left(R + \frac{1}{sC} \right) \quad (5)$$

The ratio of the Laplace transforms of potential and current, $E(s)/i(s)$ is expressed in the units of resistance, Ω , and is called *impedance*, $Z(s)$. In this case:

$$Z(s) = \frac{E(s)}{i(s)} = R + \frac{1}{sC} \quad (6)$$

The inverse of impedance is called *admittance*, $Y(s) = 1/Z(s)$. They are *transfer functions* which transform one signal, *e.g.* applied voltage, into another, *e.g.* current. Both are called *immittances*. Some other transfer functions are discussed in refs. 18, 35 and 36. It should be noticed that the impedance of a series connection of a resistance and capacitance, eqn. (6), is a sum of the contributions of these two elements: resistance, R , and capacitance, $1/sC$.

For the series connection of a resistance, R , and inductance, L , the total potential difference consists of the potential drop on both elements:

$$E(t) = i(t)R + L \frac{di(t)}{dt} \quad (7)$$

Taking into account that $\mathcal{L}[di(t)/dt] = s i(s) - i(0^+)$, and taking $i = 0$ at $t = 0$, one obtains the current response in the Laplace space:

$$i(s) = E(s) / (R + sL) \quad (8)$$

In both cases considered above the system impedance consists of the sum of two terms, corresponding to two elements: resistance and capacitance or inductance.

In general, one can write contributions to the total impedance corresponding to the resistance as R , the capacitance as $1/sC$ and the inductance as sL . Addition of impedances is analogous to the addition of resistances. Knowledge of the system impedance allows for an easy solution of the problem.

For example, when a constant voltage, E_0 , is applied at time zero to a series connection of R and C , the current is described by eqn. (5). Taking into account that the Laplace transform of a constant $\mathcal{L}(E_0) = E_0/s$, one gets:

$$i(s) = \frac{E_0}{s(R + 1/sC)} = \frac{E_0}{R} \frac{1}{s + 1/RC} \quad (9)$$

Inverse transform of (9) gives the current relaxation versus time:

$$i(t) = \frac{E_0}{R} \exp(-t / RC) \quad (10)$$

The result obtained shows that after the application of the potential step, current initially equals E_0/R and it decreases to zero as the capacitance is charged to the potential difference E_0 .

Similarly, application of the potential step to a series connection of R and L produces response given by eqn. (8) which, after substitution of $E(s) = E_0/s$, gives:

$$i(s) = \frac{E_0}{s(R + sL)} = \frac{E_0}{L} \frac{1}{s(s + R/L)} = \frac{E_0}{R} \left(\frac{1}{s} + \frac{1}{s + R/L} \right) \quad (11)$$

Inverse transform gives the time dependence of the current:

$$i(t) = \frac{E_0}{R} \left[1 - \exp\left(-\frac{Rt}{L}\right) \right] \quad (12)$$

The current starts at zero as the inductance constitutes infinite resistance at $t = 0$ and it increases to E_0/R as the effect of inductance becomes negligible in the steady-state condition.

In a similar way other problems of transient system response may be solved. More complex examples are presented, *e.g.*, in refs. 33-34. It should be added that an arbitrary signal may be applied to the system and if the Laplace transforms of the potential and current are determined, *e.g.* by numerical transform calculations, the system impedance is determined. In the Laplace space the equations (*e.g.* eqns. (9) and (11)) are much simpler than those in the time space (*e.g.* eqns. (10) and (12)) and analysis in the frequency space s allows for the determination of the system parameters. This analysis is especially important when an ideal potential step cannot be applied to the system because of the band-width limitations of the potentiostat.³⁷ In this case it is sufficient to know $i(t)$ and the real value of the potential applied to the electrodes by the potentiostat, $E(t)$, which allows numerical Laplace transformation to be carried out and the system impedance obtained.

In the cases involving more time constants, *i.e.* more than one capacitance or inductance in the circuit, the differential equations describing the system are of the second or higher order and the impedances obtained are the second or higher order functions of s .

(ii) **Alternating Voltage (av) Input Signal**

In the EIS we are interested in the system response to the application of a sinusoidal signal, *e.g.*: $E = E_0 \sin(\omega t)$, where E_0 is the signal amplitude, $\omega = 2\pi f$ is the angular frequency, and f is the av signal frequency. This problem may be solved in different ways. First, let us consider application of an av signal to a series R - C connection. Taking into account that the Laplace transform of the sine function $\mathcal{L}[\sin(\omega t)] = \omega/(s^2 + \omega^2)$, use of eqn. (5) gives:

$$i(s) = \frac{E_0 \omega}{s^2 + \omega^2} \frac{1}{R + 1/sC} = \frac{E_0 \omega}{R} \frac{1}{s^2 + \omega^2} \frac{1}{s + 1/RC} \quad (13)$$

Distribution into simple fractions leads to:

$$i(s) = \frac{E_0}{R[\omega^2 + (1/RC)^2]} \left[\omega^2 \frac{\omega}{s^2 + \omega^2} + \frac{\omega}{RC} \frac{s}{s^2 + \omega^2} - \frac{\omega}{RC} \frac{1}{s + 1/RC} \right] \quad (14)$$

and the inverse Laplace transform, taking $\mathcal{L}^{-1} [s/(s^2 + \omega^2)] = \cos \omega t$, gives:

$$i(t) = \frac{E_0}{R[\omega^2 + (1/RC)^2]} \left[\omega^2 \sin(\omega t) + \frac{\omega}{RC} \cos(\omega t) - \frac{\omega}{RC} \exp(-t/RC) \right] \quad (15)$$

The third term in eqn. (15) corresponds to a transitory response observed just after application of the av signal and it decreases quickly to zero. The steady-state equation may be rearranged into a simpler form:

$$i(t) = \frac{E_0}{R \left(1 + \frac{1}{(\omega RC)^2} \right)} \left[\sin(\omega t) + \frac{1}{\omega RC} \cos(\omega t) \right] \quad (16)$$

and by introducing $\tan \varphi = 1/\omega RC$ the following form is found:

$$i(t) = \frac{E_0}{\sqrt{R^2 + \frac{1}{(\omega C)^2}}} \sin(\omega t + \varphi) = \frac{E_0}{|Z|} \sin(\omega t + \varphi) \quad (17)$$

where φ is the phase-angle between current and potential, $\varphi = \arctan(1/\omega RC)$. It is obvious that the current has the same frequency as the applied potential but is phase-shifted by the angle φ . The value $|Z|$ has units of resistance; it is the length of a vector obtained by addition of two perpendicular vectors: R and $1/\omega C$.

2. Impedance of Electrical Circuits

In order to simplify the calculations of impedances, the result obtained for the periodic perturbation of an electrical circuit may be represented using complex notation. In the latter example the system impedance, $Z(j\omega)$, may be represented as:

$$Z(j\omega) \equiv \hat{Z} = Z' + jZ'' = R + \frac{1}{j\omega C} = R - j\frac{1}{\omega C} \quad (18)$$

and the real and imaginary parts of the impedance are: $Z' = R$ and $Z'' = -1/\omega C$, respectively. It should be noted that the complex impedance $Z(j\omega)$, eqn. (18), may be obtained from $Z(s)$, eqn. (6), by substitution: $s = j\omega$. In fact, this is the imaginary Laplace transform. The modulus of $Z(j\omega)$, eqn. (17), equals:

$$|Z| = \sqrt{(Z')^2 + (Z'')^2} = \sqrt{R^2 + (1/\omega C)^2} \quad (19)$$

and the phase-angle between the imaginary and real impedance equals $\varphi \equiv \arg(\hat{Z}) = \text{atan}(-1/\omega RC)$. It should be noticed that the sign of φ , between potential and current, described above for the impedances, is different from that found between current and potential, eqn. (17). It may be recalled that in complex notation:

$$Z(j\omega) = |Z| \exp(j\varphi) = |Z| [\cos(\varphi) + j \sin(\varphi)] \quad (20)$$

Analysis of eqn. (17) indicates that the current represents a vector of the length $i_0 = E_0/|Z|$ which rotates with the frequency ω . Current and potential are rotating vectors in the time domain, as represented in Figure 1a. Using complex notation they may be described by:

$$E = E_0 \exp(j\omega t) \text{ and } i = i_0 \exp[j(\omega t + \varphi)] \quad (21)$$

These vectors rotate with a constant frequency ω and the phase-angle, φ , between them stays constant. Instead of showing rotating vectors in time space it is possible to present immobile

Figure 1.

vectors in the frequency space, separated by the phase-angle φ . These vectors are called *phasors*; they are equal to $\tilde{E} = E_0$ and $\tilde{I} = I_0 \exp(j\varphi)$, where the initial phase shift of the potential was assumed to be zero, see Figure 1b.

In general, the complex impedance may be written for any circuit by taking R for a resistance, $1/j\omega C$ for a capacitance and $j\omega L$ for an inductance, and applying Ohm's and Kirchhoff's laws to the connection of these elements. Several examples of this method are presented below.

(i) Series R-C Circuit

In the case of a series connection of the resistance and capacitance the impedance is given by: $Z(j\omega) = R + 1/j\omega C = R - j/\omega C$. The result may be represented graphically using two types of plots: *complex plane* (also known as *Argand* or *Nyquist plots*) and *Bode plots*. The complex plane plot is a plot of Z'' versus Z' , that is, the imaginary versus the real components, plotted for various frequencies. A complex plane plot for a series connection $R-C$ ($R = 100 \Omega$, $C = 2 \times 10^{-5} \text{ F}$) circuit is shown in Figure 2. It consists of a straight line perpendicular to the real axis. Other types of graphs are Bode plots *i.e.* $\log |Z|$ (magnitude) and phase-angle, φ , versus $\log \omega$. They are also shown in Figure 2. The graph of $\log |Z|$ versus $\log \omega$, Figure 2d, contains one breakpoint or corner frequency. This point corresponds to the system characteristic frequency $\omega = 1/RC = 500 \text{ s}^{-1}$ or a time constant $\tau = RC = 0.002 \text{ s}$. The phase-angle changes from 90° at low frequencies to 0 at high frequencies. This circuit corresponds to an ideally polarized electrode in solution, e.g. a mercury electrode - supporting electrolyte solution.

Figure 2.

The complex plane plots may also be obtained for admittances. Admittance for the series $R-C$ connection equals:

$$Y(j\omega) = \frac{1}{Z(j\omega)} = \frac{1}{R - \frac{j}{\omega C}} = \frac{R}{R^2 + \frac{1}{\omega^2 C^2}} + \frac{j}{\omega C \left(R^2 + \frac{1}{\omega^2 C^2} \right)} \quad (22)$$

It represents a semi-circle on the complex plane plot, Figure 2c. It should be stressed that for capacitive circuits the imaginary impedance is always negative and the imaginary admittance is positive.

(ii) Parallel R-C Circuit

For the parallel $R-C$ connection the total admittance equals: $Y(j\omega) = 1/R + j\omega C$ such that:

$$Z(j\omega) = \frac{1}{1/R + j\omega C} = \frac{R}{1 + j\omega RC} = \frac{R}{1 + \omega^2 R^2 C^2} - \frac{j\omega R^2 C}{1 + \omega^2 R^2 C^2} \quad (23)$$

There are two limits of the impedance: $\omega = 0$, $\hat{Z} = R$ and $\omega \rightarrow \infty$, $\hat{Z} = 0$. The corresponding complex plane and Bode plots, for the same values of R and C elements as used in the series $R-C$ model above, are shown in Figure 3. The Nyquist plot shows a semicircle of radius $R/2$ and the center on the real axis, and the frequency at the semicircle maximum equal to: $\omega = 1/RC$. The circuit's characteristic breakpoint frequency (inverse of the characteristic time constant), as observed in the impedance Bode graph, is the same as for the series and the parallel $R-C$ circuits.

The complex plane admittance plot represents a straight line parallel to the imaginary axis, Figure 3c, which is similar to the impedance complex plane plot for the series R - C connection.

Figure 3.

(iii) Series: R_s + Parallel R-C Circuit

Finally, impedance of the circuit shown in Figure 4, consisting of a series connection of the resistance R_s with the parallel connection of R_{ct} - C_{dl} , is given as:

Figure 4.

$$Z(j\omega) = R_s + \frac{1}{1/R_{ct} + j\omega C_{dl}} \quad (24)$$

The corresponding complex plane and Bode plots are also shown in Figure 4 for $R_{ct} = 100 \Omega$, $R_s = 10 \Omega$ and $C_{dl} = 20 \mu\text{F}$. The main difference between circuits in Figure 3 and Figure 4 is connected with the fact that in the latter circuit, at $\omega \rightarrow \infty$, $Z \rightarrow R_s$ and $\varphi \rightarrow 0$, due to the presence of R_s , and for $\omega \rightarrow 0$ $Z \rightarrow R_s + R_{ct}$. The frequency corresponding to the maximum of Z'' is still equal to $\omega = 1/R_{ct}C_{dl} = 500 \text{ s}^{-1}$. In addition, the Bode $\log |Z|$ plot shows that there are two breakpoints (bends). For comparison, the admittance complex plane plot is also shown in Figure 4c.

3. Interpretation of the Complex Plane and Bode Plots

Complex plane (Nyquist) plots are the most often used in the electrochemical literature because they allow for an easy prediction of the circuit elements. However, they do not show all details; for example, exactly the same Nyquist impedance plots, shown in Figure 3 and Figure 4, may be obtained for different values of the capacitance C . The only difference between them will be the fact that the points on the semicircle would correspond to different frequencies. Nevertheless, Nyquist plots allow for an easy relation to the electrical model. On the other hand Bode plots contain all the necessary information. That is why Bode plots are mainly used in the circuit analysis. The Bode magnitude plots may be easily predicted from the circuit impedance.³³ Let us consider the circuit shown in Figure 4a. Its impedance is presented by eqn. (24). This equation may be rearranged into another form:

$$\hat{Z} = (R_s + R_{ct}) \frac{1 + j\omega \left(\frac{R_s R_{ct} C_{dl}}{R_s + R_{ct}} \right)}{1 + j\omega (R_{ct} C_{dl})} = (R_s + R_{ct}) \frac{1 + j\omega\tau_2}{1 + j\omega\tau_1} \quad (25)$$

where τ_1 and τ_2 are the Bode characteristic time constants. From eqn. (25) $\log(|Z|)$ is easily evaluated:

$$\log(|Z|) = \log(|R_s + R_{ct}|) + \log(|1 + j\omega\tau_2|) - \log(|1 + j\omega\tau_1|) \quad (26)$$

In order to construct asymptotic lines in the Bode magnitude plot, the contribution of each term in eqn. (26) can be considered independently and then their sum may be easily obtained. Each term $\log(|1 + j\omega\tau|)$ has two limits: when $\omega\tau \ll 1$, i.e. $\omega \ll 1/\tau$, $\log(|1 + j\omega\tau|) = 0$ and when $\omega\tau \gg 1$,

$\log(|1+j\omega\tau|) = \log \tau + \log \omega$, which correspond to a straight line with a slope of one and intercept $\log \omega = -\log \tau$.

The graphs corresponding to these lines are shown in Figure 5. The break-point frequencies in the Bode magnitude plot, Figure 4d and Figure 5, are $\omega_1 = 1/\tau_1 = 500 \text{ s}^{-1}$ and $\omega_2 = 1/\tau_2 = 5500 \text{ s}^{-1}$. The continuous line is the sum of the three asymptotes. In this way Bode magnitude graphs may be constructed for other circuits.

The Bode phase-angle graph is shown in Figure 4e. The phase-angle is described by:

$$\varphi = \text{atan}(Z''/Z') = \text{atan}\left(\frac{\omega R_{ct}^2 C_{dl}}{R_s + R_{ct} + (\omega R_{ct} C_{dl})^2 R_s}\right) \quad (27)$$

It can be shown that this function has a maximum at:

$$\omega = \frac{1}{R_{ct} C_{dl}} \sqrt{\frac{R_s + R_{ct}}{R_s}} \quad (28)$$

which, in this case, equals $\omega = 1658 \text{ s}^{-1}$. It should be noticed that the maximum of the phase-angle is different from the maximum of the imaginary part of the impedance, corresponding to the maximum of the semicircle at $Z' = R_s + R_{ct}/2$ at $\omega = 1/R_{ct} C_{dl}$. The plots of Z' and Z'' (or their logarithms) as a function of $\log \omega$ are also sometimes shown in the literature.

Figure 5.

II. IMPEDANCE MEASUREMENTS

Dc transient response of electrochemical systems is usually measured using potentiostats. In the case of EIS an additional perturbation is added to the dc signal in order to obtain the frequency response of the system. The system impedance may be measured using various techniques:

- 1) ac bridges
- 2) Lissajous curves
- 3) phase sensitive detection (PSD)
- 4) frequency response analysis (FRA)
- 5) fast Fourier transform (FFT)

Because older techniques were described in detail in refs. 18, 19, 26, 28, 30 and 31, this chapter will be focused on the last three techniques.

1. Ac Bridges

This technique was the first used to measure the double-layer parameters (principally of the dropping mercury electrode) and, later, to measure the electrode impedance in the presence of a faradaic reaction to determine the kinetics of electrode processes. The use of ac bridges provides a very good precision of measurements. It has been described in detail in refs. 18, 26, 28 and 38. The ac bridge with potentiostatic control may also be used. Although this method is slow, because bridge compensation must be carried out at each frequency manually, it is still used, principally in precise double-layer measurements.³⁹⁻⁴¹

2. Lissajous Curves

Recording of the applied av potential and the resulting ac current on a twin-beam oscilloscope produces so-called Lissajous curves (in this case an ellipse)^{18,28,30} which may be used for the determination of the impedances. Because of the frequency limitations and sensitivity to noise, this technique is not currently used in electrochemical measurements.

3. Phase Sensitive Detection (PSD)

Phase sensitive detection is used in lock-in amplifiers, which are interfaced with potentiostats.^{42,43} Only a general idea of these measurements will be presented here. In this method the measured signal, E_1 , proportional to the ac current from the potentiostat, is:

$$E_1 = E_{1,a} \sin(\omega t + \varphi_1) \quad (29)$$

where $E_{1,a}$ is the signal amplitude and φ_1 is the phase shift, is multiplied by a square-wave signal of the same angular frequency ω . The square-wave signal may be represented as a Fourier series:

$$E_2 = \frac{4}{\pi} \sum_{n=0}^{\infty} \frac{1}{2n+1} \sin[(2n+1)\omega t + \varphi_2] \quad (30)$$

where n is an integer and the amplitude of the square signal is taken as unity. The resulting signal $E_1 \times E_2$ equals:

$$\begin{aligned} E_1 E_2 &= \sum_{n=0}^{\infty} \frac{4E_1}{(2n+1)\pi} \sin(\omega t + \varphi_1) \sin[(2n+1)\omega t + \varphi_2] = \\ &= \sum_{n=0}^{\infty} \frac{2E_1}{(2n+1)\pi} \left\{ \cos[-2n\omega t + \varphi_1 - (2n+1)\varphi_2] - \cos[(2n+2)\omega t + \varphi_1 + (2n+1)\varphi_2] \right\} = \quad (31) \\ &= \frac{2E_1}{\pi} \left\{ \begin{aligned} &\cos(\varphi_1 - \varphi_2) - \cos(2\omega t + \varphi_1 + \varphi_2) \\ &+ \frac{1}{3} \cos(-2\omega t + \varphi_1 - 3\varphi_2) - \frac{1}{3} \cos(4\omega t + \varphi_1 + 3\varphi_2) \\ &+ \frac{1}{5} \cos(-4\omega t + \varphi_1 - 5\varphi_2) - \frac{1}{5} \cos(6\omega t + \varphi_1 + 5\varphi_2) + \dots \end{aligned} \right\} \end{aligned}$$

It contains one time independent component, depending on the phase difference of two signals, and is proportional to the amplitude of the measured ac signal. It reaches a maximum when the phase difference of the two signals being mixed is zero. The output signal is subsequently applied to a low-pass filter which averages the signal components having frequencies above the filter cut-off frequency. It produces a dc signal proportional to the amplitude. Because the average value of periodic functions is equal to zero, the average value of $E_1 E_2$, equation (31), equals:

$$\text{Average}(E_1 E_2) = \frac{2E_1}{\pi} \cos(\varphi_1 - \varphi_2) \quad (32)$$

The disadvantage of the lock-in technique is that it retains contributions of the harmonic frequencies $(2n+1)\omega_{\text{ref}}$, if they are present in the input signal (e.g. harmonics, noise), although their influence is attenuated by 1/3, 1/5, 1/7, etc. with increasing n . For example, when the frequency in eqn. (29) is three times the reference frequency in eqn. (30), the obtained average signal:

$$\text{Average}(E_1 E_2) = \frac{2E_1}{3\pi} \cos(\varphi_1 - 3\varphi_2) \quad (33)$$

is attenuated three times. If the reference signal is synchronized with the applied signal (they are both generated from the same source), φ_2 is equal to zero and the expressions become simplified.

A schematic diagram of a lock-in amplifier is shown in Figure 6. The measured signal is mixed with the reference square-wave signal of the same frequency and the resulting signal goes through a low-pass filter producing an average of all components. The phase shifter allows for precise adjustment of the reference phase in order to zero the phase difference $\varphi_1 - \varphi_2$. In two-phase lock-in amplifiers, the measured signal is mixed with the reference signal to obtain the in-phase component and, additionally, with the reference signal shifted by $\pi/2$ to resolve the imaginary component.

Lock-in amplifiers operate in the frequency range from 0.5 (lower limit up to 10 Hz, depending on the manufacturer) to $\sim 10^5$ Hz with a precision of 0.1 to 0.2%. Modern lock-in amplifiers are controlled by a microprocessor and permit automated measurements with auto-range selection.

4. Frequency Response Analyzers

Frequency response analyzers (FRA) are instruments which determine the frequency response of a measured system. Their functioning is different from that of lock-in amplifiers. They are based on the correlation of the studied signal with the reference.⁴⁴ The measured signal, eqn. (29), is multiplied by the sine and cosine of the reference signal of the same frequency and then integrated during one or more wave-periods:

$$\text{Re}(E_1) = \frac{1}{T} \int_0^T E_{1,a} \sin(\omega t + \varphi_1) \sin(\omega t) dt = \frac{E_{1,a}}{2} \cos(\varphi_1) \quad (34)$$

and

$$\text{Im}(E_1) = \frac{1}{T} \int_0^T E_{1,a} \sin(\omega t + \varphi_1) \cos(\omega t) dt = \frac{E_{1,a}}{2} \sin(\varphi_1) \quad (35)$$

Such integration recovers the real and imaginary parts of the measured signal. It can also be shown that all the harmonics are strictly rejected, that is correlation of $\sin(k\omega t + \varphi)$ with $\sin(\omega t)$ or with $\cos(\omega t)$ is equal to zero for $k > 1$. The advantage of the correlation process is also reduction of noise (of arbitrary frequency), its influence decreasing with the increase of the integration time. Figure 7 shows the attenuation of the output signal as a function of frequency and the number of integration cycles N . Modern FRAs carry out all the computations digitally. FRAs have a wide frequency range (12 decades) and high precision.

Recently, Diard et al.⁴⁵ studied effects of electrochemical non-linearities on impedance measurements using a FRA. They derived theoretical expressions for the error in impedance measurements using the odd harmonic test criterion⁴⁶. Measurements of the fundamental and third harmonic in the electrode response are sufficient to estimate the impedance error.

Figure 6.

Figure 7.

A comparison of PSD and FRA was recently presented by Evans,⁴⁷ as shown in Table 1.

Table 1**Comparison of PSD and FRA**

Lock-in amplifier	FRA
<p>Advantages</p> <ul style="list-style-type: none"> • Very sensitive • Effectively removes noise • Reduces harmonic distortion • Suppresses dc noise • Relatively low cost <p>Disadvantages</p> <ul style="list-style-type: none"> • Limited frequency range • Slower • Standalone readings difficult 	<p>Advantages</p> <ul style="list-style-type: none"> • Faster analysis • Wide frequency range • Removes harmonic distortion • Direct output to external device • Easy standalone measurements <p>Disadvantages</p> <ul style="list-style-type: none"> • Higher cost • Limited noise removal • Limited sensitivity

5. Fast Fourier Transform (FFT)

It has been shown in Section I.1(i) that the system impedance is defined as the ratio of Laplace transforms, eqn. (6), of potential and current. In general, the transformation parameter is complex, $s = \nu + j\omega$. The imaginary Laplace transform:

$$F(j\omega) = \int_0^{\infty} f(t) e^{-j\omega t} dt \quad (36)$$

is called the single sided Fourier transform. Taking the Fourier transform of the perturbation signal and that of the resulting signal allows determination of the transfer function, e.g. the system ac impedance may be obtained from:

$$Z(j\omega) = \frac{F[E(t)]}{F[i(t)]} = \frac{E(j\omega)}{i(j\omega)} \quad (37)$$

where symbol F denotes the Fourier transform. The fast Fourier transform (FFT) provides a fast and efficient algorithm of computation of the Fourier transform.⁴⁸ The number of points acquired must be equal to 2^k , where k is an integer.

Certain proprieties of the FFT technique influence the obtained results.^{28,48,49,50} First of all the Fourier transform defined by eqn. (36) involves integration to infinity. In practice only limited length data are transformed, causing broadening of the computed frequency spectrum. This problem is known as leakage. It may be minimized by increase of the data record acquired in the time domain. However, it will disappear when the acquisition time is equal exactly to an integer multiple of the wave repetition period. That is if the data acquisition is terminated at other times than the multiple of the wave period, sharp discontinuities of the signal are introduced (because there is no continuity between the last and the first point of the signal) which causes frequency peak broadening, that is a distribution of frequencies is obtained instead of discrete values. Therefore, synchronization of the sampling time with the wave period is necessary.

Another problem called aliasing is connected with the presence of the frequencies larger than one-half of the time domain sampling frequency. This problem may be easily eliminated by assuring that the sampling frequency is greater than (or at least equal to) twice the highest frequency present in the measured signal. In some cases the highest frequencies may be filtered

out by a low-pass filter. This minimum sampling frequency, necessary to get information about the existing signal, is called the Nyquist sampling rate.

In general, the perturbing signal may have an arbitrary form. However, in practice, the most often used perturbation signals are^{50,51,52}: 1) pulse, 2) noise, and 3) sum of sine waves.

(i) Pulse Perturbation

Fourier transform of an infinite short pulse function: $h(t) = K\delta(t)$, where $\delta(t)$ is Dirac's delta function, equals: $H(j\omega) = K$, that is it contains all the frequencies with the same amplitude K . Such a function cannot be realized in practice and must be substituted by a pulse of a short duration Δt . However, such a function does not have uniform response in the Fourier (i.e. frequency) space. Fourier transform of such a function, defined as: $h(t) = 1$ for $t = 0$ to T_0 and $h(t) = 0$ elsewhere, equals:

$$H(j\omega) = \int_0^{\infty} h(t)e^{-j\omega t} dt = \int_0^{T_0} e^{-j\omega t} dt = \frac{1 - e^{-j\omega T_0}}{j\omega} \quad (38)$$

Figure 8 presents the graph of the amplitude of $|H(j\omega)|$ as a function of frequency. It is obvious that the amplitude of the higher frequency signals is attenuated. Therefore, only a limited frequency range may be studied because the higher frequency response is too small. It was shown^{50,51} that even low level noise disturbs significantly the obtained impedance spectra.

Figure 8.

(ii) Noise Perturbation

White noise, that is noise consisting of continuous spectrum of frequencies (or a computer generated pseudo-random white noise) may be used as a perturbation signal in practical impedance measurements.^{50,51} However, single frequency components obtained by the FFT have relatively low amplitudes and long data acquisition time is necessary to obtain reliable results.^{50,51} Even low noise contamination of the measured signal leads to significantly disturbed impedance spectra.

(iii) Sum of Sine Waves

In this technique the perturbation signal is composed of a sum of selected sinusoids. This technique was introduced and extensively used by D.E. Smith and coworkers.^{50,49,53,54} The applied signal consists of a fundamental harmonic frequency f_0 and a number of odd harmonics $(2n+1)f_0$. This arrangement is superior to other perturbation wave forms.⁵⁰ All these frequencies are applied at the same time and the response to each frequency is found by the FFT. This technique has been applied by Smith and coworkers to study electrode kinetics in the frequency range 10 to 500 Hz. It should be mentioned the such technique is used in low frequency impedance analysis (below 10 Hz) in PAR 273 series potentiostats (software implemented).

Popkirov and Schindler⁵¹ have demonstrated that by the appropriate selection of phases and amplitudes of the individual sinusoidal components the measured results may be improved. First of all, signal phases may be optimized to minimize the observed peak to peak signal amplitude. This also allows the amplitudes of the individual components to be increased by over 30%, maintaining the total amplitude at its initial level, thus increasing the power of the single

frequency components. A decrease of the standard deviation of the impedance by 25% was obtained in that way. The results of such optimization are shown in Figure 9. An additional possibility is an optimization of the amplitudes. It is known that the response of electrochemical cells is different for different frequencies so that the response is weaker in the low frequency range and larger at high frequencies. Besides, higher noise is observed at low frequencies (for the same perturbation amplitude). When the amplitudes of different frequencies are optimized, that is they are selected in such a way that the response remains nearly constant, the response signal is much less sensitive to noise. An example of such optimization is displayed in Figure 10.

The main advantage of the FFT technique is that the information is obtained quickly, therefore it may be applied to study impedances evolving with time (of course, impedance must be considered constant during the time of measurements). The weakness of the FFT technique is that the response to individual frequencies is usually weaker than that when only one frequency is applied.

It should be added that other types of analysis of the system responses were also used, e.g. Laplace transform of the applied perturbation and the obtained response to determine the impedance spectra.^{28,55-61}

Figure 9.

Figure 10.

III. IMPEDANCE OF FARADAIC REACTIONS IN THE PRESENCE OF DIFFUSION

Total electrode impedance consists of the contributions of the electrolyte, the electrode-solution interface and electrochemical reactions taking place on the electrode. First, we shall consider the case of an ideally polarizable electrode, followed by semi-infinite diffusion in linear, spherical and cylindrical geometry and, finally a finite-length diffusion.

1. The Ideally Polarizable Electrode

An ideally polarizable electrode behaves as an ideal capacitor because there is no charge transfer across the solution-electrode boundary. In this case the equivalent electrical model consists of the solution resistance, R_s , in series with the double-layer capacitance, C_{dl} . Analysis of such a circuit was presented in Section I.2(i).

2. Semi-Infinite Linear Diffusion

In general, it is possible to write the expression for the impedance for any mechanisms. The procedure shown below is general and may be applied to other processes involving diffusion. For the reaction:



the current is described by:

$$i = nF[k_f C_O(0) - k_b C_R(0)] \quad (40)$$

where k_f and k_b are the potential-dependent rate constants for the forward and backward reactions: $k_f = k_o \exp[-\alpha n f (E - E^0)]$ and $k_b = k_o \exp[(1 - \alpha) n f (E - E^0)]$, k_o and E^0 are the standard rate constant and standard potential, respectively, $C_O(0)$ and $C_R(0)$ are the surface concentrations of the forms Ox and Red, α is the transfer coefficient, n number of electrons, and $f = F/RT$. When a small ac perturbation signal, $\Delta E = E_0 \exp(j\omega t)$, is applied, the current and concentrations oscillate around steady-state values: $i = i_{dc} + \Delta i$, $C_O = C_{O,dc} + \Delta C_O$, and $C_R = C_{R,dc} + \Delta C_R$, where the subscript *dc* indicates a parameter which changes only slowly with time i.e., either a steady-state term or the one that does not change with ω or its harmonics, and the symbol Δ indicates a parameter oscillating periodically with time. In general, the oscillating potential and the concentrations may be written as:

$$\Delta E = \tilde{E} \exp(j\omega t), \quad \Delta i = \tilde{i} \exp(j\omega t) \quad \Delta C_O = \tilde{C}_O \exp(j\omega t) \quad \text{and} \quad \Delta C_R = \tilde{C}_R \exp(j\omega t) \quad (41)$$

where \tilde{E} , \tilde{i} , \tilde{C}_O , and \tilde{C}_R are the phasors of the voltage, current and concentrations. Because we are interested in the ac components of these parameters, we can solve equations for ΔE , Δi , ΔC_O and ΔC_R only. In general, the current is a function of the potential and concentrations, eqn. (40), and it may be represented as an infinite Taylor series:

$$\begin{aligned} \Delta i = & \left(\frac{\partial i}{\partial E} \right) \Delta E + \left(\frac{\partial i}{\partial C_O} \right) \Delta C_O + \left(\frac{\partial i}{\partial C_R} \right) \Delta C_R \\ & + \frac{1}{2} \left(\frac{\partial^2 i}{\partial E^2} \right) (\Delta E)^2 + \frac{1}{2} \left(\frac{\partial^2 i}{\partial C_O^2} \right) (\Delta C_O)^2 + \frac{1}{2} \left(\frac{\partial^2 i}{\partial C_R^2} \right) (\Delta C_R)^2 \\ & + \left(\frac{\partial^2 i}{\partial E \partial C_O} \right) \Delta E \Delta C_O + \left(\frac{\partial^2 i}{\partial E \partial C_R} \right) \Delta E \Delta C_R + \left(\frac{\partial^2 i}{\partial C_O \partial C_R} \right) \Delta C_O \Delta C_R + \dots \end{aligned} \quad (42)$$

It can be noticed that because eqn. (40) is linear with respect to the concentrations, only first-order derivatives versus concentrations are different from zero. For small perturbations it is a good approximation to keep only the linear terms. This *linearization is a fundamental property* of EIS, therefore the amplitudes applied must be small, $\Delta E < 8/n \text{ mV}^6$ peak-to-peak, where n is the number of electrons exchanged in the reaction. Higher harmonics analysis has also been described.^{6,7,27,62} The derivatives in eqn. (42) correspond to stationary conditions and may be obtained from eqn. (40):

$$\frac{\partial i}{\partial E} = -n^2 F f \left[\alpha k_f C_O(0) + (1 - \alpha) k_b C_R(0) \right] \quad (43)$$

$$\frac{\partial i}{\partial C_O} = n F k_f \quad \text{and} \quad \frac{\partial i}{\partial C_R} = -n F k_b \quad (44)$$

In order to find concentrations, Fick's diffusion equation must be solved for ΔC . For semi-infinite linear diffusion the following equations must be solved:

$$\frac{\partial \Delta C_o}{\partial t} = D_o \frac{\partial^2 \Delta C_o}{\partial x^2} \quad \text{and} \quad \frac{\partial \Delta C_R}{\partial t} = D_R \frac{\partial^2 \Delta C_R}{\partial x^2} \quad (45)$$

Taking into account eqn. (41) and

$$\partial \Delta C_o / \partial t = j\omega \tilde{C}_o \exp(j\omega t) \quad (46)$$

eqn. (45) may be rearranged to:

$$j\omega \tilde{C}_o = D_o \frac{d^2 \tilde{C}_o}{dx^2} \quad \text{and} \quad j\omega \tilde{C}_R = D_R \frac{d^2 \tilde{C}_R}{dx^2} \quad (47)$$

with the boundary conditions:

$$x = 0: \quad \frac{d\tilde{C}_o}{dx} = \frac{\tilde{i}}{nFD_o}, \quad \frac{d\tilde{C}_R}{dx} = -\frac{\tilde{i}}{nFD_R} \quad (48)$$

$$D_o \frac{d\tilde{C}_o}{dx} + D_R \frac{d\tilde{C}_R}{dx} = 0 \quad (49)$$

$$x \rightarrow \infty: \quad \tilde{C}_o \rightarrow 0 \quad \text{and} \quad \tilde{C}_R \rightarrow 0 \quad (50)$$

where, at $x \rightarrow \infty$, only a dc concentration gradient exists. After further rearrangements one obtains:

$$\frac{d^2 \tilde{C}_o}{dx^2} = \left(\frac{j\omega}{D_o} \right) \tilde{C}_o = s_o^2 \tilde{C}_o \quad \text{and} \quad \frac{d^2 \tilde{C}_R}{dx^2} = \left(\frac{j\omega}{D_R} \right) \tilde{C}_R = s_R^2 \tilde{C}_R \quad (51)$$

which have the following solutions:

$$\tilde{C}_o(x) = A \exp(-s_o x) + B \exp(s_o x) \quad \text{and} \quad \tilde{C}_R(x) = A' \exp(-s_R x) + B' \exp(s_R x) \quad (52)$$

For semi-infinite diffusion B and B' are both equal to zero, to fulfill the condition (50). In order to determine the constants A and A' , the condition at $x = 0$ must be considered:

$$\frac{d\tilde{C}_o}{dx} = -s_o A = \frac{\tilde{i}}{nFD_o} \quad (53)$$

and substituting s_o and s_R , eqn. (50), one gets:

$$A = \tilde{C}_o(0) = -\frac{\tilde{i}}{nF\sqrt{j\omega D_o}} \quad \text{and} \quad A' = \tilde{C}_R(0) = \frac{\tilde{i}}{nF\sqrt{j\omega D_R}} \quad (54)$$

Now, it is possible to make the substitutions into eqn. (42), conserving only linear terms:

$$\tilde{i} = -\frac{n^2 F^2}{RT} \left[\alpha k_f C_O(0) + (1-\alpha) k_b C_R(0) \right] \tilde{E} - \frac{\tilde{i} k_f}{\sqrt{j\omega D_O}} - \frac{\tilde{i} k_b}{\sqrt{j\omega D_R}} \quad (55)$$

and the faradaic impedance equals $\hat{Z}_f = -\tilde{E} / \tilde{i}$ (the negative sign arises from the assumed convention in which the cathodic current is positive):

$$\hat{Z}_f = \frac{RT}{n^2 F^2} \frac{1 + \frac{k_f}{\sqrt{j\omega D_O}} + \frac{k_b}{\sqrt{j\omega D_R}}}{\alpha k_f C_O(0) + (1-\alpha) k_b C_R(0)} \quad (56)$$

The total faradaic impedance, \hat{Z}_f , consists of three terms: the first one comes from the derivative: $\partial i / \partial E$ and is called charge-transfer resistance, R_{ct} , and the two others, which are contributions from $\partial i / \partial C_i$, are called impedances of mass transfer or semi-infinite Warburg impedance⁶³⁻⁶⁶, \hat{Z}_W :

$$\hat{Z}_f = R_{ct} + \hat{Z}_W = R_{ct} + \hat{Z}_{W,O} + \hat{Z}_{W,R} \quad (57)$$

$$R_{ct} = \frac{RT}{n^2 F^2} \frac{1}{\alpha k_f C_O(0) + (1-\alpha) k_b C_R(0)} \quad (58)$$

$$\begin{aligned} \hat{Z}_{W,O} &= \frac{RT}{n^2 F^2} \frac{k_f}{\sqrt{j\omega D_O} \left[\alpha k_f C_O(0) + (1-\alpha) k_b C_R(0) \right]} \\ &= \frac{RT}{n^2 F^2} \frac{1}{\sqrt{j\omega D_O} \{ \alpha C_O(0) + (1-\alpha) C_R(0) \exp[nf(E - E^0)] \}} \end{aligned} \quad (59)$$

$$\hat{Z}_{W,R} = \frac{RT}{n^2 F^2} \frac{\exp[nf(E - E^0)]}{\sqrt{j\omega D_R} \{ \alpha C_O(0) + (1-\alpha) C_R(0) \exp[nf(E - E^0)] \}} \quad (60)$$

Assuming that the process is dc reversible, the surface concentrations are described by the Nernst equation: $C_O(0)/C_R(0) = \exp[nf(E - E^0)]$ and eqns. (59) and (60) may be written as:

$$\hat{Z}_W = \hat{Z}_{W,O} + \hat{Z}_{W,R} = \frac{RT}{n^2 F^2 \sqrt{j\omega}} \left(\frac{1}{\sqrt{D_O} C_O(0)} + \frac{1}{\sqrt{D_R} C_R(0)} \right) = \frac{\sqrt{2}}{\sqrt{j}} \frac{\sigma}{\sqrt{\omega}} \quad (61)$$

where σ is the mass transfer coefficient equal to the sum of the contributions of the forms Ox and Red:

$$\sigma = \sigma_O + \sigma_R = \frac{RT}{n^2 F^2 \sqrt{2}} \left[\frac{1}{\sqrt{D_O} C_O(0)} + \frac{1}{\sqrt{D_R} C_R(0)} \right] \quad (62)$$

Because $1/\sqrt{j} = (1/\sqrt{2})(1-j)$, the mass transfer impedance may be written as:

$$\hat{Z}_W = \sigma \omega^{-1/2} - j \sigma \omega^{-1/2} \quad (63)$$

This equation may be also obtained directly by assuming that the charge-transfer reaction is reversible and calculating the mass transfer impedance from:

$$\hat{Z}_W = \frac{dE}{di} = \sum_{i=O,R} \frac{dE}{dC_i} \frac{\tilde{C}_i}{\tilde{i}} \quad (64)$$

where, from the Nernst equation, one gets:

$$dE/dC_O = RT/nFC_O(0) \text{ and } dE/dC_R = -RT/nFC_R(0) \quad (65)$$

After substitution of eqn. (64) into (65), eqn. (63) is obtained as before. The mass transfer impedance is called, in the case of semi-infinite linear diffusion, a semi-infinite Warburg impedance. Assuming that there is only the oxidized form initially in the solution (C_O^*), the surface concentrations may be estimated from¹¹:

$$C_O(0) = C_O^* \frac{\xi \theta}{1 + \xi \theta} \text{ and } C_R(0) = C_O^* \frac{\xi}{1 + \xi \theta} \quad (66)$$

where $\xi = (D_O/D_R)^{1/2}$ and $\theta = \exp[nf(E-E^0)]$ and $\xi \theta = \exp[nf(E-E_{1/2})]$. Substituting eqn. (66) into

(58) the charge-transfer resistance may be expressed as:

$$R_{ct} = \frac{RT}{n^2 F^2 k_b C_O^*} \frac{1 + \exp[nf(E - E_{1/2})]}{\xi} = \frac{RT}{n^2 F^2 k_0 C_O^*} \frac{1 + \exp[nf(E - E_{1/2})]}{\xi^\alpha \exp[(1 - \alpha)nf(E - E_{1/2})]} \quad (67)$$

and it has a minimum at:

$$E_s = E_{1/2} + \frac{RT}{nF} \ln \frac{\alpha}{1 - \alpha} \quad (68)$$

For the processes for which the transfer coefficient, α , is equal to 0.5, the minimum of R_{ct} is observed at the half-wave potential. Similarly, the mass transfer impedance equals:

$$\begin{aligned} \hat{Z}_W &= \frac{RT}{n^2 F^2 C_O^* \sqrt{j\omega D_O}} \frac{[1 + \exp[nf(E - E_{1/2})]]^2}{\exp[nf(E - E_{1/2})]} \\ &= \frac{4RT}{n^2 F^2 C_O^* \sqrt{j\omega D_O}} \cosh^2 \left[\frac{nf(E - E_{1/2})}{2} \right] \end{aligned} \quad (69)$$

The Warburg impedance has a minimum at $E_{1/2}$. The mass transfer impedance is a vector containing real and imaginary components which are identical, that is the phase-angle: $\varphi = \text{atan}(Z_W'' / Z_W') = \text{atan}(-1) = -45^\circ$. The faradaic impedance is shown in Figure 11b (dashed line). On the complex plane plot it is a straight line with a slope of 1 and intercept R_{ct} . The total electrode impedance consists of the solution resistance, R_s , in series with the parallel connection of the double-layer capacitance, C_{dl} , and faradaic impedance, Figure 11a. This is so called Randles model.^{64,65,67} Figure 11b-d also shows complex plane and Bode plots for the total electrode impedance in the presence of slow charge-transfer kinetics. It should be stressed that the Warburg impedance cannot be represented by a connection of simple R and C elements because of the non-integer power of frequency ($\omega^{-1/2}$) and it constitutes a distributed element which can only be approximated by an infinite series of simple electrical elements.

Figure 11.

Figure 12.

In the case when the surface and bulk concentrations are the same, that is when the mass transfer impedance may be neglected, the equivalent circuit corresponds to that in Figure 4. In this case a semicircle is observed on the complex plane plots. In the other limiting case, when the charge-transfer resistance is neglected (reversible case) a straight line, with a slope of 1, is obtained on the complex plane plots.

The dependence of the mass transfer and charge-transfer impedances on the electrode potential is displayed in Figure 12. The charge-transfer and mass transfer impedances have a minimum at E_s , eqn. (68), and $E_{1/2}$, respectively, according to eqns. (67) and (69).

A procedure for assessing nonlinearities in the Randles circuit, based on nonlinear regression analysis was described recently.⁶⁸

VanderNoot⁶⁹ studied poorly separated faradaic and diffusional processes. He has found that the complex non-linear least-squares regression is capable of extracting kinetic information from impedance measurements when the ratio of the charge-transfer process time constant $t_f = R_{ct}C_{dl}$ to the diffusion process time constant $t_d = R_{ct}^2/(2\sigma^2)$, $t_f/t_d = 2\sigma^2 C_{dl}/R_{ct}$, is lower than or equal to 30.

A mechanism including two successive electron transfer reactions was analyzed by Armstrong and Firman.⁷⁰ A general approach to multistep mechanisms involving soluble species in semi-infinite diffusion was presented recently by Harrington.⁷¹ It allows for determination of the number of break-point frequencies on the Bode magnitude plot for an arbitrary mechanism and, in consequence, for the determination of the reaction mechanism and kinetics.

3. Spherical Diffusion

This case arises, e.g., when working with dropping or hanging mercury electrodes. Let us consider semi-infinite diffusion to a sphere of radius r_0 with both oxidized and reduced forms soluble in the solution. In this case eqn. (47) should be substituted by^{13,14}:

$$\frac{\partial \tilde{C}_O}{\partial t} = D_O \left(\frac{\partial^2 \tilde{C}_O}{\partial r^2} + \frac{2}{r} \frac{\partial \tilde{C}_O}{\partial r} \right) \quad \text{and} \quad \frac{\partial \tilde{C}_R}{\partial t} = D_R \left(\frac{\partial^2 \tilde{C}_R}{\partial r^2} + \frac{2}{r} \frac{\partial \tilde{C}_R}{\partial r} \right) \quad (70)$$

These equations may be rearranged into a simpler form, eqn. (51), by substitution $\tilde{u} = r\tilde{C}_O$ and $\tilde{v} = r\tilde{C}_R$:

$$\frac{d^2\tilde{u}}{dx^2} = s_O^2 \tilde{u} \quad \text{and} \quad \frac{d^2\tilde{v}}{dx^2} = s_R^2 \tilde{v} \quad (71)$$

The solution is:

$$\tilde{u} = A \exp(-\sqrt{j\omega/D_O} r) \quad \text{and} \quad \tilde{v} = A \exp(-\sqrt{j\omega/D_R} r) \quad (72)$$

Taking into account that $d\tilde{u}/dr = \tilde{C}_O + r d\tilde{C}_O/dr$ and that at $r = r_0$ (at the electrode surface) $d\tilde{C}_O/dr = \tilde{i}/nFD_O$ the following solutions are obtained:

$$\tilde{C}_O(0) = -\frac{\tilde{i} r_0}{nFD_O(1+r_0\sqrt{j\omega/D_O})} \quad \text{and} \quad \tilde{C}_R(0) = -\frac{\tilde{i} r_0}{nFD_R(1+r_0\sqrt{j\omega/D_R})} \quad (73)$$

The mass transfer impedance may be obtained from eqn. (64). Assuming a reversible dc process one obtains, similar to the case of linear diffusion:

$$\hat{Z}_W = \sum_{i=O,R} \frac{RT}{n^2 F^2 D_i C_i(0)} \frac{r_0}{\left(1 + r_0 \sqrt{\frac{j\omega}{D_i}}\right)} \quad (74)$$

or

$$\hat{Z}_W = \sum_{i=O,R} \sigma_i \omega^{-1/2} \frac{1 + y_i - j}{1 + y_i + 0.5 y_i^2} \quad (75)$$

where

$$y_i = \frac{1}{r_0} \sqrt{\frac{2D_i}{\omega}} \quad (76)$$

Influence of the nonlinearity of diffusion on the observed complex plane plots is shown in Figure 13. Spherical mass transfer causes formation of a depressed semicircle at low frequencies instead of linear behavior observed for linear semi-infinite diffusion. For very small electrodes (ultramicroelectrodes) or low frequencies the mass transfer impedances become negligible and the dc current becomes stationary. On the Bode phase-angle graph a maximum is observed at low frequencies.

Figure 13.

4. Cylindrical Electrodes

An example of cylindrical diffusion is a diffusion towards a conducting wire. Solutions for cylindrical electrodes have been given by Fleischmann et al.^{72,73} and Jacobsen and West⁷⁴. Methods presented by both groups give the same results; however, the latter is simpler. In this case the diffusion equation is similar to that for spherical diffusion, eqn. (70). The solution is shown here for the oxidized form only:

$$\frac{\partial \tilde{C}_O}{\partial t} = D_O \left(\frac{\partial^2 \tilde{C}_O}{\partial r^2} + \frac{1}{r} \frac{\partial \tilde{C}_O}{\partial r} \right) \quad (77)$$

Rearrangement for the oscillating concentration, using eqn. (46), leads to:

$$\frac{d^2 \tilde{C}_O}{dr^2} + \frac{1}{r} \frac{d\tilde{C}_O}{dr} - \left(\frac{j\omega}{D_O} \right) \tilde{C}_O = 0 \quad (78)$$

Substitution of $z = r(j\omega/D_O)^{1/2}$ gives:

$$\frac{d^2 \tilde{C}_O}{dz^2} + \frac{1}{z} \frac{d\tilde{C}_O}{dz} - \tilde{C}_O = 0 \quad (79)$$

This is a modified Bessel equation of zero order with a general solution⁷⁴:

$$\tilde{C}_O = AI_0[z] + BK_0[z] \quad (80)$$

where A and B are constants and I_0 and K_0 are zero-order modified Bessel functions. Taking into account semi-infinite diffusion conditions, that is $\tilde{C}_O \rightarrow 0$ when $r \rightarrow \infty$, leads to $A = 0$. At the electrode surface, $r = r_0$:

$$\frac{d\tilde{C}_O}{dr} = \sqrt{\frac{j\omega}{D_O}} BK_1[z_0] = \frac{i}{nFD_O} \quad (81)$$

where $z_0 = r_0(j\omega/D_O)^{1/2}$ and:

$$B = \frac{i}{nF\sqrt{j\omega D_O} K_1[z_0]} \quad (82)$$

Then, using eqns. (64) one may get:

$$\hat{Z}_W = \frac{dE}{dC_O} \frac{\tilde{C}_O}{i} = \frac{RT}{n^2 F^2 D_O C_O^*} \frac{r_0 K_0[z_0]}{z_0 K_1[z_0]} \quad (83)$$

The *function* in eqn. (83) may be evaluated using Mathematica, Maple or specific subroutines for complex modified Bessel functions. The corresponding complex plane plots are shown in Figure

14. At low frequencies cylindrical diffusion produces a constant imaginary impedance component.

Figure 14.

5. Disk Electrodes

The solution for disk electrodes was presented by Fleischmann *et al.*^{72,73}. In this case the differential equation corresponds to the normal and radial diffusion (two-dimensional) to the electrode. They obtained the following equations describing the faradaic impedance in the case of a slow charge transfer when only Ox is initially present in the solution, its concentration being C_O^* :

$$Z_f' = R_{ct} + \frac{4RT}{n^2 F^2 D_O^{1/2} \omega^{1/2} C_O^*} \int_0^\infty \left[J_1 \left(\beta \frac{a}{l} \right) \right]^2 \frac{\cos(\Theta / 2) d\beta}{\beta (1 + \beta^4)^{1/4}} \quad (84)$$

$$Z_f'' = \frac{4RT}{n^2 F^2 D_O^{1/2} \omega^{1/2} C_O^*} \int_0^\infty \left[J_1 \left(\beta \frac{a}{l} \right) \right]^2 \frac{\sin(\Theta / 2) d\beta}{\beta (1 + \beta^4)^{1/4}} \quad (85)$$

where a is the disk radius, J_1 is the Bessel function of the first kind and first order, $l^2 = D/\omega$, and $\tan\Theta = 1/\beta^2$. The first term in Z_f' corresponds to the charge-transfer resistance. The integrals in eqns. (84)-(85) were tabulated in ref. 73 as functions Φ_4 and Φ_5 of $(a^2\omega/D)$ and in a different form in ref. 72. At sufficiently high frequencies the results are similar to those for linear diffusion whereas, at low frequencies, the impedance becomes real as for spherical electrodes. The complex plane plots for the diffusion to a disk are shown in Figure 15 exhibit a flattened semicircle.

Fleischmann and Pons^{72,73,75} also considered diffusion to microring electrodes.

Figure 15.

6. Finite-Length Diffusion

In many cases the diffusion is not semi-infinite. This case is, for example, observed for polymer electrodes, for a thin mercury layer deposited on surfaces, for rotating disk electrodes, etc. In such cases, in eqn. (52) parameters B and B' are not equal to zero. Two cases may be distinguished for finite-length diffusion depending on the condition at the boundary located at a distance l from the electrode:

- 1) transfer of electroactive species is possible at $x = l$, and $C(l) = 0$, but $dC(l)/dx \neq 0$. This is the so-called conducting or transmissive boundary. It is observed, for example for the rotating disk electrode, where the diffusion layer thickness is determined by the rotation rate. And
- 2) no charge transfer is possible at $x = l$, that is $dC(l)/dx = 0$. This is the so called reflecting boundary, observed in the case of conducting polymers.

(i) **Transmissive Boundary**

In order to determine the constants A , B , A' , and B' in eqn. (52), boundary conditions must be used. At the electrode surface the concentration gradients are:

$$x = 0: \left. \frac{d\tilde{C}_O}{dx} \right|_{x=0} = -s_O A + s_O B = \frac{\tilde{i}}{nFD_O} \quad \text{and} \quad \left. \frac{d\tilde{C}_R}{dx} \right|_{x=0} = -s_R A' + s_R B' = -\frac{\tilde{i}}{nFD_R} \quad (86)$$

$$x = l: \tilde{C}_O = A \exp(-s_O l) + B \exp(s_O l) = 0 \quad \text{and} \quad \tilde{C}_R = A' \exp(-s_R l) + B' \exp(s_R l) = 0 \quad (87)$$

which leads to:

$$A = -\frac{\tilde{i}}{nF\sqrt{j\omega D_O}} \frac{\exp(s_O l)}{\exp(s_O l) + \exp(-s_O l)} \quad \text{and} \quad B = \frac{\tilde{i}}{nF\sqrt{j\omega D_O}} \frac{\exp(-s_O l)}{\exp(s_O l) + \exp(-s_O l)} \quad (88)$$

$$A' = \frac{\tilde{i}}{nF\sqrt{j\omega D_R}} \frac{\exp(s_R l)}{\exp(s_R l) + \exp(-s_R l)} \quad \text{and} \quad B' = -\frac{\tilde{i}}{nF\sqrt{j\omega D_R}} \frac{\exp(s_R l)}{\exp(s_R l) + \exp(-s_R l)} \quad (89)$$

The surface concentrations are:

$$\tilde{C}_O(0) = -\frac{\tilde{i}}{nF\sqrt{j\omega D_O}} \tanh\left(\sqrt{\frac{j\omega}{D_O}} l\right) \quad \text{and} \quad \tilde{C}_R(0) = \frac{\tilde{i}}{nF\sqrt{j\omega D_R}} \tanh\left(\sqrt{\frac{j\omega}{D_R}} l\right) \quad (90)$$

and substitution to eqn. (64) gives the mass transfer impedances:

$$\hat{Z}_W = \frac{RT}{n^2 F^2 C_O(0) \sqrt{j\omega D_O}} \tanh\left(\sqrt{\frac{j\omega}{D_O}} l\right) + \frac{RT}{n^2 F^2 C_R(0) \sqrt{j\omega D_R}} \tanh\left(\sqrt{\frac{j\omega}{D_R}} l\right) \quad (91)$$

or, assuming that the diffusion coefficients of O and R are the same, this becomes:

$$\hat{Z}_W = \frac{\sigma}{\sqrt{\omega}} \tanh\left(\sqrt{\frac{j\omega}{D}} l\right) (1 - j) \quad (92)$$

The Warburg impedance is displayed in Figure 16 a and the total impedance in Figure 16b-d. At low frequencies the function $\tanh(x) \cong x$, and \hat{Z}_W becomes real and frequency independent:

$$\hat{Z}_W(\omega \rightarrow 0) = \frac{\sqrt{2}\sigma l}{\sqrt{D}} \quad (93)$$

Therefore the low frequency limit of the electrode impedance equals:

$$\hat{Z} = R_s + R_{ct} + \frac{\sqrt{2}\sigma l}{\sqrt{D}} \quad (94)$$

(ii) **Reflective Boundary**

In this case the boundary conditions at $x = 0$ are the same as for eqn. (86) but at $x = l$ they are different, the concentration gradient being equal to zero:

$$\frac{d\tilde{C}_O}{dx} = -s_O A \exp(-s_O l) + s_O B \exp(s_O l) = 0 \quad (95)$$

and

$$\frac{d\tilde{C}_R}{dx} = -s_R A' \exp(-s_R l) + s_R B' \exp(s_R l) = 0 \quad (96)$$

They give:

$$\tilde{C}_O(0) = -\frac{\tilde{i}}{nF\sqrt{j\omega D_O}} \coth\left(\sqrt{\frac{j\omega}{D_O}} l\right) \quad \text{and} \quad \tilde{C}_R(0) = -\frac{\tilde{i}}{nF\sqrt{j\omega D_R}} \coth\left(\sqrt{\frac{j\omega}{D_R}} l\right) \quad (97)$$

and

$$\hat{Z}_W = \frac{RT}{n^2 F^2 C_O(0) \sqrt{j\omega D_O}} \coth\left(\sqrt{\frac{j\omega}{D_O}} l\right) + \frac{RT}{n^2 F^2 C_R(0) \sqrt{j\omega D_R}} \coth\left(\sqrt{\frac{j\omega}{D_R}} l\right) \quad (98)$$

or assuming equal diffusion coefficients:

$$\hat{Z}_W = \frac{\sigma}{\sqrt{\omega}} \coth\left(\sqrt{\frac{j\omega}{D}} l\right) (1-j) \quad (99)$$

Figure 16.

The corresponding Warburg and total electrode impedances are shown in Figure 16. At low frequencies $\coth(x) \cong 1/x + x/3$ and \hat{Z}_W becomes:

$$\hat{Z}_W = \frac{\sqrt{2}\sigma l}{3\sqrt{D}} - j \frac{\sqrt{2D}\sigma}{\omega l} \quad (100)$$

The imaginary part of the impedance goes to infinity and the real part to a constant value which indicates that no charge transfer occurs at low frequencies and the electrode behavior is purely capacitive. For these conditions the Warburg impedance corresponds to a series connection of the resistance $R_W = Z'_W$ and the capacitance $C_W = l/\sqrt{2D}\sigma$. The limiting value of the real part of the total cell impedance equals:

$$Z'_t = R_s + R_{ct} + \sqrt{2}\sigma l / 3\sqrt{D} \quad (101)$$

The problem of finite length diffusion in spherical and cylindrical symmetry was solved by Jacobsen and West⁷⁴.

7. Analysis of Impedance Data in the Case of Semi-Infinite Diffusion: Determination of the Kinetic Parameters

In the case of the charge transfer to diffusing species, ac voltammetry or ac polarography is usually used and the impedance curves are determined from a series of ac voltammetric curves registered at different frequencies. The methods of analysis of such curves are described below.

(i) *Randles' Analysis*^{64,65,67}

The experimentally measured ac current or total admittances are functions of the electrode potential. Figure 17 presents the dependence of the total admittances of a process limited by the diffusion of electroactive species to and from the electrode and the kinetics of the charge transfer process, on the electrode potential. Information on the kinetics of electrode process is included in the faradaic impedance. It may be simply determined from the total electrode impedance:^{64,65}

$$\frac{1}{Z_f} = \frac{1}{Z_t - R_s} - j\omega C_{dl} \quad (102)$$

It should be kept in mind that for the calculation of the impedances from admittances the following equation must be used:

$$Z' = \frac{Y'}{(Y')^2 + (Y'')^2} \quad \text{and} \quad Z'' = -\frac{Y''}{(Y')^2 + (Y'')^2} \quad (103)$$

The parameters R_s and C_{dl} must be determined in a separate experiment in a solution containing supporting electrolyte only, keeping the same distance between the working electrode and the tip of the Luggin capillary (i.e. to maintain R_s constant). This may be possible when this distance is large or the solution in the cell is exchanged without changing the electrode configuration. The other possibility is to extrapolate the admittance (or impedance) from the range where the faradaic impedance is negligible, that is from potentials more positive and more negative than the peak potential. Then, the real and imaginary components of the faradaic impedance are plotted against $\omega^{-1/2}$. They form two parallel lines with slopes of σ and intercepts of $Z'_f = R_{ct}$ and zero, Figure 18. The dependence of R_{ct} on potential allows the determination of the standard rate constant and the transfer coefficient.

Figure 17.

In order to eliminate influence of the depolarizer concentration one can also evaluate the ratio of the slope to intercept of the Randles' plot. Proper rearrangement leads to:

$$\frac{\sigma}{R_{ct}} \frac{\exp[nf[E - E_{1/2}]]}{1 + \exp[nf[E - E_{1/2}]]} = \frac{\xi k_b}{\sqrt{2D_O}} \quad (104)$$

from which the rate constant as a function of the electrode potential may be evaluated. At the reversible half-wave potential this ratio gives directly the standard rate constant:

$$\left(\frac{\sigma}{R_{ct}}\right)_{E_{1/2}} = \frac{2\xi^\alpha}{\sqrt{2D_O}} k_0 \quad (105)$$

Figure 18.

(ii) **De Levie-Husovsky Analysis**

De Levie and Husovsky⁷⁶ have proposed method based on analysis of faradaic admittances. The Faradaic admittance may be easily determined from the total impedance:

$$\hat{Y}_f = \frac{1}{Z_t - R_s} - j\omega C_{dl} \quad (106)$$

The ratio of the imaginary to real faradaic admittances equals:

$$\frac{Y_f''}{Y_f'} = \frac{\zeta}{1-\zeta} \quad (107)$$

where

$$\zeta = \frac{k_f}{\sqrt{2\omega D_O}} + \frac{k_b}{\sqrt{2\omega D_R}} = \frac{k_f}{\sqrt{2\omega D_O}} (1 + \exp[nf(E - E_{1/2})]) \quad (108)$$

From the dependence of $\log [\zeta / \{1 + \exp[nf(E - E_{1/2})]\}]$ versus E the forward rate constant is easily determined.

(iii) **Analysis of cot φ**

Another type of determination of kinetic parameters is based on the determination of the phase-angle of the faradaic impedance. From eqns. (57), (67) and (69) one may get:

$$\cot \varphi = \frac{Z_f'}{Z_f''} = 1 + \frac{R_{ct}}{\sigma} \omega^{1/2} \quad (109)$$

or after substitution:

$$\cot \varphi = 1 + \frac{\sqrt{2} D_O^{(1-\alpha)/2} D_R^{\alpha/2} \omega^{1/2}}{k_0 \exp[(1-\alpha)f(E - E_{1/2})] \{1 + \exp[-nf(E - E_{1/2})]\}} \quad (110)$$

It is clear that $\cot \varphi$ depends linearly on $\omega^{1/2}$ and on electrode potential. It has a maximum at the potential E_s described by eqn. (58). The difference between the potential of the maximum of

$\cot \varphi$ and $E_{1/2}$ allows for estimation of the transfer coefficient α . The potential dependence of $\cot \varphi$ is shown in Figure 19. The maximal value of $\cot \varphi$ is described by:

$$[\cot \varphi]_{\max} = 1 + \frac{\left(2D_O^{1-\alpha} D_R^\alpha\right)^{1/2}}{k_0 \left[\left(\frac{\alpha}{\beta}\right)^{-\alpha} + \left(\frac{\alpha}{\beta}\right)^\beta \right]} \omega^{1/2} \quad (111)$$

while at the half-wave potential it is given by:

$$[\cot \varphi]_{E_{1/2}} = 1 + \left(\frac{D_O^{1-\alpha} D_R^\alpha}{2} \right)^{1/2} \frac{\omega^{1/2}}{k_0} \quad (112)$$

Analysis of $\cot \varphi$ as a function of $\omega^{1/2}$, illustrated in Figure 20, gives access to the standard rate constant k_0 .

Figure 19.

Figure 20.

(iv) **Sluyter's Analysis**

Complex plane plots obtained in the case of a slow charge transfer with semi-infinite diffusion were presented in Figure 11a. They represent a semicircle (at high frequencies) followed by a straight line. General equations describing total real and imaginary impedance were analyzed by Sluyters and coworkers^{26,27,78,79}. The total electrode impedance is given as:

$$\hat{Z}_t = R_s + \frac{1}{\frac{1}{Z_f} + j\omega C_{dl}} \quad (113)$$

where the faradaic impedance is described by eqn. (57). This equation leads to rather complicated expressions for the real and imaginary parts of the total impedance:

$$Z' = R_s + \frac{R_{ct} + \sigma \omega^{-1/2}}{\left(\sigma \omega^{1/2} C_{dl} + 1\right)^2 + \omega^2 C_{dl}^2 \left(R_{ct} + \sigma \omega^{-1/2}\right)^2} \quad (114)$$

and

$$Z'' = \frac{\omega C_{dl} (R_{ct} + \sigma \omega^{-1/2})^2 + \sigma^2 C_{dl} + \sigma \omega^{-1/2}}{(\sigma \omega^{1/2} C_{dl} + 1)^2 + \omega^2 C_{dl}^2 (R_{ct} + \sigma \omega^{-1/2})^2} \quad (115)$$

The graphical illustration of these equations is presented in Figure 11b. Although in simple cases the process parameters may be obtained graphically, the best way to analyze the impedances is, however, by the complex nonlinear least-squares approximation technique. From such fits the following parameters may be obtained: R_s , C_{dl} , R_{ct} and the Warburg coefficient σ .

IV. IMPEDANCE OF A FARADAIC REACTION INVOLVING ADSORPTION OF REACTING SPECIES

In Section III, reactions of charge transfer to diffusing species in solution were considered. In this Section reactions involving adsorbed species in the absence of diffusion limitations will be presented. The latter condition means that the concentration gradient at the electrode surface is negligible, that is the concentrations in solution are large enough and/or currents low. Reactions involving one and two and more adsorbed species will be considered subsequently.

1. Faradaic Reaction Involving One Adsorbed Species

Let us consider the following reactions:



where index *sol* denotes species in solution and *ads* adsorbed species. The rates of these reactions may be written, assuming Langmuir adsorption isotherm for *B*, as:

$$v_1 = k_1^0 \Gamma_s a_A e^{-\beta_1 f(E-E_1^0)} - k_{-1}^0 \Gamma_B e^{(1-\beta_1)f(E-E_1^0)} \quad (118)$$

and

$$v_2 = k_2^0 \Gamma_B e^{-\beta_2 f(E-E_2^0)} - k_{-2}^0 \Gamma_s a_C e^{(1-\beta_2)f(E-E_2^0)} \quad (119)$$

where k_i^0 are the standard rate constants of these two reactions, β_i are the symmetry coefficients, Γ_A and Γ_s are the surface concentrations of the species *A* and of free adsorption sites, respectively, a_A and a_C are the surface concentrations of *A* and *C* (assumed as equal to the bulk concentrations) and E_i^0 are the standard red-ox potentials of these reactions. At the equilibrium potential, E_{eq} the net rates of both reactions are null and the following relations are obtained:

$$e^{f(E_{eq}-E_1^0)} = \Gamma_s^0 a_A / \Gamma_A^0 = (1-\Theta_0) a_A / \Theta_0 \quad (120)$$

$$e^{f(E_{eq}-E_2^0)} = \Gamma_B^0 / \Gamma_s^0 a_C = \Theta_0 / (1-\Theta_0) a_C \quad (121)$$

where index 0 indicates equilibrium conditions and a relation between surface coverage, Θ , and surface concentration was introduced: $\Gamma_i = \Theta_i \Gamma_\infty$ and Γ_∞ is the maximal surface concentration. Introduction of eqns. (120) and (121) into (118) and (119), and taking into account that: $E - E_i^0 = E - E_{eq} + E_{eq} - E_i^0 = \eta + E_{eq} - E_i^0$, where η is the overpotential, gives:

$$\begin{aligned} v_1 &= k_1^0 \Gamma_\infty a_A^{1-\beta_1} (1-\Theta_0)^{-\beta_1} \Theta_0^{\beta_1} (1-\Theta) e^{-\beta_1 f \eta} - k_{-1}^0 \Gamma_\infty a_A^{1-\beta_1} (1-\Theta_0)^{1-\beta_1} \Theta_0^{-(1-\beta_1)} \Theta e^{(1-\beta_1) f \eta} \\ &= k_1 (1-\Theta) e^{-\beta_1 f \eta} - k_{-1} \Theta e^{(1-\beta_1) f \eta} \\ &= \overset{\rightarrow}{k_1} (1-\Theta) - \overset{\leftarrow}{k_{-1}} \Theta \end{aligned} \quad (122)$$

and

$$\begin{aligned} v_2 &= k_2^0 \Gamma_\infty a_C^{\beta_2} (1-\Theta_0)^{\beta_2} \Theta_0^{-\beta_2} \Theta e^{-\beta_2 f \eta} - k_{-2}^0 \Gamma_\infty a_C^{\beta_2} (1-\Theta_0)^{-(1-\beta_2)} \Theta_0^{1-\beta_2} (1-\Theta) e^{(1-\beta_2) f \eta} \\ &= k_2 \Theta e^{-\beta_2 f \eta} - k_{-2} (1-\Theta) e^{(1-\beta_2) f \eta} \\ &= \overset{\rightarrow}{k_2} \Theta - \overset{\leftarrow}{k_{-2}} (1-\Theta) \end{aligned} \quad (123)$$

where the following new rate constants were introduced:

$$k_1 = k_1^0 \Gamma_\infty a_A^{1-\beta_1} \left(\frac{\Theta_0}{1-\Theta_0} \right)^{\beta_1} \quad k_{-1} = k_{-1}^0 \Gamma_\infty a_A^{1-\beta_1} \left(\frac{1-\Theta_0}{\Theta_0} \right)^{1-\beta_1} \quad (124)$$

$$k_2 = k_2^0 \Gamma_\infty a_C^{\beta_2} \left(\frac{1-\Theta_0}{\Theta_0} \right)^{\beta_2} \quad k_{-2} = k_{-2}^0 \Gamma_\infty a_C^{\beta_2} \left(\frac{\Theta_0}{1-\Theta_0} \right)^{1-\beta_2} \quad (125)$$

$$\overset{\rightarrow}{k_1} = k_1 e^{-\beta_1 f \eta}, \quad \overset{\leftarrow}{k_{-1}} = k_{-1} e^{(1-\beta_1) f \eta}, \quad \overset{\rightarrow}{k_2} = k_2 e^{-\beta_2 f \eta}, \quad \overset{\leftarrow}{k_{-2}} = k_{-2} e^{(1-\beta_2) f \eta} \quad (126)$$

The total observed current is:

$$i = F(v_1 + v_2) = F r_0 \quad (127)$$

At the equilibrium potential rates of reactions (2) and (3) are equal to zero, which implies an additional condition:

$$\frac{k_1 k_2}{k_{-1} k_{-2}} = 1 \quad (128)$$

that is there are only three independent rate constants in the system. Under steady-state conditions the rate of formation of adsorbed species B is the same as the rate of their consumption, therefore:

$$\frac{d\Gamma_B}{dt} = \Gamma_\infty \frac{d\Theta}{dt} = \frac{\sigma_1}{F} \frac{d\Theta}{dt} = r_1 = v_1 - v_2 = 0 \quad (129)$$

where $\sigma_1 = F \Gamma_\infty$ is the charge necessary for the total surface coverage by B . In order to calculate the reaction impedance equation describing current $i(\eta, \Theta)$, eqn. (127), and $r_1(\eta, \Theta)$, eqn. (129), should be linearized, giving:

$$\Delta i = \left(\frac{\partial i}{\partial \eta} \right)_\Theta \Delta \eta + \left(\frac{\partial i}{\partial \Theta} \right)_\eta \Delta \Theta = F \left[\left(\frac{\partial r_0}{\partial \eta} \right)_\Theta \Delta \eta + \left(\frac{\partial r_0}{\partial \Theta} \right)_\eta \Delta \Theta \right] \quad (130)$$

$$\frac{\sigma_1}{F} \frac{d\Delta\Theta}{dt} = \Delta r_1 = \left(\frac{\partial r_1}{\partial \eta} \right)_{\Theta} \Delta \eta + \left(\frac{\partial r_1}{\partial \Theta} \right)_{\eta} \Delta \Theta \quad (131)$$

A model containing higher-order term contributions in eqns. (130)-(131) to fundamental harmonic impedances was recently discussed by Darowicki^{80,81} and Diard et al.⁸² Taking into account that (see Section III.2):

$$\Delta i = \tilde{i} \exp(j\omega t), \quad \Delta r_i = \tilde{r}_i \exp(j\omega t) \quad \Delta \eta = \tilde{\eta} \exp(j\omega t) \quad \text{and} \quad \Delta \Theta = \tilde{\Theta} \exp(j\omega t) \quad (132)$$

one obtains:

$$\frac{\tilde{i}}{F} = \tilde{r}_0 = \left(\frac{\partial r_0}{\partial \eta} \right)_{\Theta} \tilde{\eta} + \left(\frac{\partial r_0}{\partial \Theta} \right)_{\eta} \tilde{\Theta} \quad (133)$$

and

$$\frac{\sigma_1}{F} j\omega \tilde{\Theta} = \left(\frac{\partial r_1}{\partial \eta} \right)_{\Theta} \tilde{\eta} + \left(\frac{\partial r_1}{\partial \Theta} \right)_{\eta} \tilde{\Theta} \quad (134)$$

Elimination of $\tilde{\Theta}$ from eqns. (133)-(134) gives the faradaic admittance as:

$$\hat{Y}_f = -\frac{\tilde{i}}{\tilde{\eta}} = -F \left(\frac{\partial r_0}{\partial \eta} \right)_{\Theta} - \frac{\frac{F^2}{\sigma_1} \left(\frac{\partial r_0}{\partial \Theta} \right)_{\eta} \left(\frac{\partial r_1}{\partial \eta} \right)_{\Theta}}{j\omega - \frac{F}{\sigma_1} \left(\frac{\partial r_1}{\partial \Theta} \right)_{\eta}} = A + \frac{B}{j\omega + C} \quad (135)$$

The first term in eqn. (135) is the inverse of the charge-transfer resistance: $A = 1/R_{ct}$. Knowing the faradaic impedance, the total electrode impedance, \hat{Z}_f , may be determined using eqn. (102).

The derivatives in eqn. (135) may be easily evaluated from eqns. (122), (123), (127) and (129):

$$A = Ff \left\{ \beta_1 \vec{k}_1 (1-\Theta) + (1-\beta_1) \overset{\leftarrow}{k}_{-1} \Theta + \beta_2 \vec{k}_2 \Theta + (1-\beta_2) \overset{\leftarrow}{k}_{-2} (1-\Theta) \right\} \quad (136)$$

$$B = \frac{F^2 f}{\sigma_1} \left(-\vec{k}_1 - \overset{\leftarrow}{k}_{-1} + \vec{k}_2 + \overset{\leftarrow}{k}_{-2} \right) \times \left\{ \beta_1 \vec{k}_1 (1-\Theta) + (1-\beta_1) \overset{\leftarrow}{k}_{-1} \Theta - \beta_2 \vec{k}_2 \Theta - (1-\beta_2) \overset{\leftarrow}{k}_{-2} (1-\Theta) \right\} \quad (137)$$

and

$$C = \frac{F}{\sigma_1} \left(\vec{k}_1 + \overset{\leftarrow}{k}_{-1} + \vec{k}_2 + \overset{\leftarrow}{k}_{-2} \right) \quad (138)$$

It is evident that parameters A and C are always positive and B may be positive or negative, depending on the values of rate constants.

2. Impedance Plots in the Case of One Adsorbed Species

The faradaic admittance of the reactions (116) and (117) is described by eqn. (135). Analysis of the complex plane plots in such a case was presented by Cao⁸³. Bai and Conway⁸⁴

presented three-dimensional plots for such a reaction. Two general cases should be considered depending on the sign of the parameter B :

I) $B < 0$

In this case the faradaic admittance may be written as:

$$\hat{Y}_f = \frac{1}{R_{ct}} - \frac{|B|}{j\omega + C} \quad (139)$$

It changes from R_{ct}^{-1} at very high frequencies to $R_{ct}^{-1} - |B|/C$ at very low frequencies. The faradaic impedance is described as:

$$\hat{Z}_f = \frac{1}{\hat{Y}_f} = R_{ct} + \frac{R_{ct}^2 |B|}{j\omega + C - R_{ct} |B|} = R_{ct} + \frac{R_a}{1 + j\omega R_a C_a} = R_{ct} + \frac{1}{\frac{1}{R_a} + j\omega C_a} \quad (140)$$

where:

$$R_a = \frac{R_{ct}^2 |B|}{C - R_{ct} |B|} \quad \text{and} \quad C_a = \frac{1}{R_{ct}^2 |B|} \quad (141)$$

The limit of faradaic impedance at infinite frequency is also called the transfer impedance, R_t , while the limit at zero frequency is called the polarization resistance, R_p :

$$\lim_{\omega \rightarrow 0} (Z_f) = R_p \quad \text{and} \quad \lim_{\omega \rightarrow \infty} (Z_f) = R_t \quad (142)$$

In our case $R_p = R_{ct} + R_{ct}^2 |B| / (C - R_{ct} |B|)$ and $R_t = R_{ct}$. Equation (24) represents a series connection of the charge-transfer resistance with parallel connection of the resistance R_a and pseudocapacitance C_a . The complete equivalent circuit in this case is represented in Figure 21. The observed complex plane plots depend on the sign of the denominator of R_a .

Figure 21.

a) $C - R_{ct} |B| > 0$

In this case all the elements are positive and the faradaic impedance represents one semicircle on the complex plane plots, see Figure 22. When $C_a \gg C_{dl}$ the total impedance represents two semicircles, Figure 22. When $A \gg |B|/C$ the faradaic impedance is equal to R_{ct} . The complex plane plots are analogous to those shown in Figure 4 and represent one capacitive semicircle.

Figure 22.

b) $C - R_{ct} |B| = 0$

In this case the faradaic impedance is:

$$\hat{Z}_f = R_{ct} - j \frac{1}{\omega C_a} \quad (143)$$

which corresponds to a series connection of R_{ct} and C_{dl} . The corresponding complex plane plots are presented in Figure 23.

Figure 23.

c) $C - R_{ct} |B| < 0$

In this case the parameter R_a is negative and the corresponding complex plane plots are displayed in Figure 24.

Figure 24.

II) $B = 0$

When $B = 0$ the faradaic impedance is real and equals R_{ct} . One semicircle is observed in the complex plane plots, Figure 4.

III) $B > 0$

In this case the faradaic admittance is given by:

$$\hat{Y}_f = \frac{1}{R_{ct}} + \frac{B}{j\omega + C} = \frac{1}{R_{ct}} + \frac{1}{R_o + j\omega L} \quad (144)$$

with

$$R_o = C / B \quad \text{and} \quad L = 1 / B \quad (145)$$

and the faradaic impedance by:

$$\hat{Z}_f = \frac{1}{\frac{1}{R_{ct}} + \frac{1}{R_o + j\omega L}} \quad (146)$$

which corresponds to the parallel connection of the charge-transfer resistance with series connection of the resistance R_o and inductance L , Figure 21b. In this case $R_p = R_{ct}R_o/(R_{ct} + R_o)$. The equivalent circuit and the corresponding complex plane plots of faradaic and total impedances are shown in Figure 25. Diard et al.⁸⁵ determined conditions under which such a low frequency pseudo-inductive loop may be found.

Figure 25.

The above analysis shows that in the simple case of one adsorbed intermediate (according to Langmuirian adsorption) various complex plane plots may be obtained, depending on the relative values of the system parameters. These plots are described by various equivalent circuits, which are only the electrical representations of the interfacial phenomena. In fact, there are no real capacitances, inductances or resistances in the circuit (faradaic process). These parameters originate from the behavior of the kinetic equations and they are functions of the rate constants, transfer coefficients, potential, diffusion coefficients, concentrations, etc. Besides, all these parameters are highly nonlinear, that is they depend on the electrode potential. It seems that the electrical representation of the faradaic impedance, however useful it may sound, is not necessary in the description of the system. The system may be described in a simpler way directly by the equations describing impedances or admittances (see also chap. 8). In a system following Frumkin adsorption isotherm discontinuous impedances may be obtained.⁸⁶

It should be added that for the system involving one adsorbed species described above there are two sets of kinetic parameters giving the same experimental curves⁸⁷. In fact

permutation of the kinetic parameters: $k_1 \leftrightarrow k_2$, $k_{-1} \leftrightarrow k_{-2}$, and $\beta_1 \leftrightarrow \beta_2$ leaves the same values of the dc current, the charge-transfer resistance and the parameters B and C . The problem of identifiability and distinguishability of electrode processes was further studied by Bertier et al.⁸⁸⁻⁹¹

The impedance of a more complex process involving coupling between adsorption and diffusion was studied by Armstrong and coworkers.^{92,93}

3. Faradaic Impedance in the Case Involving Two Adsorbed Species

Typical examples of processes involving two or more adsorbed species are reactions of corrosion or anodic dissolution of metals, oxygen evolution, etc. In the case of two adsorbed species B and C , the electrochemical reactions may be written as:^{84,94,95}



and



The rates of eqns. (147)-(149) may be expressed with respect to the equilibrium potential, similarly to eqns. (122) and (123):

$$v_1 = \vec{k}_1(1 - \Theta_1 - \Theta_2) - \overset{\leftarrow}{k}_{-1}\Theta_1 \quad (150)$$

$$v_2 = \vec{k}_2\Theta_1 - \overset{\leftarrow}{k}_{-2}\Theta_2 \quad (151)$$

and

$$v_3 = k_3\Theta_2 - k_{-3}(1 - \Theta_1 - \Theta_2) \quad (152)$$

where Θ_1 and Θ_2 are the surface coverages by B and C , respectively, and rate constants k_3 and k_{-3} are potential independent. From the condition at the equilibrium potential: $v_1 = v_2 = v_3 = 0$ the following condition for the rate constants is obtained (cf. eqn. 128):

$$\frac{k_1 k_2 k_3}{k_{-1} k_{-2} k_{-3}} = 1 \quad (153)$$

The charge is exchanged in reactions (1) and (2) only, therefore the total current is given as:

$$i = F(v_1 + v_2) = Fr_0 \quad (154)$$

Mass balance for Θ_1 and Θ_2 gives, similarly to eqn. (129):

$$\frac{\sigma_1}{F} \frac{d\Theta_1}{dt} = v_1 - v_2 = r_1 \quad (155)$$

$$\frac{\sigma_2}{F} \frac{d\Theta_2}{dt} = v_2 - v_3 = r_2 \quad (156)$$

Taking into account that r_0 , r_1 and r_2 are the functions of η , Θ_1 and Θ_2 , linearization of eqns. (154)-(156) and introduction of phasors gives:

$$\tilde{i} = F \left[\left(\frac{\partial r_0}{\partial \eta} \right)_{\Theta_1, \Theta_2} \tilde{\eta} + \left(\frac{\partial r_0}{\partial \Theta_1} \right)_{\eta, \Theta_2} \tilde{\Theta}_1 + \left(\frac{\partial r_0}{\partial \Theta_2} \right)_{\eta, \Theta_1} \tilde{\Theta}_2 \right] \quad (157)$$

$$j\omega \frac{\sigma_1}{F} \tilde{\Theta}_1 = \left(\frac{\partial \eta_1}{\partial \eta} \right)_{\Theta_1, \Theta_2} \tilde{\eta} + \left(\frac{\partial \eta_1}{\partial \Theta_1} \right)_{\eta, \Theta_2} \tilde{\Theta}_1 + \left(\frac{\partial \eta_1}{\partial \Theta_2} \right)_{\eta, \Theta_1} \tilde{\Theta}_2 \quad (158)$$

and

$$j\omega \frac{\sigma_1}{F} \tilde{\Theta}_2 = \left(\frac{\partial r_2}{\partial \eta} \right)_{\Theta_1, \Theta_2} \tilde{\eta} + \left(\frac{\partial r_2}{\partial \Theta_1} \right)_{\eta, \Theta_2} \tilde{\Theta}_1 + \left(\frac{\partial r_2}{\partial \Theta_2} \right)_{\eta, \Theta_1} \tilde{\Theta}_2 \quad (159)$$

Eqns. (157)-(159) present a system of three equations with three unknowns: Θ_1 , Θ_2 and $\tilde{i}/\tilde{\eta}$. The faradaic admittance is determined as:

$$\hat{Y}_f = \frac{1}{\hat{Z}_f} = \frac{\tilde{i}}{\tilde{\eta}} = A + \frac{B + j\omega C}{j\omega D - \omega^2 + E} \quad (160)$$

where:

$$A = \frac{1}{R_{ct}} = -F \left(\frac{\partial r_0}{\partial \eta} \right)_{\Theta_1, \Theta_2} \quad (161)$$

$$B = -\frac{F^3}{\sigma_1 \sigma_2} \left\{ \begin{array}{l} - \left(\frac{\partial r_0}{\partial \Theta_1} \right) \left(\frac{\partial \eta_1}{\partial \eta} \right) \left(\frac{\partial \eta_1}{\partial \Theta_2} \right) + \left(\frac{\partial r_0}{\partial \Theta_1} \right) \left(\frac{\partial \eta_1}{\partial \Theta_2} \right) \left(\frac{\partial r_2}{\partial \eta} \right) \\ - \left(\frac{\partial r_0}{\partial \Theta_2} \right) \left(\frac{\partial \eta_1}{\partial \Theta_1} \right) \left(\frac{\partial r_2}{\partial \eta} \right) + \left(\frac{\partial r_0}{\partial \Theta_2} \right) \left(\frac{\partial \eta_1}{\partial \eta} \right) \left(\frac{\partial r_2}{\partial \Theta_1} \right) \end{array} \right\} \quad (162)$$

$$C = -F^2 \left[\frac{1}{\sigma_1} \left(\frac{\partial r_0}{\partial \Theta_1} \right) \left(\frac{\partial \eta_1}{\partial \eta} \right) + \frac{1}{\sigma_2} \left(\frac{\partial r_0}{\partial \Theta_2} \right) \left(\frac{\partial r_2}{\partial \eta} \right) \right] \quad (163)$$

$$D = -F \left[\frac{1}{\sigma_1} \left(\frac{\partial \eta_1}{\partial \Theta_1} \right) + \frac{1}{\sigma_2} \left(\frac{\partial r_2}{\partial \Theta_2} \right) \right] \quad (164)$$

and

$$E = \frac{F^2}{\sigma_1 \sigma_2} \left[\left(\frac{\partial \eta_1}{\partial \Theta_1} \right) \left(\frac{\partial r_2}{\partial \Theta_2} \right) - \left(\frac{\partial \eta_1}{\partial \Theta_2} \right) \left(\frac{\partial r_2}{\partial \Theta_1} \right) \right] \quad (165)$$

where the negative sign before the parameters A , B and C originates from the current definition (positive current for reduction). If the reactions (147)-(149) are written as oxidations this sign should be omitted. Calculation of the derivatives show that parameters A , D and E are always positive and parameters B and C may be positive or negative.

The faradaic impedance may be obtained from eqn. (160) as:

$$\hat{Z}_f = \frac{1}{A} + \frac{B + j\omega C}{A^2[(D + B/A) + j\omega(E + C/A) - \omega^2]} \quad (166)$$

The polarization resistance is: $R_p = R_{ct} + B/[A^2(D + B/A)]$.

4. Impedance Plots in the Case of Two Adsorbed Species

The second term in eqn. (166) represents a second-order electrochemical impedance⁹⁵ and its denominator may be expressed in the following form:

$$1 + j\omega 2\zeta / \omega_n - (\omega / \omega_n)^2 \quad (167)$$

where ω_n is called the undamped natural frequency and ζ is the damping ratio of the system³² expressed as:

$$\omega_n = \sqrt{D + B/A} \quad \text{and} \quad \zeta = \frac{1}{2} \frac{E + C/A}{\sqrt{D + B/A}} \quad (168)$$

Depending on the value of the parameter ζ the poles of the second term of eqn. (167) are real or imaginary. Taking into account eqn. (167) there are 54 theoretically different cases of poles and zeros. They were considered systematically in ref. 95. The faradaic impedance may be represented by many different equivalent circuits, depending on the sign of parameters B and C and relative values of all the parameters⁹⁴. Its complex plane plots display different forms from two capacitive semicircles through various capacitive/inductive loops to two inductive loops. In order to obtain the total impedance, the double-layer capacitance and solution resistance should be added to the faradaic impedance. Some examples complex plane plots of faradaic impedances are presented in Figure 26.

Figure 26.

5. Faradaic Impedance for the Process Involving Three or More Adsorbed Species

Similarly to the case of two adsorbed species presented above, more complicated cases may be considered. Such a case is often found in corrosion.⁹⁶ Assuming existence of three adsorbed species a system of equations similar to eqns. (157)-(159) may be written:

$$-\frac{\tilde{i}}{F} + \left(\frac{\partial r_0}{\partial \eta}\right) \tilde{\eta} + \left(\frac{\partial r_0}{\partial \Theta_1}\right) \tilde{\Theta}_1 + \left(\frac{\partial r_0}{\partial \Theta_2}\right) \tilde{\Theta}_2 + \left(\frac{\partial r_0}{\partial \Theta_3}\right) \tilde{\Theta}_3 = 0 \quad (169)$$

$$\left(\frac{\partial r_1}{\partial \eta}\right) \tilde{\eta} + \left[\left(\frac{\partial r_1}{\partial \Theta_1}\right) - j\omega \frac{\sigma_1}{F}\right] \tilde{\Theta}_1 + \left(\frac{\partial r_1}{\partial \Theta_2}\right) \tilde{\Theta}_2 + \left(\frac{\partial r_1}{\partial \Theta_3}\right) \tilde{\Theta}_3 = 0 \quad (170)$$

$$\left(\frac{\partial r_2}{\partial \eta}\right) \tilde{\eta} + \left(\frac{\partial r_2}{\partial \Theta_1}\right) \tilde{\Theta}_1 + \left[\left(\frac{\partial r_2}{\partial \Theta_2}\right) - j\omega \frac{\sigma_2}{F}\right] \tilde{\Theta}_2 + \left(\frac{\partial r_2}{\partial \Theta_3}\right) \tilde{\Theta}_3 = 0 \quad (171)$$

and

$$\left(\frac{\partial r_3}{\partial \eta}\right) \tilde{\eta} + \left(\frac{\partial r_3}{\partial \Theta_1}\right) \tilde{\Theta}_1 + \left(\frac{\partial r_3}{\partial \Theta_2}\right) \tilde{\Theta}_2 + \left[\left(\frac{\partial r_3}{\partial \Theta_3}\right) - j\omega \frac{\sigma_3}{F}\right] \tilde{\Theta}_3 = 0 \quad (172)$$

where Θ_i are surface coverages of adsorbed species, σ_i their charges necessary for monolayer coverage, and r_i are the corresponding mass balances and relations between adsorbed species, as in eqns. (155)-(156), which may be different for different mechanisms. Eqns. (169)-(172) are solved using methods for the solution of the system of linear equations (e.g. Cramer's method). In the case of three adsorbed species, very complicated complex plane plots may be obtained. Some examples are presented in ref. 96.

A general model of a multistep mechanism involving adsorption and diffusion was recently given by Harrington.⁹⁷

V. IMPEDANCE OF SOLID ELECTRODES

1. Frequency Dispersion and Electrode Roughness

The general model of the ideally polarizable electrode presented in Section III.1, (see also eqn. (17) and Figure 2), and that in the presence of a faradaic reaction, Section III.2, Figure 4a, are found experimentally on liquid electrodes, (e.g. mercury, amalgams, indium-gallium, etc.). On solid electrodes⁹⁸ deviations from the ideal behavior are often observed. On ideally polarizable solid electrodes the electrical equivalent model cannot be usually represented (with except of monocrystalline electrodes in the absence of adsorption) as a series connection of the solution resistance and double-layer capacitance. However, on solid electrodes a frequency dispersion is observed, that is the observed impedances cannot be represented by connection of simple $R-C-L$ elements. The impedance of such systems may be approximated by an infinite series of parallel $R-C$ circuits i.e. a transmission line (see Section VI, Figure 41b, ladder circuit). The impedances may often be represented by an equation without simple electrical representation, through so-called distributed elements. The Warburg impedance is an example of a distributed element.

Problems similar to those observed on ideally polarizable solid electrodes arise also in the presence of faradaic reactions at these electrodes. Below, various models used for explanation of solid electrode impedance behavior are presented.

2. Constant Phase Element

Dispersion of the measured complex dielectric constant is known from dielectric relaxation experiments.¹⁸ The complex dielectric constant ε^* may be represented as:

$$\frac{\varepsilon^* - \varepsilon_\infty}{\varepsilon_s - \varepsilon_\infty} = \int_0^\infty \frac{G(\tau)}{1 + j\omega\tau} d\tau \quad (173)$$

where ε_∞ and ε_s are the dielectric constants determined at $\omega \rightarrow \infty$ and $\omega \rightarrow 0$, respectively, and $G(\tau)$ is the time constants distribution function. When there is only one relaxation time constant, that is $G(\tau) = \delta(\tau - \tau_0)$, eqn. (173) simplifies to:

$$\frac{\varepsilon^* - \varepsilon_\infty}{\varepsilon_s - \varepsilon_\infty} = \frac{1}{1 + j\omega\tau_0} \quad (174)$$

Cole and Cole⁹⁹ described the observed distribution of relaxation times as:

$$\frac{\varepsilon^* - \varepsilon_\infty}{\varepsilon_s - \varepsilon_\infty} = \frac{1}{1 + (j\omega\tau_0)^\phi} \quad (175)$$

where ϕ is a constant between 0 and 1. When $\phi = 1$ there is only one time constant in the system (no dispersion) and the eqn. (173) reduces to eqn. (174). Eqn. (175) represents a semicircle

rotated by $(1-\phi)90^\circ$ on the complex plane. This behavior can be explained by eqn. (173) with the distribution function $G(\tau)$ described as:

$$G(\tau) = \frac{1}{2\pi\tau} \frac{\sin[(1-\phi)\pi]}{\cosh[\phi \ln(\tau / \tau_0)] - \cos[(1-\phi)\pi]} \quad (176)$$

It represents a lognormal distribution that is it is a normal distribution of a function of $\ln(\tau/\tau_0)$. An example of such a distribution function is shown in Figure 27. For $\phi = 1$ the distribution function becomes the Dirac's delta function.

Figure 27.

The impedance of the ideally polarizable electrode may be represented as a series connection of the solution resistance and the double-layer capacitance, which produces a straight line, perpendicular to the real axis, on the complex plane plots. However, on solid electrodes a straight line with angle lower than $\pi/2$ is often observed, Figure 28a. In order to describe such behavior a model of distributed time constants, similarly to that used by Cole and Cole⁹⁹, was proposed.¹⁰⁰ It was supposed¹⁰¹ that such a distribution may arise from: (i) a microscopic roughness caused by scratches, pits, etc., always present on solid surfaces, which causes coupling of the solution resistance with the surface capacitance and (ii) a capacitance dispersion of interfacial origin, connected with slow adsorption of ions and chemical inhomogeneities of the surface. In such cases the double-layer capacitance may be expressed in terms of a so-called constant phase element, CPE. Its impedance is given by:

$$\hat{Z}_{CPE} = \frac{1}{T(j\omega)^\phi} \quad (177)$$

where T is a constant in $F \text{ cm}^{-2} \text{ s}^{\phi-1}$ and ϕ is related to the angle of rotation of a purely capacitive line on the complex plane plots: $\alpha = 90^\circ(1-\phi)$, Figure 28a. Eqn. (177) may also be written as:

$$\hat{Z}_{CPE} = \frac{1}{T\omega^\phi} [\cos(\phi\pi/2) - j \sin(\phi\pi/2)] \quad (178)$$

and it represents a "leaking" capacitor, which has non-zero real and imaginary components. Only when $\phi = 1$, $T \equiv C_{dl}$ and purely capacitive behavior is obtained. In general, eqn. (177) may represent pure capacitance for $\phi = 1$, infinite Warburg impedance for $\phi = 0.5$, pure resistance for $\phi = 0$ and pure inductance for $\phi = -1$. Brug et al.¹⁰⁰ presented a method for estimation of the average double-layer capacitance, \bar{C}_{dl} , from the value of T . Assuming that the electrode impedance may be expressed as a sum of the solution resistance and the impedance of the CPE element, and using the Cole-Cole formula for the distributed time constants, the total impedance may be expressed as:

$$\hat{Z} = R_s + \frac{1}{(j\omega)^\phi T} = R_s \left[1 + \frac{1}{(j\omega)^\phi (TR_s)} \right] = R_s \left[1 + \frac{1}{(j\omega\tau_0)^\phi} \right] \quad (179)$$

where $\tau_0 = R_s \bar{C}_{dl}$. It leads to:

$$T = \bar{C}_{dl}^{\phi} R_s^{-(1-\phi)} \quad (180)$$

which allows for the estimation of the average double-layer capacitance in the presence of the CPE element.

In the presence of the faradaic reaction, assuming that the faradaic impedance can be expressed as a simple equivalent resistance, the complex plane plots represent a rotated semicircle, Figure 28b, instead of a semicircle centered on the Z' axis.¹⁰²⁻¹⁰⁴ Similarly, the double-layer capacitance in the presence of the faradaic reaction may be obtained as:¹⁰⁰

$$T = \bar{C}_{dl}^{\phi} \left[R_s^{-1} + R_{ct}^{-1} \right]^{1-\phi} \quad (181)$$

An example of the application of eqn. (181) to the reduction of protons and tris-oxalato ferric ions was presented by Brug et al.¹⁰⁰. Lasia and Rami⁸⁷ studied the hydrogen evolution reaction on polycrystalline Ni in 1 M NaOH. They obtained rotated semicircles on the complex plane plots and the values of the parameter T and ϕ were potential dependent; however, the double-layer capacitances estimated from eqn. (181) were constant, equal to $\sim 38 \mu\text{F cm}^{-2}$, which is a reasonable value taking into account some surface roughness. Similar results were also obtained on rhodium.¹⁰⁵

Figure 28.

VanderNoot¹⁰⁶ tried to extract the distribution function $G(\tau)$ from the CPE model. He has found that the Fourier inversion method is not suitable but the maximum entropy deconvolution works relatively well. However, because this is an ill posed problem the results obtained are very sensitive to the experimental errors (noise).

Historically, the CPE phenomenon was usually attributed to surface roughness. Pajkossy et al.^{101,107} studied recently the origins of the CPE. They found that surface roughness of the order found on polycrystalline metals could lead to the CPE behavior only at much higher frequencies than those observed experimentally. They concluded that an increase in the surface roughness of polycrystalline Pt practically did not change (even slightly increased) the ϕ parameter. However, it was found that the capacitance dispersion increases markedly with the addition of chloride ions.¹⁰¹

Experiments carried out on monocrystalline Au(111) and Au(100) electrodes in the absence of specific adsorption did not show any frequency dispersion.¹⁰⁷ Dispersion was observed, however, in the presence of specific adsorption of halide ions. It was attributed slow adsorption and diffusion of these ions and phase transitions (reconstructions). In their analysis they expressed the electrode impedance as: $\hat{Z} = R_s + (j\omega \hat{C}_{int})^{-1}$ where \hat{C}_{int} is a complex electrode capacitance. In the case of a simple CPE circuit this parameter equals: $\hat{C}_{int} = T(j\omega)^{\phi-1}$. However, analysis of the ac impedance spectra in the presence of specific adsorption revealed that the complex plane capacitance plots (C''_{int} vs. C'_{int}) show formation of deformed semicircles. Consequently, they proposed an electrical equivalent model shown in Figure 29, in which instead of the CPE there is a double-layer capacitance in parallel with a series

connection of the adsorption resistance and capacitance, R_{ad} and C_{ad} , and the semiinfinite Warburg impedance connected with the diffusion of adsorbing species. Comparison of the measured and calculated capacitances (using the model in Figure 29) for Au(111) in 0.1 M $HClO_4$ in the presence of 0.15 mM NaBr is shown in Figure 30.

Figure 29.

Figure 30.

Similar analysis of complex impedances obtained from the frequency dispersion on a passive stainless steel was carried out by Devaux et al.¹⁰⁸

Stoynov¹⁰⁹ has extended the CPE model for finite thickness diffusion. He introduced a so-called bounded CPE (BCP) impedance or finite constant phase element:

$$\hat{Z}_{BCP} = \frac{1}{T(j\omega)^\phi} \tanh\left[R_s T(j\omega)^\phi\right] \quad (182)$$

where R_s is the solution resistance. In fact, at high frequencies, eqn. (182) reduces to a simple CPE, eqn. (177) and at low frequencies it reduces to R_s . For $\phi = 0.5$ BCP has a similar form to that of the impedance in the case of the finite length diffusion. Just as the CPE represents infinite diffusion for $\phi = 0.5$, the BCP represents finite length diffusion for the same value of ϕ . Complex plane plots for the BCP element are presented in Figure 31. This element has a physical meaning for $\phi < 0.6$.¹⁹

Figure 31.

3. Fractal Model

Solid surfaces are usually irregular and their detailed geometry is not known. In order to describe their geometry the concept of fractals was introduced.¹¹⁰ This concept is based on self-similarity of surfaces implying different scaling. The difference between simple and fractal magnification is shown in Figure 32.¹¹¹ Simple magnification only increases the size of the object while the fractal magnification reveals its self-similarity at different scales. Such magnification process may continue. The line enclosing the object in Figure 32c is the so-called von Koch line,^{112,113} it is continuous, of infinite length and is nowhere differentiable. It is interesting to note that the observed (measured) length of the von Koch line is scaled in a complex way: its length depends on the yardstick used to measure it. In the example in Figure 32 the object is magnified three times and the line length is magnified 4 times. This leads to the fractal dimension of the von Koch line $D_H = (\ln 4)/(\ln 3) = 1.262$.^{111,114} In general, the fractal dimension of the line may be between 1 and 2. Such reasoning may also be used for surfaces for which the fractal dimensions may be between 2 and 3. Fractal geometry was introduced to electrochemistry by Le Méhauté et al.¹¹⁵ It was shown by Nyikos, Pajkossy and coworkers^{113,114, 116-122} that fractal geometry of ideally polarizable (i.e. blocking) interfaces generates a CPE behavior described by eqn. (177) in Section V.2. However, it should be stressed that, in general, there is no simple relation between the fractal dimension D_H and the parameter ϕ ¹²³ of the CPE

although higher fractal dimensions lead to smaller values of ϕ .¹¹⁴ The fractal theory was subsequently extended to irregular or quasi-random surfaces lacking well defined self-similarity.^{119,120} Pajkossy and Nyikos¹²⁴ carried out simulations of blocking electrodes with a self-similar spatial capacitance distribution and found that the calculated impedances exhibited the CPE behavior. The fractal theory was also tested experimentally using fractal electrodes prepared by microelectronic techniques.¹¹⁸

Subsequently, the fractal theory was extended to faradaic processes.^{111,114,117,118,125,126} De Levie^{111,125} has shown that the impedance of a fractal electrode, in the absence of mass transfer control, is given as:

$$\hat{Z} = R_s + \frac{1}{b} \left(\frac{1}{\frac{1}{R_{ct}} + j\omega C_{dl}} \right)^\phi \quad (183)$$

where the parameters b is given by:

$$b = f_g \rho^{\phi-1} \quad (184)$$

ρ is the solution resistivity and f_g is a factor depending on the fractal surface geometry¹¹⁰, which may be based on von Koch curves¹²⁷, Cantor bars^{128,129,130}, Sierpinski carpets^{131,132,133}, etc.⁹⁸ When the surface is flat and homogeneous, $\phi = 1$, $f_g = 1$, $b = 1$ and eqn. (184) reduces to eqn. (112). According to de Levie¹¹¹ eqn. (183) may be applied to fractal electrodes in equilibrium, i.e. in the absence of the dc current which may introduce a local interfacial potential difference. When the exact fractal structure is unknown the parameter b cannot be obtained and the only parameters accessible are:

$$C_{exp} = b^{1/\phi} C_{dl} \quad \text{and} \quad R_{ct,exp} = b^{1/\phi} R_{ct} \quad (185)$$

Figure 32.

Examples of the complex plane plots obtained for fractal electrodes are presented in Figure 33.

Figure 33.

With decrease of parameter ϕ the semicircles become deformed (skewed). The complex plane impedance plots obtained from eqn. (183), are formally similar to those found by Davidson and Cole¹³⁴ in their dielectric studies. Kinetic analysis of the hydrogen evolution reaction on surfaces displaying fractal ac impedance behavior was carried out by Lasia and coworkers¹³⁵⁻¹³⁷ who obtained rate constants expressed as: $k_{i,exp} = b^{1/\phi} k_i$. In order to compare the intrinsic activities of such electrodes with that of polycrystalline nickel the ratio of $k_{i,exp} / C_{dl,exp} = k_i / C_{dl}$ was used. It was found that this ratio has similar values for Raney Ni and polycrystalline Ni, therefore the intrinsic activity of these electrodes is similar and the observed increase in activity of Raney Ni electrodes arises from their very large real surface area.

In general, self-similar fractal surfaces do not exist in the real world. The fractal models may only approximate random surfaces. Besides, eqn. (183) for $\phi = 0.5$ is formally identical with the semi-infinite porous model presented below. The fractal model in the presence of diffusion was discussed in refs. 111 and 118. Experimental verifications of the fractal model were also carried out for some electrodes.^{118,121,138} It was also stated that the fractal dimension of the surface may be found from dc experiments.^{114,118,139,140}

4. Porous Electrode Model

In electrocatalysis there is a great interest in increasing the real surface area of electrodes. In such cases porous electrodes are used. Because modeling of real electrodes is difficult, a simpler model is usually used in which it is assumed that pores have cylindrical shape with a length l and a radius r .^{24,141-145}

In order to describe the impedance of such electrodes first a dc solution must be found. Two cases are considered below: (i) porous electrodes in the absence of internal diffusion and (ii) in the presence of axial diffusion. It is assumed that the electrical potential and concentration of electroactive species depend on the distance from the pore orifice only and there is always an excess of the supporting electrolyte (*i.e.* migration can be neglected).

(i) Porous Electrodes in the Absence of Internal Diffusion

In this case it is assumed that the concentration of the electroactive species is independent of the distance along a pore. In the next Section we shall see when such an assumption is valid. The axially flowing dc current, I , which enters the pore, flows towards the walls and its value decreases with the distance x from the pore orifice, Figure 34.

Figure 34.

This decrease of the current is proportional to the current flowing to the wall:

$$\frac{dI}{dx} = -\frac{(2\pi r dx)j}{dx} = -2\pi r j \quad (186)$$

where $2\pi r dx$ is the surface area of a pore section dx and j is the current density. Because of Ohm's law a potential drop along the pore also arises:

$$\frac{dE}{dx} = -I \left(\frac{\rho dx}{\pi r^2} \right) \frac{1}{dx} = -I \left(\frac{\rho}{\pi r^2} \right) \quad (187)$$

where ρ is the specific solution resistance and $(\rho dx/\pi r^2)$ is the resistance of the section dx of the solution in the pore. The last term in the parentheses in eqn. (187) may be called the solution resistance per unit length of the pore, $R = \rho/\pi r^2$ and is expressed in $\Omega \text{ cm}^{-1}$. Similarly, the current flowing through an element dx of the surface area, $(2\pi r dx)j$, may be represented as E/Z , where Z is the impedance of pore walls per unit of the pore length, in $\Omega \text{ cm}$. It can be shown that $Z = Z_{el}/2\pi r$ where Z_{el} is the specific impedance of pore walls in $\Omega \text{ cm}^2$. Z_{el} consists of the faradaic, Z_f , and the double-layer impedance: $Z_{el} = (1/Z_f + j\omega C_{dl})^{-1}$.

(a) *De Levie's treatment*

De Levie¹⁴⁶ was the first to describe the impedance of porous electrodes. He represented eqns. (186) and (187) in the following form:

$$\frac{dI}{dx} = -\frac{E}{\hat{Z}} \quad (188)$$

$$\frac{dE}{dx} = -RI \quad (189)$$

Taking the second derivative of eqn. (189) and substituting eqn. (188) one obtains:

$$\frac{d^2E}{dx^2} = -R \frac{dI}{dx} = \left(\frac{R}{\hat{Z}} \right) E \quad (190)$$

This equation describes changes of the electrical potential as a function of pore length. De Levie assumed that the impedance of pore walls is independent of the pore distance (\hat{Z} is not a function of distance) which implies that there is no net dc current. The solution is:

$$E = C_1 e^{-\sqrt{R/\hat{Z}}x} + C_2 e^{\sqrt{R/\hat{Z}}x} \quad (191)$$

where C_1 and C_2 are the integration constants. Taking into account the boundary conditions:

$$x = 0 \quad E = E_0$$

and

$$x = l \quad dE/dx = 0$$

where E_0 is the potential at $x = 0$, the dc solution is:

$$E = E_0 \frac{\cosh \left[\sqrt{\frac{R}{\hat{Z}}} (l-x) \right]}{\cosh \left(\sqrt{\frac{R}{\hat{Z}}} l \right)} \quad (192)$$

and

$$\left(\frac{dE}{dx} \right)_{x=0} = -E_0 \sqrt{\frac{R}{\hat{Z}}} \tanh \left(\sqrt{\frac{R}{\hat{Z}}} l \right) = -I_0 R \quad (193)$$

The total pore impedance, \hat{Z}_{por} , is then obtained as:

$$\hat{Z}_{por} = \frac{E_0}{I_0} = \sqrt{R\hat{Z}} \coth \left(\sqrt{\frac{R}{\hat{Z}}} l \right) \quad (194)$$

This equation may be rearranged into:

$$\hat{Z}_{por} = \frac{R_{\Omega,p}}{\Lambda^{1/2}} \coth(\Lambda^{1/2}) \quad (195)$$

where $R_{\Omega,p} = \rho l / \pi r^2$ and $\Lambda = (2\rho l^2 / r) / \hat{Z}_{el}$. It is evident that the faradaic impedance of pore walls was assumed potential independent despite the fact that the potential changes with the pore depth. The faradaic impedance may be obtained assuming that the Butler-Volmer equation describes adequately the electrochemical process. Although original development was carried out using electrode potential E , a more adequate representation of impedance would be with respect to the overpotential η :

$$\frac{1}{\hat{Z}_f} = \frac{1}{R_{ct}} = \frac{dj}{d\eta} = j_0 n f \left[\alpha e^{-\alpha n f \eta} + (1 - \alpha) e^{(1 - \alpha) n f \eta} \right] \quad (196)$$

Of course, under dc conditions, when $\omega = 0$, $\hat{Z}_{el} = R_{ct}$. For the ensemble of n pores and in the presence of the solution resistance outside the pores, the total impedance becomes:

$$\hat{Z}_t = R_s + \frac{\hat{Z}_{por}}{n} \quad (197)$$

Eqn. (195) predicts observation of a straight line at 45° at high frequencies, followed by a semicircle, Figure 35a.

Figure 35.

At low frequencies the impedance becomes real:

$$Z(\omega = 0) = R_p = \sqrt{\frac{\rho R_{ct}}{2\pi^2 r^3}} \coth\left(\sqrt{\frac{2\rho}{r R_{ct}}} l\right) \quad (198)$$

Behavior of the porous electrode depends on the *penetration depth*, λ , of the alternating signal into the pore. This parameter is defined as: $\Lambda = l/\lambda$, or $\lambda = (r \hat{Z}_{el} / 2\rho)^{1/2}$. Eqn. (195) has two limiting cases. First, when $\lambda \gg l$, $\Lambda \rightarrow 0$, $\coth(\Lambda^{1/2}) \rightarrow \Lambda^{-1/2}$, and the equation becomes:

$$\hat{Z}_{por} = \frac{R_{\Omega,p}}{\Lambda} = \frac{1}{2\pi r l} \hat{Z}_{el} \quad (199)$$

where $s = 2\pi r l$ is the total pore surface area. Eqn. (199) represents simply the impedance of a flat electrode having surface area s . In this case the ac signal penetrates to the bottom of the pore and the electrode behaves as a flat one; then its impedance may be described by a semicircle on the complex plane plot, Figure 35b.

Another limiting case is obtained when the penetration depth is much smaller than the pore length, $\lambda \ll l$, that is the pores behave as semiinfinite channels; then $\Lambda \rightarrow \frac{1}{4}$, $\coth(\Lambda^{1/2}) \rightarrow 1$, and:

$$\hat{Z} = \frac{R_{\Omega,p}}{\Lambda^{1/2}} = \left(\frac{\rho}{2\pi^2 r^3}\right)^{1/2} \hat{Z}_{el} \quad (200)$$

In this case the complex plane plot presents a deformed semicircle, Figure 35c. In such a case, plotting $Z_i = |Z|^2 \sin(2\phi)$ vs. $Z_r = |Z|^2 \cos(2\phi)$ gives a perfect semicircle.¹⁴⁶ Eqn. (200) is formally identical with eqn. (183) for the fractal model with $\phi = 0.5$ and these two models are indistinguishable.

In further papers the impedance of double-layer was substituted by the CPE:

$$\hat{Z}_{el} = \left[1 / \hat{Z}_f + (j\omega)^\phi T \right]^{-1} \quad (201)$$

An example of porous behavior was presented by Los *et. al.*¹⁴⁷ for the hydrogen evolution reaction on LaPO₄-bonded Ni powder electrodes in 30% NaOH. Examples of the complex plane plots are shown in Figure 36. Using the CNLS fit, the parameters R_{ct} , T , and C_{dl} were determined.

Figure 36.

(b) *Rigorous treatment*

It is obvious that the de Levie's treatment is an approximation, because \hat{Z}_f , and in consequence \hat{Z}_{el} , are potential dependent. In the rigorous treatment, eqns. (186) and (187), should be solved. The second derivative of eqn. (187), written using the Butler-Volmer expression for current and overpotentials is:^{148,149}

$$\frac{d^2\eta}{dx^2} = \frac{2\rho}{r} j = \frac{2\rho j_0}{r} \left[e^{\alpha n f \eta} - e^{-(1-\alpha) n f \eta} \right] = \frac{2\rho j_0}{r} \left[e^{b_1 \eta} - e^{-b_2 \eta} \right] \quad (202)$$

Assuming that $\alpha = 0.5$ and $b = 0.5nf$, eqn. (202) may be written in a simpler form as:

$$\frac{d^2\eta}{dx^2} = \frac{4\rho j_0}{r} \sinh(b\eta) \quad (203)$$

The first integration of eqn. (202) gives, taking into account that at $x = l$, $d\eta/dx = 0$ and $\eta_l = \eta(l)$:

$$\frac{d\eta}{dx} = - \left\{ (4\rho j_0 / r) \left[\exp(b_1 \eta) / b_1 + \exp(-b_2 \eta) / b_2 - \exp(b_1 \eta_l) / b_1 - \exp(-b_2 \eta_l) \right] \right\}^{1/2} \quad (204)$$

Eqn. (204) may be solved analytically only for the case of semiinfinite length of pores and for $\alpha = 1/2$, $1/3$ and $2/3$.¹⁴⁴ In a general case, it may be solved numerically. Let us consider now the case of semiinfinite pores, *i.e.* when the potential at the bottom of the pore drops to zero, $\eta_l = 0$. In this case eqn. (204) may be rearranged to:

$$\frac{d\eta}{dx} = -4 \sqrt{\frac{\rho j_0}{r}} \sinh\left(\frac{b\eta}{2}\right) \quad (205)$$

which has a solution:

$$\tanh\left(\frac{b\eta}{4}\right) = \tanh\left(\frac{b\eta_0}{4}\right) \exp\left(-2\sqrt{\frac{\rho j_0 b}{r}}x\right) \quad (206)$$

It may be noticed that the eqn. (206) is formally identical with that developed for the Gouy-Chapman theory of the double-layer. Substitution of eqn. (189) into (205) gives the expression for the steady-state current on porous electrodes:

$$I = 4\pi r \sqrt{\frac{rj_0}{\rho b}} \sinh(b\eta_0 / 2) \quad (207)$$

which gives, at negative potentials, the Tafel slope of $2 \ln(10)/\alpha f = 0.118/\alpha$ V at 25°C. This result indicates that the Tafel slope on porous electrodes is doubled over its normal value.

Knowing the potential distribution in pores, the pore impedance may be obtained by numerical summation of the impedances of small sections Δx of the pore walls, starting from the bottom of the pore:

$$\hat{Z}_i = \left(\frac{\rho}{\pi r^2}\right) \Delta x + 1 / \left[(2\pi r \Delta x) / \hat{Z}_{el,i} + 1 / \hat{Z}_{i-1} \right] \quad (208)$$

where $\hat{Z}_{el,i}$ is the specific electrode impedance at the distance x . The solution obtained may be compared with de Levie's solution, eqn. (195). Complex plane plots obtained for the same conditions using two different approaches are displayed in Figure 37.

Figure 37.

The analysis of the results indicates that the resistance at $\omega = 0$, R_p , obtained using the correct analysis is twice that found from de Levie's equation. Besides, the plot of squared impedances produces a deformed ellipsoid, instead of a perfect semicircle. It has been shown¹⁴⁷ that the CNLS fit of the simulated impedances to the de Levie equation (195) is not good, there being systematic differences between these two curves, Figure 37. However, when the CPE is used instead of the double-layer capacitance, the approximation is good. The values obtained for of the parameter ϕ are between 0.91 and 0.93.¹⁴⁹ In this case the use of the CPE only hides the inadequacy of the model.

(ii) *Porous Electrodes in the Presence of Axial Diffusion*

During electrolysis, concentration changes in the pores. This problem has been addressed in numerous papers.^{148,150-155} Simplifications such as assuming totally irreversible reaction kinetics, semiinfinite pores or assuming that the concentration gradient in pores is exponential were usually made. Recently, Lasia¹⁵⁶ solved the problem for a quasi-reversible process and a finite pore length. It was assumed that the electrode process could be described by the current-overpotential equation:

$$j = j_0 \left(\frac{C_O}{C_O^*} e^{b\eta} - \frac{C_R}{C_R^*} e^{-b\eta} \right) \quad (209)$$

where C_i and C_i^* represent surface and bulk concentrations of Ox and Red, respectively. Assuming that the diffusion coefficients of the two forms are identical, eqn. (209) can be rearranged into:

$$j = j_0 \left[a \left(e^{b\eta} + m e^{-b\eta} \right) - (m+1) e^{-b\eta} \right] \quad (210)$$

where $a = C_O/C_O^*$ and $m = C_O^*/C_R^*$. The current flowing through the section dx of the pore walls is related to the changes of concentration:

$$j = -\frac{nF}{2\pi r dx} \frac{dN}{dt} = -\frac{nFr}{2} \frac{dC}{dt} \quad (211)$$

or taking into account diffusion:

$$\frac{\partial a}{\partial t} = D \frac{\partial^2 a}{\partial x^2} - \frac{2}{nFrC_O^*} j \quad (212)$$

which, under steady-state conditions, reduces into:

$$\frac{d^2 a}{dx^2} - \frac{2}{nFrC_O^*} j = 0 \quad (213)$$

The potential drop in the pore is still described by eqn. (202), with the current given by eqn. (210). Eqns. (202) and (213) may be combined together as:

$$\frac{d^2 \eta}{dx^2} = v \frac{d^2 a}{dx^2} \quad \text{where} \quad v = nFDC_O^* \rho \quad (214)$$

Eqn. (214) has the analytical solution:

$$\eta - \eta_0 = v(a - 1) \quad (215)$$

which allows elimination of one variable from eqns. (202) and (213). In a general case the first integration may be carried out analytically and the next numerically. The derived dependence of η and a as functions of distance may be used to calculate the impedance.

The value of the parameter v determines whether the porous behavior is determined by the potential or concentration drop. When $v \ll 1$ V the system behavior is determined principally by the concentration gradient and when $v \gg 1$ V it is determined by the potential drop. For typical conditions: $D = 10^{-5} \text{ cm}^2 \text{ s}^{-1}$, $\rho = 10 \text{ } \Omega \text{ cm}$ and $C^* = 10^{-3}$ to 10^{-2} M , $v \sim 10^{-5}$ to 10^{-4} V . For these conditions the porous behavior is determined by the concentration gradient and the potential gradient down pores is negligible. Only for the extreme conditions where the solvent or the supporting electrolyte (at high concentration) undergo the red-ox reaction, may the process be limited by the potential drop in the pores.

In a limiting case when the potential drop in the pore may be neglected, an analytical solution of eqn. (213) may be obtained:

$$a = \gamma + (1 - \gamma) \frac{\cosh[\sqrt{B}(l - x)]}{\cosh(\sqrt{B}l)} \quad (216)$$

where:

$$\gamma = \frac{e^{2b\eta_0} + m}{m+1} \quad \text{and} \quad B = \frac{2j_0}{nFrDC_O^*} \left(e^{b\eta_0} + m e^{-b\eta_0} \right) \quad (217)$$

Knowing the dc solution, the electrode impedance may be calculated. As usual, the current, eqn. (212), must be linearized:

$$\Delta j = \left(\frac{\partial j}{\partial \eta} \right)_a \Delta \eta + \left(\frac{\partial j}{\partial a} \right)_\eta \Delta a \quad (218)$$

Then, the expression for the impedance is obtained as:

$$\frac{1}{Z_f} = \frac{\tilde{j}}{\tilde{\eta}} = \left(\frac{\partial j}{\partial \eta} \right) + \left(\frac{\partial j}{\partial a} \right) \frac{\tilde{a}}{\tilde{\eta}} \quad (219)$$

In order to find a solution for the oscillating concentration, eqn. (212) must be solved for Δa . Substitution and rearrangement gives:

$$\frac{d^2(\tilde{a}/\tilde{\eta})}{dx^2} - \left(\frac{\tilde{a}}{\tilde{\eta}} \right) \left[\frac{j\omega}{D} + \frac{2}{nFrDC_O^*} \left(\frac{dj}{da} \right) \right] - \frac{2}{nFrDC_O^*} \left(\frac{dj}{d\eta} \right) = 0 \quad (220)$$

or

$$\frac{d^2 \tilde{y}}{dx^2} - \tilde{y} K - L = 0 \quad (221)$$

where:

$$\tilde{y} = \tilde{a}/\tilde{\eta} \quad K = \frac{j\omega}{D} + \frac{2}{nFrDC_O^*} \left(\frac{dj}{da} \right) \quad L = \frac{2}{nFrDC_O^*} \left(\frac{dj}{d\eta} \right) \quad (222)$$

with the boundary conditions:

$$x = 0 \quad \tilde{y} = 0$$

and

$$x = l \quad d\tilde{y}/dx = 0$$

The analytical solution of eqn. (221) is:

$$\frac{\tilde{a}}{\tilde{\eta}} = \frac{L}{K} \left\{ -1 + \frac{\cosh[\sqrt{K}(l-x)]}{\cosh(\sqrt{K}l)} \right\} \quad (223)$$

Now, substitution into eqn. (219) gives the faradaic impedance and using eqn. (208) the total impedance may be calculated numerically. The presence of the concentration gradient in the pores produces two potential-dependent semicircles, Figure 38 and Figure 39. It should be added that at high frequencies still a part of a straight line at the angle of $\pi/4$ may be observed as in Figure 39.

In real cases the problem is much more complicated, because various pores are present and, in fact, a pore size distribution and the exact surface morphology is unknown.

Figure 38.

Figure 39.

(iii) Other Pore Geometries

For pores of geometry different from cylindrical, at high frequencies where the impedance is determined by the double-layer charging, instead of a straight line some forms of arc may also be obtained.

The impedance of a V-grooved electrode was studied by de Levie.¹⁵⁷ Such surfaces may be prepared, for example, by abrasion. De Levie described the impedance of a groove per unit groove length as:

$$\hat{Z} = \frac{\rho}{\tan\beta} \frac{I_0(\lambda)}{\lambda I_1(\lambda)} \quad (224)$$

where ρ is the specific solution resistance, β is the angle between groove wall and the normal to the surface, I_0 and I_1 are the modified Bessel functions of zero and first order and:

$$\lambda = 2 \sqrt{\frac{\rho l}{Z_s \beta}} \quad (225)$$

l is the groove depth (normal to the surface) and Z_s is the double-layer impedance per unit of true surface area. Eqn. (225) reduces to the impedance of a perfectly flat surface for $\beta = 90^\circ$ and to the impedance of cylindrical porous electrode for $\beta = 0^\circ$. Recently, Gunning¹⁵⁸ obtained an exact solution of the de Levie grooved surface in the form of an infinite series. Comparison with the de Levie equation shows that the deviations arise at higher frequencies.

Keiser et al.¹⁵⁹ studied the impedance of arbitrary shaped pores. They simulated the complex plane plots in the absence of a faradaic process, Figure 40. Instead of a straight line at 45° , observed for cylindrical pores at high frequencies, different forms of plateaux or a semicircle were observed.

Figure 40.

Eloot et al.¹⁶⁰ suggested a new general matrix method for calculations involving noncylindrical pores, in which the pore is divided into sections and for each section a transmission line model with constant impedances was used. Direct simulations of the impedances for porous electrodes were also carried out using a random walk method.^{161,162}

5. Generalized Warburg Element

Macdonald¹⁸ introduced a generalized finite-length Warburg element described as:

$$\hat{Z} = \frac{R_s}{A_0 R_s (j\omega)^\phi} \tanh \left[A_0 R_s (j\omega)^\phi \right] \quad (226)$$

to describe non-uniform diffusion under finite-length transmissive conditions, where R_s is the solution resistance. For $\phi = 0.5$, $A_0 = l / (R_s \sqrt{D})$, and it represents a finite-length diffusion. Non-uniform diffusion arises for example when the diffusion coefficient is a function of the distance. This equation is formally identical with Stoynov's finite constant phase element BCP, eqn. (182). However, Stoynov¹⁰⁹ stated that eqn. (226) represents uniform finite-length diffusion and not the non-uniform diffusion case.

A similar equation but containing the function *coth* was used by Inzelt and Láng¹⁶³ to describe the diffusional impedance of conducting polymers under reflective conditions (see

Section III.6(ii) and eqn. (99)). An electrical model containing this element accounted well for the impedance spectra with a minimal number of free parameters.

Although models including impedance represented by eqn. (226) may well describe some experimental data, the physical significance of the parameter A_0 for $\phi < 0.5$ is not clear .

VI. CONDITIONS FOR "GOOD" IMPEDANCES

1. Linearity, Causality, Stability, Finiteness

The impedance technique is often applied to various electrochemical systems which were never studied before. The complex plane and Bode plots obtained often display shapes that had never been encountered previously. Before starting the analysis and modeling of the experimental results one should be certain that the impedances are valid. There is a general mathematical procedure which allows for the verification of the impedance data. It was introduced by Kramers¹⁶⁴ and Kronig,¹⁶⁵ further developed by Bode¹⁶⁶ and later applied to EIS.^{18, 167-177} During the impedance measurements a small ac perturbation is applied to the system. The impedance derived is valid provided that the following four criteria are met:^{33,169}

- *Linearity*: A system is linear when its response to a sum of individual input signals is equal to the sum of the individual responses. This also implies that the system is described by a system of linear differential equations (see e.g. eqns. (2) and (7)). Electrochemical systems are usually highly nonlinear and the impedance is obtained by linearization of equations (see e.g. eqns. (42) and (130)) for small amplitudes. For the linear systems the response is independent of the amplitude. It is easy to verify the linearity of the system: if the obtained impedance is the same when the amplitude of the applied ac signal is halved then the system is linear. Besides, linear systems cannot exhibit hysteresis in their response at $\omega = 0$.
- *Causality*: The response of the system must be entirely determined by the applied perturbation, that is the output depends only on the present and past input values. The causal system cannot predict what its future input will be. Causal systems are also called physically realizable systems. If the system is at rest and a perturbation is applied at $t = 0$, the response must be zero for $t < 0$. In the complex plane the above criterion requires that, for $t < 0$, $\omega = 0$. Moreover, the integral on and inside a closed path C of an analytic function (i.e. it has a derivative at each point)¹⁷⁸ must be equal to zero:

$$\oint_C Z(s) ds = 0 \quad (227)$$

If the function $Z(s)$ has singularities then the sum of the residuals of the poles a_i must equal zero:

$$\frac{1}{2\pi j} \oint_C \frac{Z(s)}{s - a_i} ds = f(a_i) \quad \text{and} \quad \sum_i f(a_i) = 0 \quad (228)$$

Eqns. (227) and (228) are mathematical forms of causality. The system is casual if it does not have any singularities, eqn. (227), or the sum of residues is zero, eqn. (228). Physical meaning of these equations is that the system does not generate noise independent of the applied signal.

- *Stability*: The stability of a system is determined by its response to inputs. A stable system remains stable unless excited by an external source and it should return to its original state once the perturbation is removed and the system cannot supply power to the output irrespective of the input. The system is stable if its response to the impulse excitation approaches zero at long times or when every bounded input produces a bounded output. Mathematically this means that the function does not have any singularities that cannot be avoided. The impedance $Z(s)$ must satisfy the following conditions: $Z(s)$ is real when s is real

(that is when $\omega \rightarrow 0$) and $\text{Re}[Z(s)] \geq 0$ when $\nu \geq 0$ ($s = \nu + j\omega$, see Section I.1(i)). This last condition ensures that there are no negative resistances in the system. The impedance measurements must also be stationary, that is the measured impedance must not be time dependent. This condition may be easily checked by repetitive recording of the impedance spectra; then the obtained Bode plots should be identical.

- *Finiteness*: The real and imaginary components of the impedance must be finite-valued over the entire frequency range $0 < \omega < \infty$. In particular, the impedance must tend to a constant real value for $\omega \rightarrow 0$ and $\omega \rightarrow \infty$.

2. Kramers-Kronig Transforms

The Kramers-Kronig relations hold provided the four above constraints are satisfied and allow the calculation of the imaginary impedance from the real part:

$$Z''(\omega) = -\left(\frac{2\omega}{\pi}\right) \int_0^{\infty} \frac{Z'(x) - Z'(\omega)}{x^2 - \omega^2} dx \quad (229)$$

the real impedance from the imaginary part, if the high frequency asymptote for the real part is known:

$$Z'(\omega) = Z'(\infty) + \frac{2}{\pi} \int_0^{\infty} \frac{xZ''(x) - \omega Z''(\omega)}{x^2 - \omega^2} dx \quad (230)$$

the real impedance from the imaginary part, if the zero-frequency asymptote of the real part is known:

$$Z'(\omega) = Z'(0) + \left(\frac{2\omega}{\pi}\right) \int_0^{\infty} \frac{\left(\frac{\omega}{x}\right) Z''(x) - Z''(\omega)}{x^2 - \omega^2} dx \quad (231)$$

the polarization resistance R_p from the imaginary part:

$$R_p = Z'(\infty) - Z'(0) = \left(\frac{2}{\pi}\right) \int_0^{\infty} \frac{Z''(x)}{x} dx \quad (232)$$

or the phase-angle from the magnitude (modulus):

$$\varphi(\omega) = \left(\frac{2\omega}{\pi}\right) \int_0^{\infty} \frac{\ln|Z(x)|}{x^2 - \omega^2} dx \quad (233)$$

Similar transformations may also be carried out for admittances. Such procedures are important when the impedance goes to infinity at low frequencies (blocking electrodes, CPE, semi-infinite mass transfer, etc.). The major difficulty in applying the Kramers-Kronig relations is that the integration must be performed over the whole frequency range from zero to infinity. However, the impedance results are known only over a finite frequency range. The discrepancies that arise may be attributed to the errors of integration or to failure to satisfy the four above conditions.

Kendig and Mansfeld¹⁷⁹ used eqn. (232) and supposed that the imaginary impedance is symmetric. They carried out integration between the frequency corresponding to the maximum of the imaginary impedance and infinity, and multiplied the result by two. However, their method is limited to systems containing one time constant.

Macdonald *et. al.*¹⁶⁷⁻¹⁶⁹ and Dougherty and Smedley¹⁷⁷ used a polynomial approximation of the impedance function, followed by analytical integration of the polynomials. However,

extrapolation of polynomials over a large frequency range may be unreliable. Haili¹⁸⁰ extrapolated Z' as proportional to ω as $\omega \rightarrow 0$ and as inversely proportional to ω as $\omega \rightarrow \infty$ and $Z' \rightarrow R_s$.

Esteban and Orazem^{170,171} proposed using eqns. (230) and (231) simultaneously to calculate the impedance below the lowest measured frequency, ω_{\min} , and continue the integration procedure to three or four decades of smaller frequency, ω_0 . The latter parameter is chosen in such a way that the real impedance goes to a constant value while the imaginary impedance goes to zero at ω_0 .

Later, Orazem and coworkers^{175,181,182} used an approximation to the experimental impedance by the Voigt model (Figure 41) followed by a transformation of the model data. To take into account the inductive loops they proposed using negative resistances. This method was applied to approximate the impedance from various circuits containing resistive, capacitive and inductive elements, Warburg impedance, CPE, etc. Because each parallel R - C circuit is transformable, the entire circuit must also be transformable. In this method the explicit Kramers-Kronig integration is replaced by the fit to the Voigt model. If the data cannot be well approximated, it means that they are not transformable. Such an approximation may be written as:

Figure 41.

$$Z'(\omega) = R_s + \sum_{k=1}^M \frac{R_k}{1 + (\omega R_k C_k)^2} = R_s + \sum_{k=1}^M \frac{R_k}{1 + (\omega \tau_k)^2} \quad (234)$$

and

$$Z''(\omega) = - \sum_{k=1}^M \frac{\omega R_k \tau_k}{1 + (\omega \tau_k)^2} \quad (235)$$

where $\tau_k = R_k C_k$ and M is the number of R - C elements used in the Voigt circuit to approximate the experimental impedance. The problem with this approach is the initial selection of R_k and C_k parameters in the complex nonlinear least-squares approximation, which are unknown. Similarly, Boukamp and Macdonald¹⁸³ proposed an approximation of the experimental impedances using a distribution of relaxation times. They represented the function $G(\tau)$ in eqn. (173), written for

immittances, as a sum of M discrete delta functions: $G(\tau) = \sum_{m=1}^M g_m \delta(\tau - \tau_m)$, where g_m are

dimensionless weighting coefficients and τ_m characteristic time constants to be determined.

This method was further modified by Boukamp¹⁸⁴ who also used the Voigt circuit but with a fixed distribution of time constants τ_k , that is the time constants were defined and the adjustable parameters were R_k . Parameters τ_k were chosen as equal to the inverse of the experimental angular frequencies ω_k , which are usually logarithmically distributed (5 to 10 per decade). Under such conditions eqns. (234) and (235) become linear in the R_k values and the problem of approximation reduces from iterative nonlinear to a linear single matrix inversion. The method is quite robust with respect to the choice of the distribution and range of τ_k values. In practice 6 to 7 time constants per frequency decade ($\tau_k = 1/\omega_k$) should be selected to get a good approximation. Through inspection of the relative residual plots it is possible to isolate data

that do not comply with the Kramers-Kronig transformations. The sign of R_k parameters is not important but the time constants are always positive (by definition), the negative τ_k could mask some non Kramers-Kronig transformable behavior.

Macdonald¹⁸⁵ proposed another form of the Kramers-Kronig integrals in which integration to infinity and the poles are avoided.

In the case of blocking electrodes the impedance goes to infinity as $\omega \rightarrow 0$. For such electrodes the admittance Kramers-Kronig transformation could be used. Alternatively, a suitable parallel resistance could be added to the system (in such a system the impedance must always be real and equal to this shunt resistance at $\omega = 0$) and then carry out the transformation of the data obtained.¹⁸⁶

In general, Kramers-Kronig transforms constitute a very sensitive criterion of the validity of the ac impedance data. An example of such analysis is shown in Figure 42.¹⁷⁷

Figure 42.

It has been shown that instead of Kramers-Kronig transforms another method involving a coherence function^{28,187} could be used to validate the data. The coherence function, γ , is defined as:^{188,189}

$$\gamma_{xy} = \left(\frac{\overline{S_{xy} S_{xy}^*}}{\overline{S_{xx} S_{yy}}} \right)^{1/2} \quad (236)$$

where $\overline{S_{xx}}$ is the average input signal power spectrum, $\overline{S_{yy}}$ is the average output signal power spectrum, $\overline{S_{xy}}$ is the average crosspower spectrum, symbol * denotes the complex conjugate, and $S_{xx}(\omega)$ is the power spectrum of parameter x as defined by its Fourier transform X :

$$S_{xx}(\omega) = X(\omega)X^*(\omega) \quad (237)$$

The power spectra may be directly obtained using dynamic signal analyzers which measure signals as a function of time and perform the fast Fourier transform. The coherence function takes values between zero and one and it characterizes statistical validity of the frequency response measurements: it is equal to one when perfect coherence exists. This function may be used when the Fourier-transformed data exist and the Kramers-Kronig transforms are difficult to use (unbounded impedance, truncated data, etc.).¹⁸⁷

3. Non-Stationary Impedances

As mentioned above the measured system should be stationary and should not evolve with time. In practice, such conditions cannot always be met. For example, corrosion process may continue during the experiment and change the measured impedance. Such measurements should be carried out quickly. However, very often the most interesting features are observed at low frequencies and the experiment may take hours. In such cases it is possible to follow evolution of impedances with time at one frequency and then repeat the experiment many times at different frequencies.¹⁹⁰ In order to use such a method the initial conditions must always be the

same. This method was applied recently to follow the electrochemical impedance of a guillotined aluminum electrode.¹⁹⁰ Stoynov et al.¹⁹¹⁻¹⁹⁴ introduced a new mathematical method for non-stationary impedances involving four-dimensional analysis and so-called rotating Fourier transforms. Although the simulations were carried out they were not applied in experimental studies of non-stationary systems.

VII. MODELING OF EXPERIMENTAL DATA

1. Selection of the Model

The aim of the analysis of the EIS data is to elucidate the electrode process and to derive its characteristic parameters. It should be stressed here that the EIS is a very sensitive technique but it does not provide a direct measure of the physical phenomena. Other electrochemical experiments (dc, transients) should also be carried out, together with good physical knowledge of the system (solution and surface composition, thickness, porosity, presence of various layers, hydrodynamic conditions, etc.). Interpretation of impedance data requires use of an appropriate model. This is a quite difficult task which must be carried out very carefully.

The modeling may be classified as: (i) physico-chemical, process^{175,181,195,196} or structural^{19,197,198,199} modeling and (ii) measurement,^{195,196} formal¹⁹ or mathematical^{200,201} modeling. Process modeling links measured impedances with physicochemical parameters of the process (kinetic parameters, concentrations, diffusion coefficients, sample geometry, hydrodynamic conditions, etc.). Measurement modeling explains the experimental impedances in terms of mathematical functions in order to obtain good fit between the calculated and experimental impedances. In the latter case the parameters obtained do not necessarily have a clear physico-chemical significance.

Ideally, first the measurement modeling should be carried out, the number and the nature of the circuit elements should be identified and then the process modeling should be carried out. Such a procedure is relatively elementary for a circuit containing simple elements: R , C , and L . It may also be carried out for the circuits containing distributed elements that can be described by a closed form equation: CPE, semiinfinite, finite length or spherical diffusion, etc. However, many different conditions arise from the numerical calculations, e.g. for porous electrodes (correct solution), nonlinear diffusion (to disk, cylinder, etc.) or nonuniform diffusion, nonhomogeneous materials (conducting polymers), etc. In such cases *a priori* model predictions are difficult or impossible. It should be stressed that proper modeling is the most difficult part of the analysis, and is often misunderstood and wrongly interpreted.

Usually, an equivalent circuit is chosen and the fit to the experimental data is performed using the complex nonlinear least-squares technique (CNLS). However, the model deduced from the reaction mechanism may have too many adjustable parameters while the experimental impedance spectrum is simple. For example, a system with one adsorbed species, Section IV.2, may produce two semicircles in the complex plane plots, but experimentally only one semicircle is often identified. In such a case approximation to a full model introduces too many free parameters and a simpler model containing one time constant should be used. Therefore, first, the number and nature of parameters should be determined and, then, the process model constructed in consistency with the parameters found and the physico-chemical properties of the process.

Another problem of data modeling is connected with the fact that the same data may be represented by different equivalent circuits.²⁰⁰ For example, the system containing one capacitive

loop, Figure 4, may be exactly described by either of the two equivalent circuits shown in Figure 43.

Figure 43.

In fact, that the admittance of these two circuits may be written in the general form:

$$Y = \frac{a_1 j\omega + a_0}{j\omega + b_0} = a_1 + \frac{a_0 - a_1 b_0}{j\omega + b_0} \quad (238)$$

where

$$a_1 = R_1^{-1}, a_0 = 1/(C_2 R_1 R_2) \text{ and } b_0 = (R_1^{-1} + R_2^{-1})/C_2 \text{ for circuit (a)} \quad (239)$$

or

$$a_1 = R_1^{-1} + R_2^{-1}, a_0 = 1/(C_2 R_1 R_2) \text{ and } b_0 = 1/(R_1 C_2) \text{ for circuit (b)}$$

and these two cases are indistinguishable. Equation (238) indicates that there is only one time constant of the system (see eqn. (25)). Similarly, a system displaying two capacitive loops, i.e. having two time constants, Figure 23, may be adequately described by the three circuits in Figure 44.

Figure 44.

Their admittance may be written as:

$$Y = \frac{a_2 (j\omega)^2 + a_1 j\omega + a_0}{(j\omega)^2 + b_1 j\omega + b_0} \quad (240)$$

And the behaviors of these three circuits are also indistinguishable, that is for a proper choice of the parameters they display the same impedance spectrum over at all frequencies.

Circuits the most often used in measurement modeling are: the Voigt, ladder and Maxwell circuits, as presented in Figure 45.

Figure 45.

Zoltowski²⁰⁰ proposed using ladder circuits for measurement modeling, substituting circuit resistances and capacitances by the CPE elements.

Very often modeling depends on the errors of the experimental data. Orazem et al.¹⁹⁶ studied approximation of synthetic data corresponding to the impedance response of a single electrochemical reaction on a rotating disk electrode under the conditions of nonuniform current and potential distribution. The complex plane plot represented a depressed semicircle. The authors found that the input data could be quite well approximated by a circuit consisting of a solution resistance in series with the parallel connection of a resistance and a CPE element (see Figure 28) and three other circuits containing two time constants (ladder, Voigt and mixed). These authors also studied a more complex case. They stated that the ambiguity demonstrated above is common to model identification for all electrochemical measurements and presents the greatest challenge for the analysis of impedance data. For example, impedance of a porous electrode may be described by the Voigt circuit with a sufficient number of R - C elements or by eqn. (195). Development of a proper model requires knowledge of the chemistry and physics of

the system, some prior information about it and good understanding of the characteristics of the measured values. Such a model identification procedure should be supported by a series of measurements at different potentials, temperatures, concentrations, disk rotation rates, etc.

Stoynov and collaborators^{19,197-199} developed mathematical methods for the structural and parameter identification from impedance data. They also used spectral analysis which could identify the number and nature of time constants existing in the system.

Direct use of equivalent circuits may lead to more complex data analysis. For example, for a system containing one adsorbed species, eqn. (139), may be described by the ladder circuit shown in Figure 21. The parameters R_a and C_a describing the faradaic impedance, eqn. (141), are complex functions of the parameters A , B , and C while direct use of eqn. (135) leads to simpler data analysis, i.e. parameters A , B , and C are simpler functions of the kinetic parameters than the electric parameters R_a and C_a .

2. CNLS Approximations

(i) CNLS Method

After validated data are obtained one can proceed with modeling. To do this a complex nonlinear least-squares (CNLS) program is used.^{18,202-204} This is a nonlinear least-squares fit of the real and imaginary parts, or magnitude and phase-angle of the experimental impedance/admittance to a given model. In general, the sum of squares:

$$S = \sum_{i=1}^N \left\{ w_i' \left[Z_i' - Z_{i,calc}' \right]^2 + w_i'' \left[Z_i'' - Z_{i,calc}'' \right]^2 \right\} \quad (241)$$

must be minimized, where Z_i' and Z_i'' are the real and imaginary parts of the experimental impedances at the frequencies ω_i , $Z_{i,calc}'$ and $Z_{i,calc}''$ are the values calculated from a given model, w_i' and w_i'' are the statistical weights of the data, and the summation runs over all N experimentally used frequencies. The minimization is most often carried out using the iterative Marquard-Levenberg algorithm.^{202,203,205} Because of the iterative nature of the algorithm the initial choice of the parameters is very important: they must lie relatively close to the real values, otherwise the CNLS method may become divergent. Usually, a simpler model is first used, several parameters determined, then they are kept constant as new parameters are added and, finally, all the parameters are used as adjustable. Such a procedure may be tricky and in some cases local minima are found. In such cases it is advisable to repeat the approximation starting with different initial parameter values. If the process converges to another minimum, the relative values of the weighted sum of squares or χ^2 should be compared. Sometimes vary flat minima are obtained leading to large values of the relative standard deviations of the measured parameters.

Another problem is connected with the goodness of fit and the number of free parameters used in the approximating function. The identification procedure may give the number and nature of the elements in the circuit. The number of adjustable parameters should be kept to a minimum. Usually, the approximation starts with the smallest possible number of parameters, then an additional parameter is added and the decrease in the sum of squares must be compared. Such decrease must be statistically important. It may be tested using the F-test for the additional parameter.²⁰⁶ Addition of some elements in the circuit may be connected with addition of more than one parameter. The F-test of addition of k parameters to the approximating function is described as:

$$F_{\text{exp}} = \frac{[S(N-p) - S(N-p-k)]/k}{S(N-p)/(N-p)} \quad (242)$$

where $S(N-p)$ is the sum of squares, eqn. (241), for p parameters and $N-p$ degrees of freedom, $S(N-p-k)$ is the sum of squares for $p+k$ free parameters and N is the number of points. This parameter should be compared with function $F(k, N-p, \alpha)$ for k and $N-p$ degrees of freedom, and a level of confidence α , from the statistical tables. If F_{exp} is lower than $F(k, N-p)$, the hypothesis that the function has $p+k$ parameters must be rejected. This test should be applied with prudence and always the *smallest possible number of added parameters* k should be used. It may happen that when k parameters are added only the first one increases the value of $F_{\text{exp}} > F(1, N-p, \alpha)$, although for k parameters F_{exp} is also $> F(k, N-p, \alpha)$.

Besides comparing the sum of squares the comparison of the experimental and simulated data should be carried out using complex plane and Bode plots. The phase-angle Bode plot is particularly sensitive in detection of time constants. Boukamp²⁰³ proposed to study the residual sum of squares after subtracting the assumed model values from the total impedance data. If the model is valid the residuals should behave randomly. If they display regular tendencies it may mean that the model is not correct and further elements should be added. However, the variations of the residuals should be statistically important.

Macdonald²⁰⁷ studied precision of the parameters determined by the EIS. He added a noise to the simulated impedance data and used the CNLS technique to determine the parameters together with their standard deviation. Using this technique it was possible to determine how the impedance errors are transferred to the determined parameters, depending on their relative values. This method allows sensitivity of the parameters to the random noise to be determined.

(ii) *Statistical Weights*

The choice of statistical weights in the CNLS fit is very important. Because the measured impedances may vary at different frequencies over several orders of magnitude when unitary weights ($w_i = 1$) are used, only the largest impedances contribute to the sum of squares S . In such a case low time constants may be overlooked. In general, several repetitions of the experiment allows for the determination of the standard deviation of each point (σ_i' and σ_i'') and the statistical weights may be obtained as: $w_i' = (\sigma_i')^{-2}$ and $w_i'' = (\sigma_i'')^{-2}$. Although this is the best approach such a procedure is time consuming and rarely used in practice. Another alternative proposed by Macdonald¹⁸ was to use proportional weighting, that is taking weights inversely proportional to the measured or estimated impedances: $w_i = 1/Z_i^2$ or $w_i = 1/Z_{i,\text{calc}}^2$. Such weighting methods mean that the real and imaginary parts of the impedance may be independently determined and that their precisions are independent. However, in practice, these parameters are often measured using the same sensitivity for both components; therefore, a better weighting procedure may be use of modulus weighting: $w_i = 1/(Z_i'^2 + Z_i''^2)$.^{203,208}

Orazem and coworkers^{195,196,209,210} studied the error structure of the impedances measured using a Solartron FRA. They found that the standard deviations of the real and imaginary impedances are identical and may be described by:

$$\sigma_i = \alpha |Z_i'| + \beta |Z_i''| + \gamma \frac{|Z_i|^2}{R_m} \quad (243)$$

where α , β and γ are constant parameters determined for a given instrumental system and R_m is the value of the current-measuring resistor. Such an error structure was verified for solid state and electrochemical systems under a wide variety of experimental conditions, and for errors ranging from $m\Omega$ to $M\Omega$, and allowed for better determination of system parameters.

(iii) AC Modeling Programs

Several programs for the EIS modeling are available:

- J.R. Macdonald's program^{18,202}, written in FORTRAN, source code available. It contains various models already predefined, many weighting possibilities, and allows for easy modifications of the subroutines for the model impedance calculations. FORTRAN is a language which contains intrinsically complex number calculations which facilitates the programming process. Its disadvantage is a special formatted data input (however, it can be easily corrected).
- Boukamp' program²⁰³ written in Pascal, distributed with EG&G software, is very popular. Equivalent circuits are constructed from several predefined elements. There is no possibility of changing the subroutines or introducing new equations.
- Scribner Associates, Inc. developed a software (Zplot) for data acquisition and analysis. It is based on Macdonald's algorithm and the data analysis was simplified. It uses a number of predefined circuits without the possibility of modification.
- Sirotech Ltd.²¹¹ developed a software which performs a similar task and is able to choose the best equivalent circuit.
- Several software packages (often with very limited modeling capabilities) come with the hardware, e.g. from Gamry Instruments, Inc.: EIS900; BAS-Zahner (Thales); Eco Chemie BV: Autolab; Tacussel: Z-Computer, etc.
- Some other programs have been developed in the literature without being widely commercialized.^{204,212-215}

VIII. INSTRUMENTAL LIMITATIONS

EIS measurements should be carried out over a wide frequency range in order to identify all time constants in the circuit (usually 10 frequencies per decade). The highest frequency depends on the potentiostat used, because at high frequencies, it may introduce a phase shift, and on the stray capacitance and inductance of the experimental setup (cables, cell, etc.). A typical range in modern systems is 20 to 50 kHz, although they may range to MHz. With increase of sensitivity the potentiostats tend to slow down and the response on a 10 mA current scale is much faster than that on 10 μ A scale. Much higher frequencies up to 10 MHz were used by Barański et al.^{216,217} but the experiments were carried out without a potentiostat on ultramicroelectrodes. Corrections for slow response of the potentiostat may be carried out and increases the effective bandwidth by about one order of magnitude.²¹⁸ If the response of the electronic system is linear the parasitic impedances, \hat{Z}_{in} and \hat{Z}_{oc} , together with the complex sensibility, \hat{S} , Figure 46, may be obtained from:

$$\hat{S} \hat{Z}_m = \hat{Z}_{in} + \frac{1}{\frac{1}{\hat{Z}_{el}} + \frac{1}{\hat{Z}_{oc}}} \quad (244)$$

where \hat{Z}_m is the measured impedance and \hat{Z}_{el} is the impedance of the electrochemical cell. Three measurements: one in the open circuit and two with two different resistances instead of \hat{Z}_{el} allow the determination of three unknown complex parameters and further correction of the measured impedance. Such corrections should be repeated at each frequency and the cable configuration used for calibration should be the same as for the electrochemical measurements. Another method involving two working electrodes for high frequency (≤ 5 MHz) impedance measurements was proposed by Schöne and Wiesbeck.²¹⁹

Figure 46.

The lowest frequency typically used is 10^{-3} Hz. This limit is connected with the possible changes in the state of the electrode during long-period measurements. At this frequency measurements averaged over five wave periods take 1 hour 23 min. The measurement at all frequencies takes a much longer time.

The use of FRAs may lead to erroneous results when the frequency is swept too fast.^{30,220} The change of frequency may lead to a transient regime. If the measurements are performed during this transient, error is introduced into the results. It depends on the initial phase of the sinusoidal excitation. It can be neglected when 10 cycles of signal integration and at least five steps per decade are used in measurements. This error becomes negligible at higher frequencies (> 10 Hz for the Solartron) because of the internal delay of the measurements at each frequency.

It is relatively easy to get good precision of measurements for impedances between 1 and $10^5 \Omega$ at frequencies below 5×10^4 Hz. However, for lower and higher impedances, distortions may be observed. Very high impedances are found, for example, in measurements of protective coatings on metallic surfaces and very low impedances are found in molten salts. The errors for high impedance measurements originate from the finite potentiostat input impedance. Such resistance should be at least 100 times larger than the measured impedance; if not, a calibration procedure is necessary.

Another distortion is observed at very low impedances, corresponding to an inductance in series with the electrode impedance. It is observed at high frequencies and leads to large positive imaginary impedances.^{221,222} This inductance arises from that of the leads and the current measuring resistor. Such effects may be often minimized by shortening the cables and shielding the reference electrode.

The distance between the working electrode and the Luggin capillary may also affect the impedance measurements and lead to artifacts.²²³ In principle, increase of the distance between the Luggin capillary tip and working electrode should only increase the solution resistance, which shifts the complex plane plot along the real axis. Figure 47 presents examples of the complex plane plots obtained at several distances in acetic acid.

Figure 47.

Such behavior arises from the contribution of the reference electrode to the measured impedances and it was explained introducing the resistance and capacitance of the reference electrode and a capacitive coupling between the reference electrode and counter and working electrodes.²²³ Similar artifacts, observed at high frequencies, are also observed in highly

conducting solutions²²⁴ when the Luggin capillary is located too close to the electrode surface. They can be minimized by inserting a thin platinum wire into the Luggin capillary and the salt bridge.²²⁴⁻²²⁶

IX. CONCLUSION

EIS has become a mature and well understood technique. It is now possible to acquire, validate and quantitatively interpret the experimental impedances. The above review was dedicated to the understanding of the fundamental processes of diffusion and faradaic reaction at electrodes. However, the most difficult problem in EIS is modeling of the electrode processes, that is where most of the problems and errors arise. There is almost an infinite variety of different reactions and interfaces that can be studied (corrosion, coatings, conducting polymers, batteries and fuel cells, semiconductors, electrocatalytic reactions, chemical reactions coupled with faradaic processes, etc.) and the main effort is now applied to understand and analyze these processes. These applications will be subject of a second review by the author in a forthcoming volume in this series.

List of Figures

Figure 1. Representation of ac signals: (a) rotating voltage and current vectors in time space; (b) voltage and current phasors in frequency space.....	7
Figure 2. Complex plane (b), (c) and Bode (d), (e), plots for a series connection of a resistance and a capacitance, (a) ; $R = 100 \Omega$, $C = 20 \mu\text{F}$	8
Figure 3. Complex plane (b), (c) and Bode (d), (E), plots for a parallel connection of R and C (a); $R = 100 \Omega$, $C = 20 \mu\text{F}$	9
Figure 4. Complex plane (b), (c) and Bode (d), (e), plots for the circuit (a); $R_s = 10 \Omega$, $R_{ct} = 100 \Omega$, $C_{dl} = 20 \mu\text{F}$	9
Figure 5. Construction of the Bode magnitude plot for the circuit in Figure 4a using eqn. (26). The solid line is a sum of all three contributions.	10
Figure 6. Schematic operation of a lock-in amplifier.	12
Figure 7. Frequency response of a FRA averaging filter for different numbers of integration cycles ⁴⁴	12
Figure 8. FFT amplitude, $ H(j\omega) $, of the pulse function, eqn. (38), of duration $T_0 = 1 \text{ s}$	14
Figure 9. FFT analysis of the sum of sine waves perturbation; left - no optimization, right - optimization of phases; a) perturbation voltage in the time domain, b) perturbation voltage in the frequency domain, c) complex plane plots of simulated impedance spectra with 5% noise added to the current response. Solid lines show response without noise. ⁵¹	15
Figure 10. FFT analysis of the sum of sine waves perturbation; left - no optimization, right - optimization of amplitudes; a) perturbation voltage in the time domain, b) perturbation voltage in the frequency domain, c) current response with 10% noise added, presented in frequency domain, d) complex plane plots of simulated impedance spectra with 10% noise added to the current response. Solid lines show response without noise. ⁵¹	15
Figure 11. Complex plane (b) and Bode (c), (d), plots for the semi-infinite linear diffusion model (a); in (b) continuous line: total impedance, dashed line: faradaic impedance; $R_s = 10 \Omega$, $R_{ct} = 100 \Omega$, $C_{dl} = 20 \mu\text{F}$, $\sigma = 10 \Omega \text{ s}^{-1/2}$	20
Figure 12. Dependence of logarithms of R_{ct} and $ Z_w $ on potential for $\alpha = 0.4$	20
Figure 13. Complex plane (a) and Bode (b), (c) plots for semi-infinite spherical diffusion; sphericity parameter $\sqrt{2D_i} / r_0$: (a) ∞ - linear diffusion, (b) 0.02, (c) 0.05, (d) 0.1, (e) $0.2 \text{ s}^{-1/2}$; $R_s = 10 \Omega$, $R_{ct} = 100 \Omega$	21
Figure 14. Faradaic (dashed line) and total (continuous line) impedance for a reversible reaction in the conditions of semi-infinite cylindrical diffusion, $R_s = 10 \Omega$	23
Figure 15. Faradaic (dashed line) and total (continuous line) impedances in the conditions of the diffusion to a disk and a reversible charge transfer.	23
Figure 16. Faradaic (a) and total (b)-(d) impedances for: a) - linear semi-infinite, b) - finite transmissive, and c) - finite reflective boundaries, $R_s = 10 \Omega$, $R_{ct} = 100 \Omega$	25
Figure 17. Dependence of the real and imaginary admittances for a diffusion-kinetic process on the electrode potential.	26
Figure 18. Dependence of real and imaginary parts of the faradaic impedance of a diffusion-kinetic process on $\omega^{-1/2}$ at constant potential.	27
Figure 19. Dependence of $\cot \varphi$ as a function of potential for TiCl_4 reduction in $\text{H}_2\text{C}_2\text{O}_4$ at various frequencies. ⁷⁷	28

Figure 20. Dependence of $\cot \phi$ vs. $\omega^{1/2}$ for TiCl_4 reduction in $\text{H}_2\text{C}_2\text{O}_4$. Data from ref. 77.....	28
Figure 21. Equivalent circuit for the case of one adsorbed species: a) for $B < 0$, b) $B > 0$	32
Figure 22. Complex plane plots for the case of one adsorbed species and $B < 0$, eqns. (139)- (140); continuous line - total impedance, dashed line - faradaic impedance; parameters used: $R_{ct} = 100 \Omega$, $R_a = 100 \Omega$, $C_a = 2 \times 10^{-3} \text{ F}$, $C_{dl} = 2 \times 10^{-5} \text{ F}$, $R_s = 10 \Omega$	32
Figure 23. Complex plane plot for the case of one adsorbed species, $B < 0$ and $C - R_{ct} B = 0$; continuous line - total impedance, dashed line - faradaic impedance; parameters used: $R_{ct} =$ 100Ω , $C_a = 2 \times 10^{-3} \text{ F}$, $C_{dl} = 2 \times 10^{-5} \text{ F}$, $R_s = 10 \Omega$	33
Figure 24. Complex plane plot for the case of one adsorbed species, $B < 0$ and $C - R_{ct} B < 0$; continuous line - total impedance, dashed line - faradaic impedance; parameters used: $R_{ct} =$ 100Ω , $R_a = -200 \Omega$, $C_a = 2 \times 10^{-3} \text{ F}$, $C_{dl} = 2 \times 10^{-5} \text{ F}$, $R_s = 10 \Omega$	33
Figure 25. Complex plane plots for the case of one adsorbed species and $B > 0$, eqns. (144)- (146); continuous line - total impedance, dashed line - faradaic impedance; parameters used: $R_{ct} = 100 \Omega$, $R_o = 40 \Omega$, $L = 0.2 \text{ H}$, $C_{dl} = 2 \times 10^{-5} \text{ F}$, $R_s = 10 \Omega$	33
Figure 26. Some examples of the complex plane plots obtained for the case of two adsorbed species. ⁹⁴	36
Figure 27. The distribution function $\tau G(\tau)$ versus $\ln(\tau/\tau_0)$ according to eqn. (176).....	38
Figure 28. Complex plane plots in the presence of a CPE element: a) ideally polarizable electrode, b) in the presence of faradaic reaction.....	39
Figure 29. Equivalent-circuit model of the electrode in the presence of adsorption. ¹⁰⁷	40
Figure 30. Nyquist plot of complex capacitances for Au(111) in 0.1 M HClO_4 in the presence of bromide ions; Br^- concentrations given in the figure, upper three curves at $E = 0.3 \text{ V}$, lower three curves at $E = 0.1 \text{ V}$ vs. SCE. ¹⁰⁷	40
Figure 31. Complex plane plots for the bounded thickness impedance (BCP) for $R_s = 100 \Omega$, $T =$ $0.01 \text{ F cm}^{-2} \text{ s}^{\phi-1}$, and different values of parameter ϕ	40
Figure 32. Comparison of a simple (b) and fractal (c) magnifications of the image (a). ¹¹¹	41
Figure 33. Complex plane plots on fractal electrodes for different values of parameter ϕ	41
Figure 34. Pore model.....	42
Figure 35. Complex plane plots for a porous electrode according to de Levie's model, eqn. (195): (a) general case, eqn.(195); (b) limiting case for shallow pores, eqn. (199); (c) limiting case for very deep pores, eqn. (200)......	44
Figure 36. Complex plane plots for LaPO_4 -bonded Ni powder electrodes during hydrogen evolution in 30% NaOH at 70°C . ¹⁴⁷	45
Figure 37. Complex plane plots for a porous electrode at different overpotentials; pore parameters: $l = 0.05 \text{ cm}$, $r = 10^{-4} \text{ cm}$, $\rho = 10 \Omega \text{ cm}$, $j_0 = 10^{-6} \text{ A cm}^{-2}$, η_0 : a) 0.025, b) 0.1, c) 0.2, d) 0.3, e) 0.4, and f) 0.5 V. Continuous lines - simulated, dashed lines - calculated using de Levie's model, eqn.(195). ¹⁴⁹	46
Figure 38. Complex plane plots for a porous electrode in the presence of a concentration gradient at different overpotentials; $l = 0.05 \text{ cm}$, $r = 10^{-4} \text{ cm}$, $\rho = 10 \Omega \text{ cm}$, $D = 10^{-5} \text{ cm}^2 \text{ s}^{-1}$, $m = 1$, $j_0 =$ $10^{-7} \text{ A cm}^{-2}$, $C_O^* = 0.01 \text{ M}$	48
Figure 39. Influence of the depolarizer concentration on the complex plane plots for a porous electrode; $j_0 = 10^{-6} \text{ A cm}^{-2}$, $\eta = 0.2 \text{ V}$, concentrations in mol cm^{-3} are indicated in the figure, other parameters as in Figure 38.	48
Figure 40. Calculated impedances for various shapes of a single pore blocking electrode. ¹⁵⁹	49
Figure 41. Voigt (a) and ladder (b) models.....	52

Figure 42. Impedance spectrum for an Al electrode in water (a) and its Kramers-Kronig transforms, (b) and (c). ¹⁷⁷	53
Figure 43. Alternative circuits for the impedance behavior of a system containing one capacitive loop.....	55
Figure 44. Three circuits describing a system displaying two capacitive loops: (a) ladder, (b) Voigt, (c) mixed.	55
Figure 45. Typical circuits used in ac modeling; they are experimentally indistinguishable: (a) Voigt, (b) Maxwell, (c) ladder. ¹⁸	55
Figure 46. Equivalent circuit for the case of a slow response of the potentiostat.....	59
Figure 47. Impedance diagrams for different distances x between the working electrode and the Luggin capillary tip in: (a) 80% acetic acid; (b) 100% acetic acid. ²²³	59

References

- ¹ D.C. Graham, *Chem. Rev.*, **41** (1947) 441.
- ² R. Parsons, *Modern Aspects of Electrochemistry*, Vol. 1, 1954, p. 103.
- ³ P. Delahay, *Double Layer and Electrode Kinetics*, Wiley-Interscience, New York, 1965.
- ⁴ D.M. Mohilner in *Electroanalytical Chemistry*, A.J. Bard, Ed., Dekker, New York, 1966, p. 241.
- ⁵ B. Breyer and H.H. Bauer, *Alternating Current Polarography and Tensammetry, Chemical Analysis Series*, P.J. Elving and I.M. Kolthoff, Eds., Wiley-Interscience, New York, 1963.
- ⁶ D.E. Smith in *Electroanalytical Chemistry*, A.J. Bard, Ed., Dekker, New York, Vol. 1, 1966, p. 1.
- ⁷ A.M. Bond, *Modern Polarographic Techniques in Analytical Chemistry*, Dekker, New York, 1980.
- ⁸ P. Delahay, *New Instrumental Methods in Electrochemistry*, Interscience, New York, 1954.
- ⁹ K.J. Vetter, *Electrochemical Kinetics*, Academic Press, New York, 1967.
- ¹⁰ D.D. Macdonald, *Transient Techniques in Electrochemistry*, Plenum Press, New York, 1977.
- ¹¹ A.J. Bard and L.R. Faulkner, *Electrochemical Methods*, Wiley, New York, 1980.
- ¹² *Instrumental Methods in Electrochemistry*, Southampton Electrochemistry Group, Ellis Horwood, Chichester, 1985.
- ¹³ E. Gileadi, *Electrode Kinetics for Chemists, Engineers, and Material Scientists*, VCH, New York, 1993.
- ¹⁴ C.M.A. Brett and A.M. Oliveira Brett, *Electrochemistry, Principles, Methods, and Applications*, Oxford University Press, 1993.
- ¹⁵ Z. Galus, *Fundamentals of Electrochemical Analysis*, Ellis Horwood, New York, 1994.
- ¹⁶ H.B. Oldham and J.C. Myland, *Fundamentals of Electrochemical Science*, Academic Press, San Diego, 1994.
- ¹⁷ *Physical Electrochemistry, Principles, Methods, and Applications*, I. Rubinstein, Ed., Dekker, New York, 1995.
- ¹⁸ J.R. Macdonald, *Impedance Spectroscopy Emphasizing Solid Materials and Systems*, Wiley, New York, 1987.
- ¹⁹ Z.B. Stoyanov, B.M. Grafov, B.S. Savova-Stoynova, V.V. Elkin, and B.B. Damaskin, *Electrochemical Impedance*, Nauka, Moscow, 1991 (in Russian).
- ²⁰ R.D. Armstrong, M.F. Bell, and A.A. Metcalfe in *Electrochemistry. A Specialist Periodical Report*, H.R. Thirsk, Ed., The Chemical Society, Burlington House, London, 1978, Vol. 6, p. 98.
- ²¹ W.I. Archer and R.D. Armstrong, in *Electrochemistry. A Specialist Periodical Report*, H.R. Thirsk, Ed., The Chemical Society, Burlington House, London, 1980, Vol. 7, p. 157.
- ²² D.D. Macdonald in *Techniques for Characterization of Electrodes and Electrochemical Processes*, Ed. by R. Varma and J.R. Selman, J. Wiley & Sons, New York, 1991, p. 515.
- ²³ F. Mansfeld and W.J. Lorenz in *Techniques for Characterization of Electrodes and Electrochemical Processes*, Ed. by R. Varma and J.R. Selman, J. Wiley & Sons, New York, 1991, p. 581.
- ²⁴ S. Szpak in *Techniques for Characterization of Electrodes and Electrochemical Processes*, Ed. by R. Varma and J.R. Selman, J. Wiley & Sons, New York, 1991, p. 677.
- ²⁵ *Electrochemical Impedance: Analysis and Interpretation*, Ed. by J.R. Scully, D.C. Silverman and M.W. Kendig, ASTM, Philadelphia, 1993.

- ²⁶ M. Sluyters-Rehbach and J.H. Sluyters, *Analytical Chemistry*, Ed. by A.J. Bard, Marcel Dekker, 1970, Vol. 4, p. 1.
- ²⁷ M. Sluyters-Rehbach and J.H. Sluyters, *Comprehensive Treatise of Electrochemistry*, Plenum Press, 1984, Vol. 9, p. 177.
- ²⁸ D.D. Macdonald and M.C.H. McKurbe in *Modern Aspects of Electrochemistry*, Ed. by J. O'M. Bockris, B.E. Conway and R.E. White, Plenum Press, 1982, Vol. 14, p. 61.
- ²⁹ D.D. Macdonald and M.C.H. McKurbe in *Electrochemical Corrosion Testing, ASTM Special Publ. 727*, ASTM, Philadelphia, 1981.
- ³⁰ C. Gabrielli, *Identification of Electrochemical Processes by Frequency Response Analysis*, Technical Report No 004, Solartron, Hampshire, 1984.
- ³¹ C. Gabrielli, *Use and Applications of Electrochemical Impedance Techniques*, Technical Report No 24, Solartron, Hampshire, 1990.
- ³² G. Doetsch, *Laplace Transformation*, Dover, New York, 1953.
- ³³ J.J. DiStefano, III, A.R. Stubberud and I.J. Williams, *Theory and Problems of Feedback and Control Systems*, 2nd. ed., Schaum's Outline Series, McGraw-Hill, New York, 1990.
- ³⁴ S. Goldman, *Transformation Calculus and Electrical Transients*, Prentice-Hall, New York, 1950.
- ³⁵ C. Gabrielli, M. Keddarn, and H. Takenouti, *Electrochim. Acta*, **35** (1990) 1553.
- ³⁶ C. Gabrielli and B. Tribollet, *J. Electrochem. Soc.*, **141** (1994) 957.
- ³⁷ A.A. Pilla in *Electrochemistry. Calculations, Simulation and Instrumentation*, Ed. by J.S. Mattson, H.B. Mark, Jr., and H.C. MacDonald, Marcel Dekker, New York, 1972, p. 139.
- ³⁸ R.D. Armstrong, W.P. Race, and H.R. Thirsk, *Electrochim. Acta*, **13** (1968) 215.
- ³⁹ A. Muszalska and J. Jarzebska, *J. Electroanal. Chem.*, **318** (1991) 145.
- ⁴⁰ M.M. Gomez, R. Motilla, and E. Diez, *Electrochim. Acta*, **34** (1989) 831.
- ⁴¹ K. Chandrasekara Pillai, W.E. Waghorne, and O. Wilson, *J. Electroanal. Chem.*, **252** (1988) 151.
- ⁴² *A Lock-In Primer*, EG&G, Princeton Applied Research, Princeton, 1986.
- ⁴³ R. de Levie and A.A. Husovsky, *J. Electroanal. Chem.*, **20** (1969) 181.
- ⁴⁴ P.E. Wellstead, *Frequency Response Analysis*, Technical Note No 10, Solartron Instruments.
- ⁴⁵ J.-P. Diard, B. Le Gorrec, and C. Montella, *J. Electroanal. Chem.*, **377** (1994) 61.
- ⁴⁶ C. Gabrielli, M. Keddarn and H. Takenouti in *Electrochemical Methods in Corrosion Research*, M. Duprat, Ed., Materials Science Forum, Vol. 8, 1986, p. 417.
- ⁴⁷ N.J. Evans, *Electrochemistry Newsletter*, April 1996, p. 11.
- ⁴⁸ E.O. Birgham, *The Fast Fourier Transform*, Prentice-Hall, N.J., 1974.
- ⁴⁹ D.E. Smith, *Anal. Chem.*, **48** (1976) 221A.
- ⁵⁰ S.C. Creason, J.W. Hayes, and D.E. Smith, *J. Electroanal. Chem.*, **47** (1973) 9.
- ⁵¹ G.S. Popkirov and R.N. Schindler, *Bulgarian Chem. Commun.*, **27** (1994) 459.
- ⁵² G.S. Popkirov and R.N. Schindler, *Rev. Sci. Instrum.*, **64** (1993) 3111.
- ⁵³ R.J. Schwall, A.M. Bond, R.J. Loyd, J.G. Larsen, and D.E. Smith, *Anal. Chem.*, **49** (1977) 1797.
- ⁵⁴ A.J. Bond, R.J. Schwall, and D.E. Smith, *J. Electroanal. Chem.*, **85** (1977) 231.
- ⁵⁵ A.A. Pilla, *J. Electrochem. Soc.*, **117** (1970) 467.
- ⁵⁶ A.A. Pilla in *Electrochemistry. Calculations, Simulation, and Instrumentation*, J.S. Mattson, H.B. Mark, Jr., and H.C. MacDonald, Jr., Eds., Marcel Dekker, New York, 1972, p. 139.
- ⁵⁷ K. Doblhofer and A.A. Pilla, *J. Electroanal. Chem.*, **39** (1972) 91.
- ⁵⁸ C. Gabrielli, M. Keddarn, and J.F. Lizee, *J. Electroanal. Chem.*, **205** (1986) 59.

- ⁵⁹ J. Ye and K. Doblhofer, *J. Electroanal. Chem.*, **272** (1989) 11, 29.
- ⁶⁰ M. Neumannspallart and M. Elman, *J. Electroanal. Chem.*, **327** (1994) 33.
- ⁶¹ A.A. Sagüés, S.C. Krans, and E.I. Moreno, *Electrochim. Acta*, **41** (1996) 1239, 2661.
- ⁶² J.S. Gill, L.M. Callow, and J.D. Scantlebury, *Corrosion*, **39** (1983) 61.
- ⁶³ E. Warburg, *Ann. Phys. Chem.*, **67** (1899) 493.
- ⁶⁴ J.E.B. Randles, *Disc. Farad. Soc.*, **1** (1947) 11.
- ⁶⁵ D.C. Grahame, *J. Electrochem. Soc.*, **99** (1952) 370C.
- ⁶⁶ S.R. Taylor and E. Gileadi, *Corr. Sci.*, **51** (1995) 664.
- ⁶⁷ J.E.B. Randles, *Transactions of the Symposium on Electrode Processes*, Philadelphia, 1959, E. Yeager, Ed., Wiley, New York, p. 209.
- ⁶⁸ X. Wu and W. Zhang, *J. Electroanal. Chem.*, **383**, (1995) 1.
- ⁶⁹ T.J. VanderNoot, *J. Electroanal. Chem.*, **300** (1991) 199.
- ⁷⁰ R.D. Armstrong and R.E. Firman, *J. Electroanal. Chem.*, **45** (1973) 3.
- ⁷¹ D.A. Harrington, *J. Electroanal. Chem.*, **403** (1996) 11.
- ⁷² M. Fleischmann, S. Pons and J. Daschbach, *J. Electroanal. Chem.*, **317** (1991) 1.
- ⁷³ *Ultramicroelectrodes*, Ed. by M. Fleischmann, S. Pons, D.R. Rolison and P.P. Schmidt, Datatech Systems, Inc., Morganton, NC, 1987, Chap. 2.
- ⁷⁴ T. Jacobsen and K. West, *Electrochim. Acta*, **30** (1995) 255.
- ⁷⁵ M. Fleischmann and S. Pons, *J. Electroanal. Chem.*, **250** (1988) 277.
- ⁷⁶ R. De Levie and A.A. Husovsky, *J. Electroanal. Chem.*, **22** (1969) 29.
- ⁷⁷ D.E. Smith, *Anal. Chem.*, **35** (1963) 610.
- ⁷⁸ J.H. Sluyters, *Rec. Trav. Chim.* **79** (1960) 1092.
- ⁷⁹ M. Sluyters-Rehbach and J.H. Sluyters, *J. Electroanal. Chem.*, **4** (1970) 1.
- ⁸⁰ K. Darowicki, *Electrochim. Acta*, **40** (1995) 767.
- ⁸¹ K. Darowicki, *Electrochim. Acta*, **42**, 1073 (1997).
- ⁸² J.-P. Diard, B. Le Gorrec, and C. Montella, *Electrochim. Acta.*, **42**, 1053 (1997).
- ⁸³ C.-N. Cao, *Electrochim. Acta*, **35** (1990) 831.
- ⁸⁴ L. Bai and B.E. Conway, *Electrochim. Acta*, **38** (1993) 1803.
- ⁸⁵ J.-P. Diard, B. Le Gorrec, and C. Montella, *J. Electroanal. Chem.*, **326** (1992) 13.
- ⁸⁶ F. Berthier, J.-P. Diard and C. Montella, *J. Electrochem. Soc.*, **410** (1996) 247.
- ⁸⁷ A. Lasia and A. Rami, *J. Electroanal. Chem.*, **294** (1990) 123.
- ⁸⁸ F. Berthier, J.-P. Diard, L. Pronzato, and E. Walter, *Proceedings of the 10th IFAC Symposium on System Identification*, 4-6 July 1994, Copenhagen.
- ⁸⁹ F. Berthier, J.-P. Diard, C. Montella, L. Pronzato, and E. Walter, *J. Chim. Phys.*, **90** (1993) 2069.
- ⁹⁰ F. Berthier, J.-P. Diard, P. Landaud, and C. Montella, *J. Electroanal. Chem.*, **362** (1993) 13.
- ⁹¹ F. Berthier, J.-P. Diard, L. Pronzato, and E. Walter, *Automatica*, **32** (1996) 973.
- ⁹² R.D. Armstrong and M. Henderson, *J. Electroanal. Chem.*, **39** (1972) 81.
- ⁹³ R.D. Armstrong, R.E. Firman, and H.R. Thirsk, *Farad. Discuss. Chem. Soc.*, **56** (1973) 244.
- ⁹⁴ C.-N. Cao, *Electrochim. Acta*, **35** (1990) 837.
- ⁹⁵ J.-P. Diard, B. Le Gorrec, C. Montella and C. Montero-Ocampo, *J. Electroanal. Chem.*, **352** (1993) 1.
- ⁹⁶ L. Bai and B.E. Conway, *J. Electrochem. Soc.*, **137** (1990) 3737.
- ⁹⁷ D.A. Harrington, *J. Electroanal. Chem.*, **403**, 11 (1996).
- ⁹⁸ R.C. Salvarezza and A.J. Arvia, *Modern Aspects of Electrochemistry*, Vol. 30, R.E. White, B.E. Conway, and J. O'M. Bockris, Eds., Plenum.

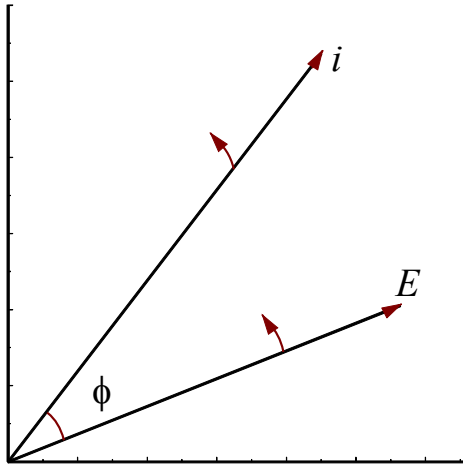
- ⁹⁹ K.S. Cole and R.H. Cole, *J. Chem. Phys.*, **9** (1941) 341.
- ¹⁰⁰ G.J. Brug, A.L.G. van den Eeden, M. Sluyters-Rehbach, and J.H. Sluyters, *J. Electroanal. Chem.*, **176** (1984) 275.
- ¹⁰¹ T. Pajkossy, *J. Electroanal. Chem.*, **364** (1994) 111.
- ¹⁰² Z.A. Rotenberg and N.V. Nekrasove, *Sov. Electrochem.*, **25** (1989) 651.
- ¹⁰³ U. Rammlet and G. Reinhard, *Corr. Sci.*, **27** (1987) 373.
- ¹⁰⁴ U. Rammlet and G. Reinhard, *Electrochim. Acta*, **35** (1990) 1045.
- ¹⁰⁵ P.K. Wrona, A. Lasia, M. Lessard, and H. Ménard, *Electrochim. Acta*, **37** (1992) 1283.
- ¹⁰⁶ T.J. VanderNoot, *J. Electroanal. Chem.*, **386** (1995) 57.
- ¹⁰⁷ T. Pajkossy, T. Wandlowski, and D.M. Kolb, *J. Electroanal. Chem.*, **414** (1996) 209.
- ¹⁰⁸ R. Devaux, A.M. de Bedelievre, C. Duret-Thual, and M. Keddam, *Electrochim. Acta*, **38** (1993) 1615.
- ¹⁰⁹ Z. Stoynov, *Electrochim. Acta*, **35** (1990) 1493.
- ¹¹⁰ B.B. Mandenbrot, *The Fractal Geometry of the Nature*, Freeman, San Francisco, 1982.
- ¹¹¹ R. de Levie, *J. Electroanal. Chem.*, **281** (1990) 1.
- ¹¹² H. von Koch, *Ark. Mat. Astron. Fys.*, **1** (1904) 681.
- ¹¹³ L. Nyikos and T. Pajkossy, *Electrochim. Acta*, **30** (1985) 1533.
- ¹¹⁴ T. Pajkossy, *J. Electroanal. Chem.*, **300** (1991) 1.
- ¹¹⁵ A. Le Méhauté and G. Crépy, *Solid State Ionics*, **9/10** (1983) 17; A. Le Méhauté, G. Crépy and A. Hurd, *C. R. Acad. Sci, Paris*, **306** (1988) 117.
- ¹¹⁶ L. Nyikos and T. Pajkossy, *J. Electrochem. Soc.*, **133** (1986) 2061.
- ¹¹⁷ L. Nyikos and T. Pajkossy, *Electrochim. Acta*, **31** (1986) 1347.
- ¹¹⁸ T. Pajkossy and L. Nyikos, *Electrochim. Acta*, **34** (1989) 171.
- ¹¹⁹ A.P. Borossy, L. Nyikos and T. Pajkossy, *Electrochim. Acta*, **36** (1991) 163.
- ¹²⁰ L. Nyikos and T. Pajkossy, *Electrochim. Acta*, **35** (1990) 1567.
- ¹²¹ A. Sakharova, L. Nyikos and T. Pajkossy, *Electrochim. Acta*, **37** (1992) 973.
- ¹²² T. Pajkossy, *Heterogen. Chem. Rev.*, **2** (1995) 143.
- ¹²³ M. Keddam and H. Takenouti, *Electrochim. Acta*, **33** (1988) 445.
- ¹²⁴ T. Pajkossy and L. Nyikos, *J. Electroanal. Chem.*, **332** (1992) 55.
- ¹²⁵ R. de Levie, *J. Electroanal. Chem.*, **261** (1989) 1.
- ¹²⁶ W. Mulder, *J. Electroanal. Chem.*, **326** (1992) 231.
- ¹²⁷ J.C. Wang, *Electrochim. Acta*, **33** (1987) 707.
- ¹²⁸ S.H. Liu, *Phys. Rev. Lett.*, **55** (1985) 529.
- ¹²⁹ T. Kaplan S.H. Liu and L.J. Gray, *Phys. Rev.*, **34** (1986) 4870.
- ¹³⁰ T. Kaplan, L.J. Gray and S.H. Liu, *Phys. Rev. B*, **35** (1987) 5379.
- ¹³¹ B. Sapoval, *Solid State Ionics*, **23** (1987) 253.
- ¹³² B. Sapoval, J.-N. Chazalviel and J. Peyrière, *Solid State Ionics*, **28/30** (1988) 1441.
- ¹³³ B. Sapoval, J.-N. Chazalviel and J. Peyrière, *Phys. Rev. A*, **38** (1988) 5867.
- ¹³⁴ D.W. Davidson and R.H. Cole, *J. Chem. Phys.*, **19** (1951) 1484.
- ¹³⁵ A. Rami and A. Lasia, *J. Appl. Electrochem.*, **22** (1992) 376.
- ¹³⁶ L. Chen and A. Lasia, *J. Electrochem. Soc.*, **139** (1992) 3458.
- ¹³⁷ P. Los, A. Rami, and A. Lasia, *J. Appl. Electrochem.*, **23** (1993) 135.
- ¹³⁸ E. Chassaing, B. Sapoval, G. Daccord and R. Lenormand, *J. Electroanal. Chem.*, **279** (1990) 67.
- ¹³⁹ T. Pajkossy and L. Nyikos, *Electrochim. Acta*, **34** (1989) 181.
- ¹⁴⁰ R. de Levie and A. Vogt, *J. Electroanal. Chem.*, **278** (1990) 25; **281** (1990) 23.

- ¹⁴¹ A.N. Frumkin, *Zh. Fiz. Khim.*, **23** (1949) 1477.
- ¹⁴² O.S. Ksenzhek, *Russ. J. Phys. Chem.*, **36** (1962) 331.
- ¹⁴³ A. Winsel, *Z. Elektrochem.*, **66** (1962) 287.
- ¹⁴⁴ F.A. Posey, *J. Electrochem. Soc.*, **111** (1962) 1173.
- ¹⁴⁵ J.M. Bisang, K. Jüttner, and G. Kreysa, *Electrochim. Acta*, **39** (1994) 1297.
- ¹⁴⁶ R. de Levie, in P. Delahay (Ed.), *Advances in Electrochemistry and Electrochemical Engineering*, Vol. 6, Interscience, New York, 1967, p. 329.
- ¹⁴⁷ P. Los, A. Lasia, H. Ménard, and L. Brossard, *J. Electroanal. Chem.*, **360** (1993) 101.
- ¹⁴⁸ K. Scott, *J. Appl. Electrochem.*, **13** (1983) 709.
- ¹⁴⁹ A. Lasia, *J. Electroanal. Chem.*, **397** (1995) 27.
- ¹⁵⁰ J.S. Newman and C.W. Tobias, *J. Electrochem. Soc.*, **109** (1962) 1183.
- ¹⁵¹ L.G. Austin and H. Lerner, *Electrochim. Acta*, **9** (1964) 1469.
- ¹⁵² S.K. Rangarajan, *J. Electroanal. Chem.*, **22** (1969) 89.
- ¹⁵³ M. Keddama, C. Rakomotavo, and H. Takenouti, *J. Appl. Electrochem.*, **14** (1984) 437.
- ¹⁵⁴ C. Cachet and R. Wiart, *J. Electroanal. Chem.*, **195** (1985) 21.
- ¹⁵⁵ I.D. Raistrick, *Electrochim. Acta*, **35** (1990) 1579.
- ¹⁵⁶ A. Lasia, *J. Electroanal. Chem.*, **428**, 155 (1997).
- ¹⁵⁷ R. de Levie, *Electrochim. Acta*, **10** (1965) 113.
- ¹⁵⁸ J. Gunning, *J. Electroanal. Chem.*, **392** (1995) 1.
- ¹⁵⁹ H. Keiser, K.D. Beccu, and M.A. Gutjahr, *Electrochim. Acta*, **21** (1976) 539.
- ¹⁶⁰ K. Eloot, F. Debuyck, M. Moors, and A.P. van Peteghem. *J. Appl. Electrochem.*, **25** (1995) 326, 334.
- ¹⁶¹ T.C. Halsey and M. Leibig, *Electrochim. Acta*, **36** (1991) 1699.
- ¹⁶² M. Leibig and T. Halsey, *J. Electroanal. Chem.*, **358** (1993) 77.
- ¹⁶³ G. Inzelt and G. Láng, *J. Electroanal. Chem.*, **378** (1994) 39.
- ¹⁶⁴ H.A. Kramers, *Phys. Zeit.*, **30** (1929) 52.
- ¹⁶⁵ R. de L. Kronig, *J. Opt. Soc. Am.*, **12** (1926) 547.
- ¹⁶⁶ H.W. Bode, *Network Analysis and Feedback Amplifier Design*, Van Nostrand, New York, 1945.
- ¹⁶⁷ D.D. Macdonald, M. Urquidi-Macdonald, *J. Electrochem. Soc.*, **132** (1985) 2316.
- ¹⁶⁸ M. Urquidi-Macdonald, S. Real and D.D. Macdonald, *J. Electrochem. Soc.*, **133** (1986) 2018.
- ¹⁶⁹ M. Urquidi-Macdonald, S. Real and D.D. Macdonald, *Electrochim. Acta*, **35** (1990) 1559.
- ¹⁷⁰ J.M. Esteban and M.E. Orazem, *J. Electrochem. Soc.*, **138** (1991) 67.
- ¹⁷¹ M.E. Orazem, J.M. Esteban and O.C. Moghissi, *Corrosion*, **47** (1991) 248.
- ¹⁷² D.D. Macdonald and M. Uurquidi-Macdonald, *J. Electrochem. Soc.*, **137** (1990) 515.
- ¹⁷³ M. Urquidi-Macdonald and D.D. Macdonald, *J. Electrochem. Soc.*, **137** (1990) 3306.
- ¹⁷⁴ D. Townley, *J. Electrochem. Soc.*, **137** (1990) 3305.
- ¹⁷⁵ P. Agarwal, M.E. Orazem, and L.H. Garcia-Rubio in *Electrochemical Impedance: Analysis and Interpretation*, ASTM STP 1188, J.R. Scully, D.C. Silverman, and M.W. Kending, Eds., ASTM, Philadelphia, 1993, p. 115.
- ¹⁷⁶ C. Gabrielli, M. Keddama, and H. Takenouti, in *Electrochemical Impedance: Analysis and Interpretation*, ASTM STP 1188, J.R. Scully, D.C. Silverman, and M.W. Kending, Eds., ASTM, Philadelphia, 1993, p. 140.
- ¹⁷⁷ B.J. Dougherty and S.I. Smedley in *Electrochemical Impedance: Analysis and Interpretation*, ASTM STP 1188, J.R. Scully, D.C. Silverman, and M.W. Kending, Eds., ASTM, Philadelphia, 1993, p. 154.

- ¹⁷⁸ R.V. Churchill and J.W. Brown, *Complex Variables and Applications*, McGraw-Hill, New York, 1990.
- ¹⁷⁹ M. Kendig and F. Mansfeld, *Corrosion*, **39** (1983) 466.
- ¹⁸⁰ C. Haili, M.Sc. Thesis, University of California, Berkeley, 1987.
- ¹⁸¹ P. Agarwal, M.E. Orazem, and L.H. Garcia-Rubio, *J. Electrochem. Soc.*, **139** (1992) 1917.
- ¹⁸² P. Agarwal and M.E. Orazem, *J. Electrochem. Soc.*, **142**, 4159 (1995).
- ¹⁸³ B.A. Boukamp, J.R. Macdonald, *Solid State Ionics*, **74** (1994) 85.
- ¹⁸⁴ B.A. Boukamp, *J. Electrochem. Soc.*, **142** (1995) 1885.
- ¹⁸⁵ J.R. Macdonald, *Electrochim. Acta*, **38** (1993) 1883.
- ¹⁸⁶ G. Láng, L. Kocsis, and G. Inzelt, *Electrochim. Acta*, **38** (1993) 1047.
- ¹⁸⁷ J.-P. Diard, P. Landaud, J.-M. Le Canut, B. Le Gorrec and C. Montella, *Electrochim. Acta*, **39** (1994) 2585.
- ¹⁸⁸ J. Max, *Méthodes et techniques de traitement du signal*, 4th edition, Masson, Paris (1985).
- ¹⁸⁹ J.S. Bendat and A.G. Piersol, *Measurements and Analysis of Random Data*, Wiley, New York, 1966.
- ¹⁹⁰ G.T. Burstein and C. Liu, *Electrochim. Acta*, **39** (1994) 873.
- ¹⁹¹ Z.B. Stoynov and B.S. Savova-Stoynov, *J. Electroanal. Chem.*, **183** (1985) 133.
- ¹⁹² B. Savova-Stoynov and Z.B. Stoynov, *Electrochim. Acta*, **37** (1992) 2353.
- ¹⁹³ Z.B. Stoynov, *Electrochim. Acta*, **37** (1992) 2357.
- Z. Stoynov, *Electrochim. Acta*, **38** (1993) 1919.
- ¹⁹⁵ M.E. Orazem, P. Agarwal, A.N. Jansen, P.T. Wojcik, and L.H. Garcia-Rubio, *Electrochim. Acta*, **38** (1993) 1903.
- ¹⁹⁶ M.E. Orazem, P. Agarwal, L.H. Garcia-Rubio, *J. Electroanal. Chem.*, **378** (1994) 51.
- ¹⁹⁷ Z.B. Stoynov and B. Savova-Stoynova, *J. Electroanal. Chem.*, **209** (1986) 11.
- ¹⁹⁸ Z. Stoynov, *Electrochim. Acta*, **34** (1989) 1187.
- ¹⁹⁹ Z. Stoynov, *Electrochim. Acta*, **35** (1990) 1493.
- ²⁰⁰ P. Zoltowski, *J. Electroanal. Chem.*, **375** (1994) 45.
- ²⁰¹ P. Zoltowski, *Polish J. Chem.*, **68** (1994) 1171.
- ²⁰² J.R. Macdonald, J. Schoonman, and A.P. Lehen, *J. Electroanal. Chem.*, **131** (1982) 77.
- ²⁰³ B.A. Boukamp, *Solid State Ionics*, **20** (1986) 31.
- ²⁰⁴ R.H. Milocco, *J. Electroanal. Chem.*, **273** (1989) 243.
- ²⁰⁵ W.H. Press, S.A. Teukolsky, W.V. Vetterling, and B.P. Flannery, *Numerical Recipes. The Art of Scientific Computing*, Cambridge University Press, Cambridge, 1992.
- ²⁰⁶ P.R. Bevington, *Data Reduction and Error Analysis for the Physical Sciences*, McGraw-Hill, New York, 1969.
- ²⁰⁷ J.R. Macdonald, *J. Electroanal. Chem.*, **307** (1991) 1.
- ²⁰⁸ P. Zoltowski, *J. Electroanal. Chem.*, **178** (1984) 11.
- ²⁰⁹ P. Agarwal, O.D. Crisalle, M.E. Orazem, and L.H. Garcia-Rubio, *J. Electrochem. Soc.*, **142**, 4149 (1995).
- ²¹⁰ P. Agarwal, M.E. Orazem, and L.H. Garcia-Rubio, *Electrochim. Acta*, **41** (1996) 1017.
- ²¹¹ Equivalent Circuit Analysis Technology, Sirotech Ltd., Ness-Ziona, Israel, 1994.
- ²¹² Y.-T. Tsai and D.W. Whitmore, *Solid State Ionics*, **7** (1982) 129.
- ²¹³ M.W. Kendig, E.M. Meyer, G. Lindberg, and F. Mansfeld, *Corr. Sci.*, **23** (1983) 1007.
- ²¹⁴ J.-P. Diard, B. Le Gorrec, and C. Montella, *J. Electroanal. Chem.*, **205** (1986) 77.
- ²¹⁵ G.W. Walter, D.N. Nguyen, and M.A.D. Madurasinghe, *Electrochim. Acta*, **37** (1992) 245.
- ²¹⁶ A.S. Barański and A. Szulborska, *Electrochim. Acta*, **41** (1996) 985.

- ²¹⁷ A.S. Barański and A. Moyana, *Langmuir*, **12** (1996) 3295.
- ²¹⁸ A.S. Barański and W. Lu, *J. Electroanal. Chem.*, **260** (1989) 1.
- ²¹⁹ G. Schöne and W. Wiesbeck, *J. Electroanal. Chem.*, **229** (1987) 407.
- ²²⁰ C. Gabrielli, M. Keddam and J.F. Lizee, *J. Electroanal. Chem.*, **163** (1984) 419.
- ²²¹ H. Göhr, M. Mirnik, and C.A. Shiller, *J. Electroanal. Chem.*, **180** (1984) 273.
- ²²² S.A.G.R. Karunathilaka, R. Barton, M. Hughes, and N.A. Hampson, *J. Appl. Electrochem.*, **15** (1985) 251.
- ²²³ S. Chechirlian, P. Eichner, M. Keddam, H. Takenouti, and H. Mazille, *Electrochim. Acta*, **35** (1990) 1125.
- ²²⁴ A. Lasia and P. Los, unpublished data, 1991.
- ²²⁵ W. Botter, Jr., D.M. Soares, and O. Teschke, *J. Electroanal. Chem.*, **267** (1989) 279.
- ²²⁶ S. Fletcher and M.D. Horne, *J. Electroanal. Chem.*, **297** (1991) 297.

(a)



(b)

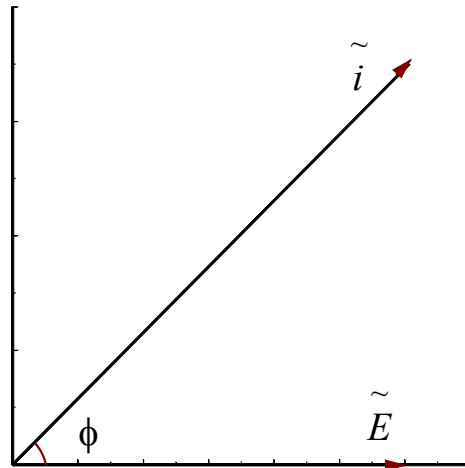
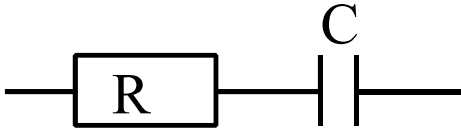
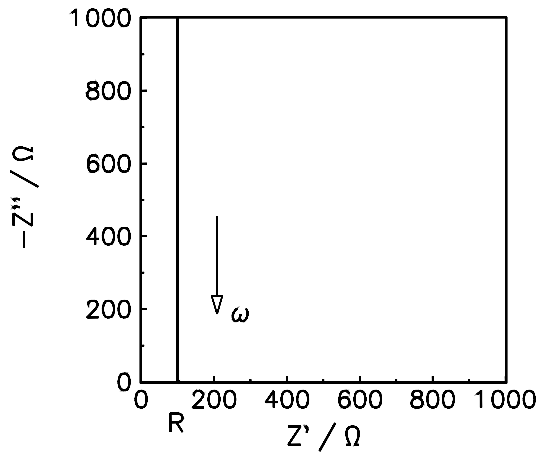


Figure 1. Representation of ac signals: (a) rotating voltage and current vectors in time space; (b) voltage and current phasors in frequency space.

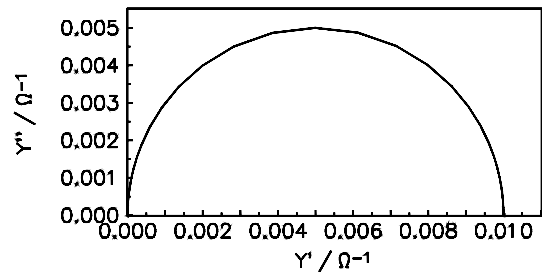
a)



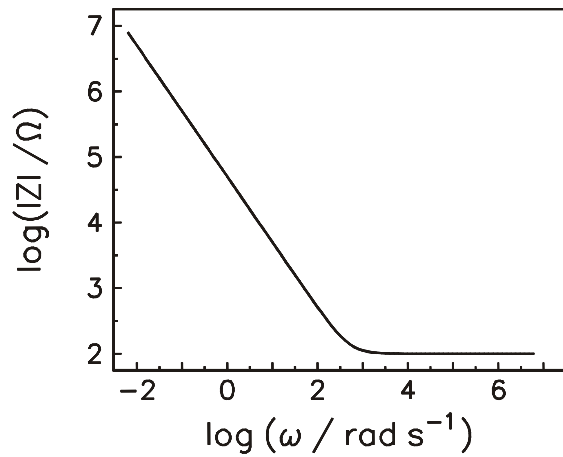
b)



c)



d)



e)

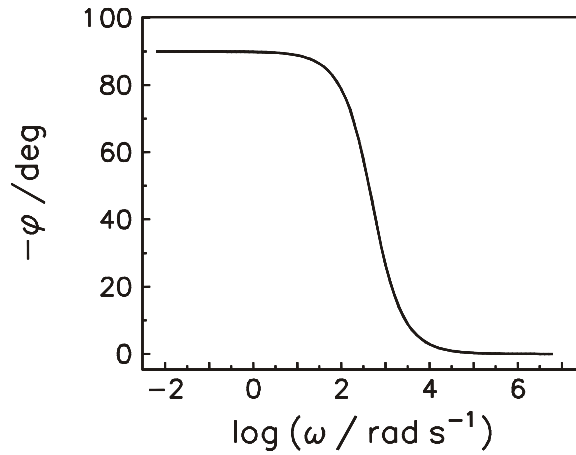
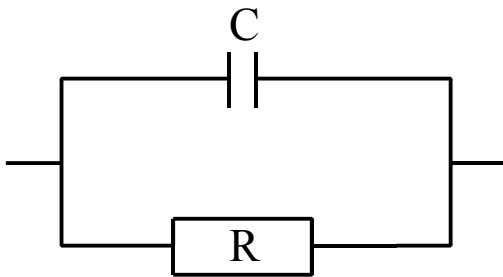
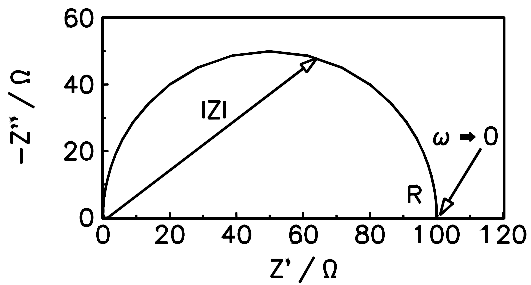


Figure 2. Complex plane (b), (c) and Bode (d), (e), plots for a series connection of a resistance and a capacitance, (a) ; $R = 100 \Omega$, $C = 20 \mu\text{F}$.

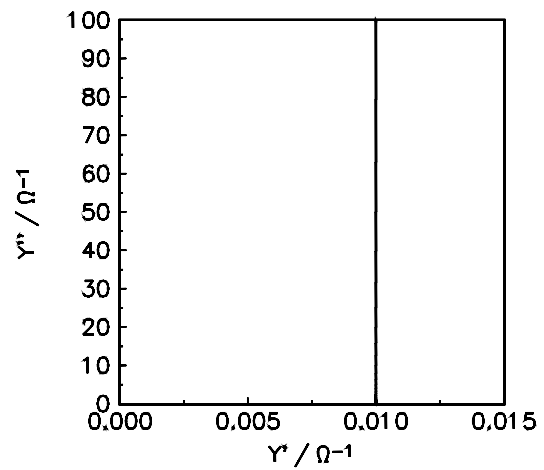
a)



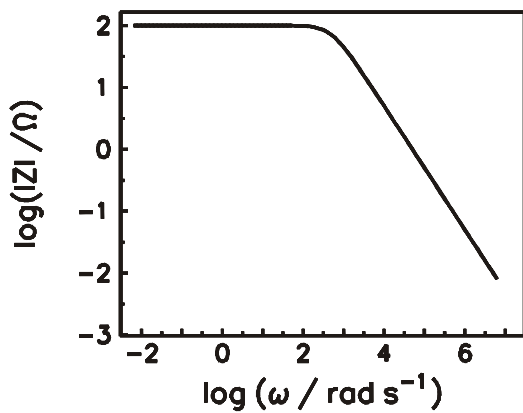
b)



c)



d)



e)

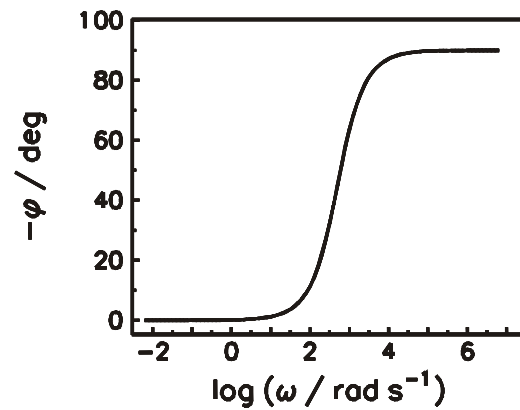
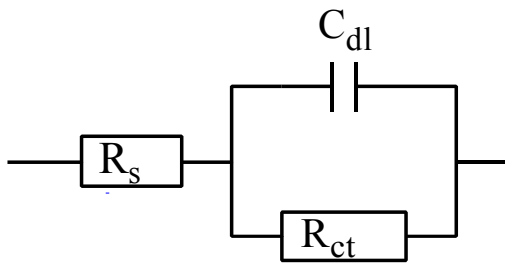
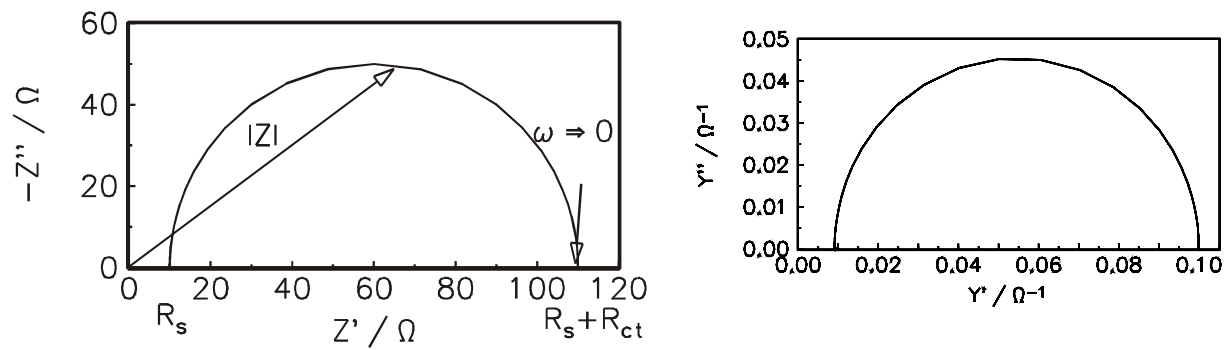


Figure 3. Complex plane (b), (c) and Bode (d), (E), plots for a parallel connection of R and C (a); $R = 100 \Omega$, $C = 20 \mu\text{F}$.

a)

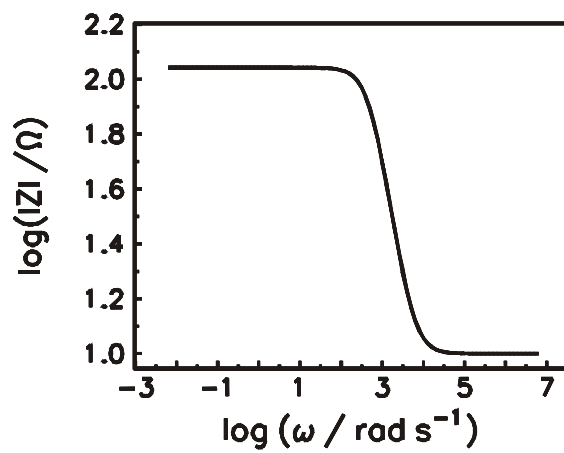


b)



c)

d)



e)

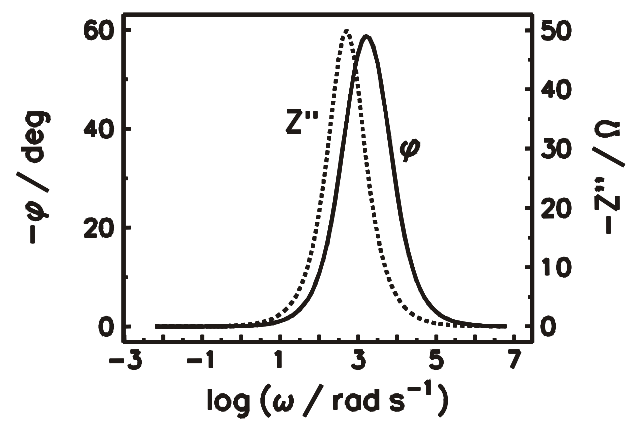


Figure 4. Complex plane (b), (c) and Bode (d), (e), plots for the circuit (a); $R_s = 10 \Omega$, $R_{ct} = 100 \Omega$, $C_{dl} = 20 \mu\text{F}$.

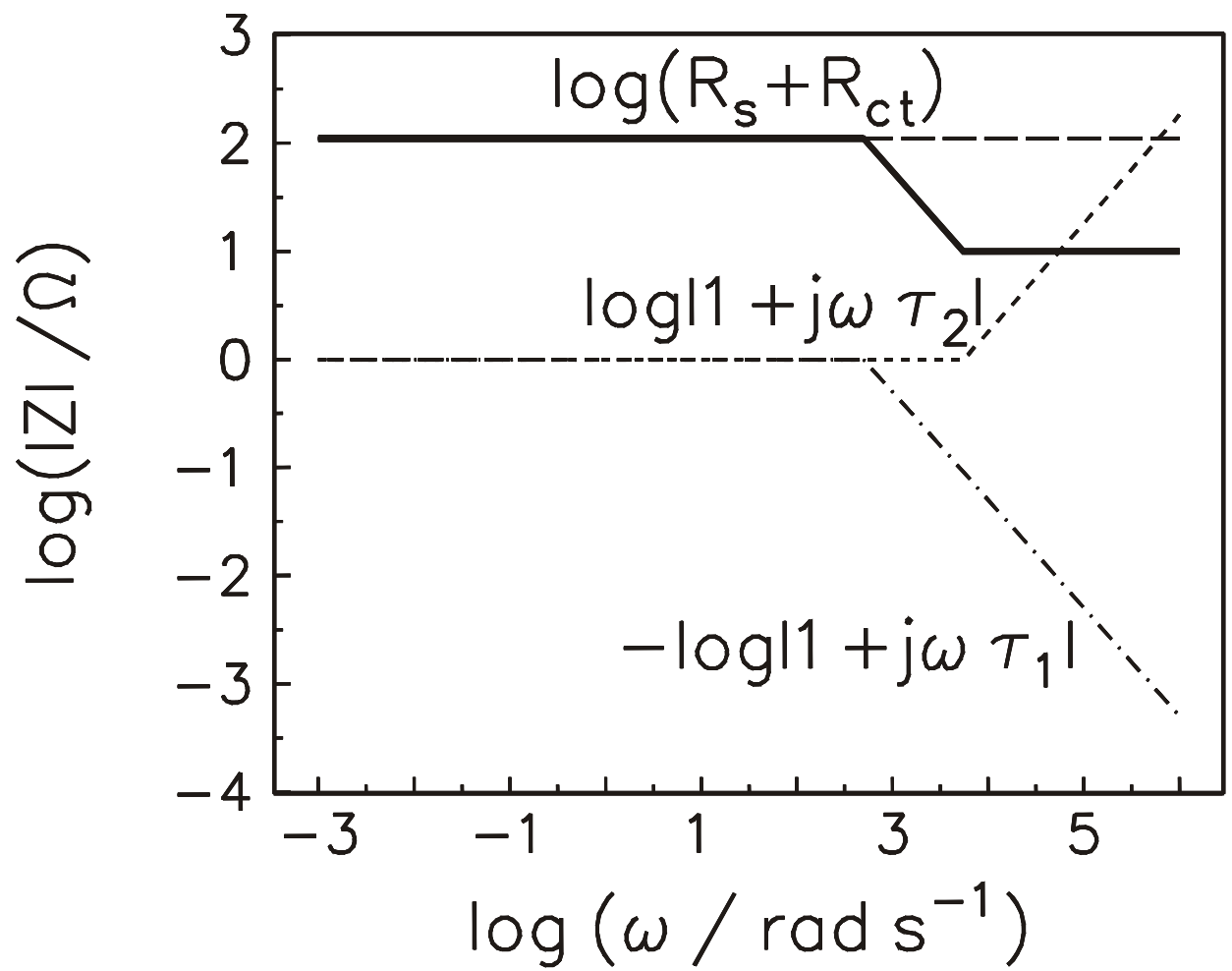


Figure 5. Construction of the Bode magnitude plot for the circuit in Figure 4a using eqn. (26). The solid line is a sum of all three contributions.

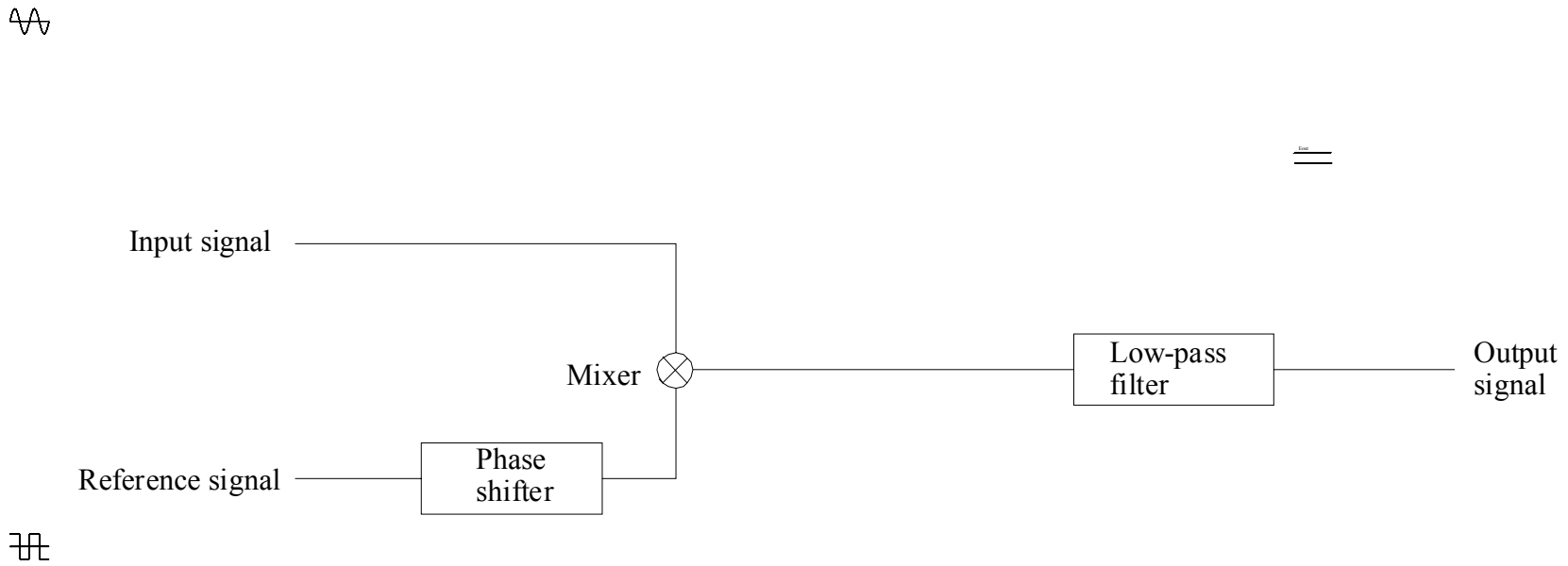


Figure 6. Schematic operation of a lock-in amplifier.

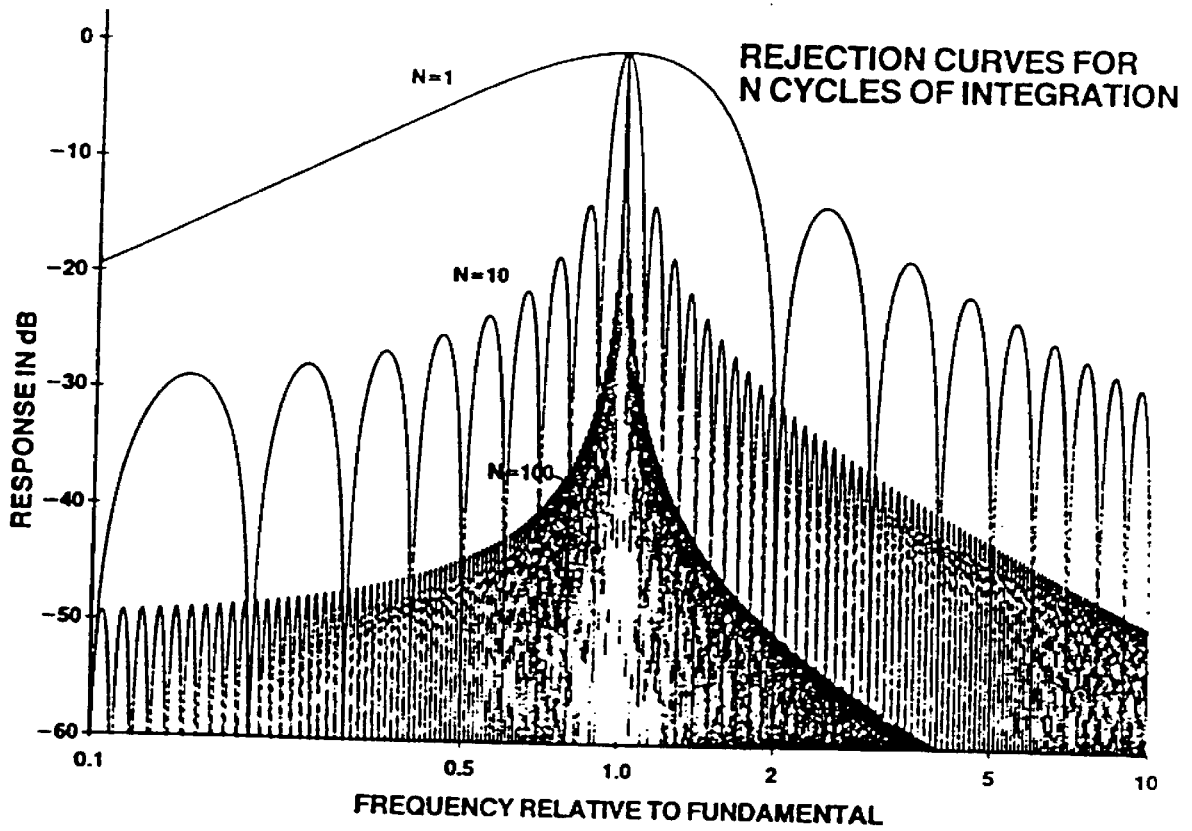


Figure 7. Frequency response of a FRA averaging filter for different numbers of integration cycles.⁴⁴

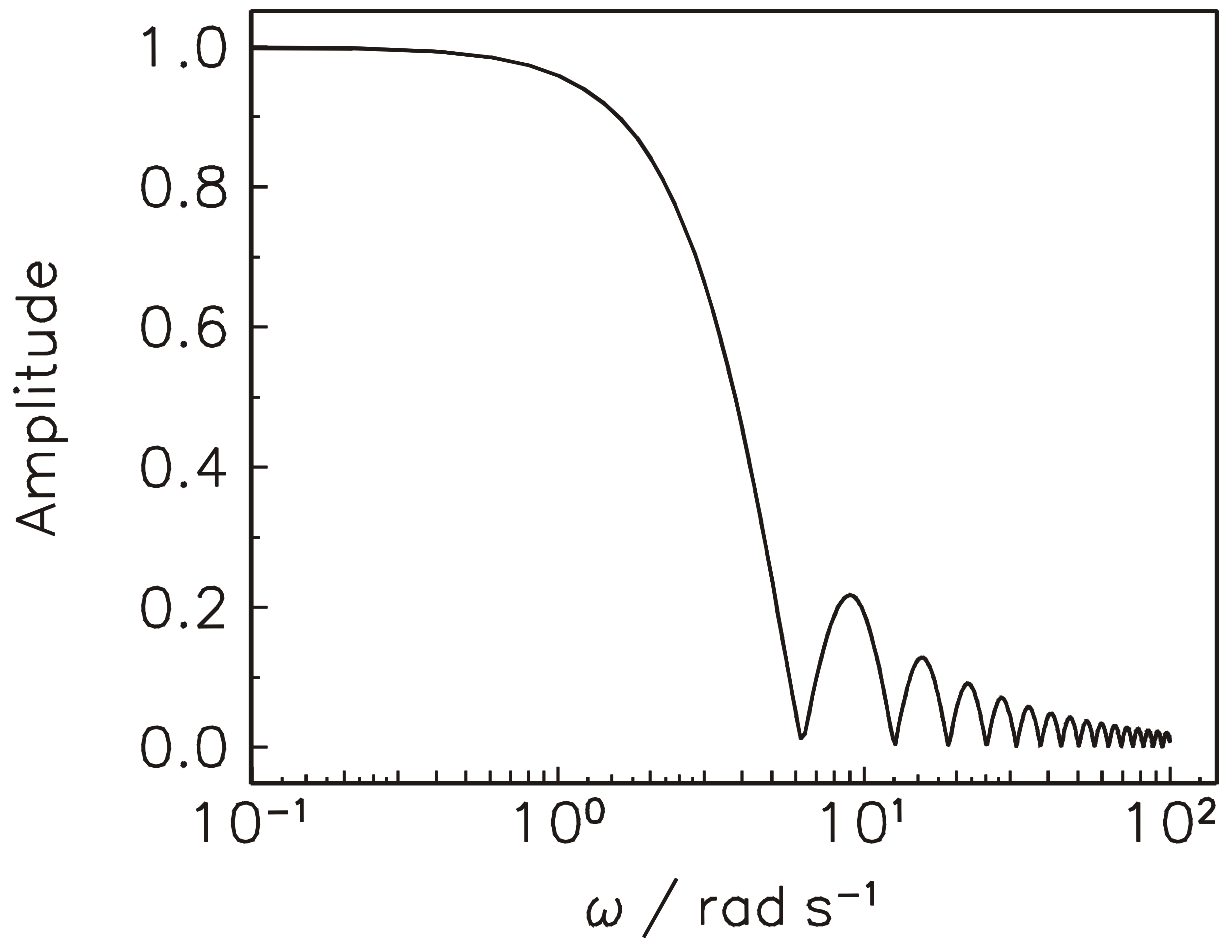


Figure 8. FFT amplitude, $|H(j\omega)|$, of the pulse function, eqn. (38), of duration $T_0 = 1$ s.

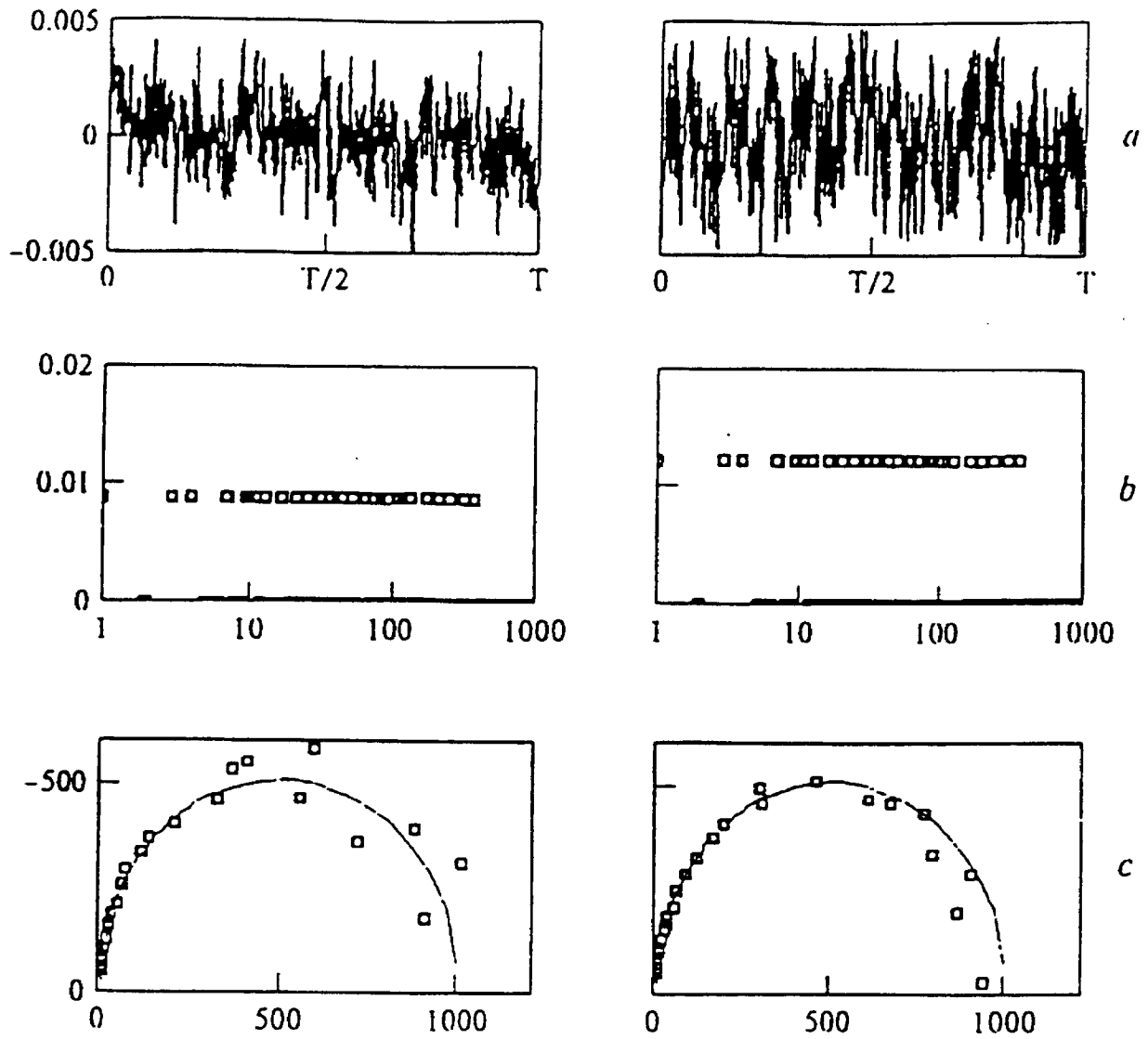


Figure 9. FFT analysis of the sum of sine waves perturbation; left - no optimization, right - optimization of phases; a) perturbation voltage in the time domain, b) perturbation voltage in the frequency domain, c) complex plane plots of simulated impedance spectra with 5% noise added to the current response.⁵¹ Solid lines show response without noise.

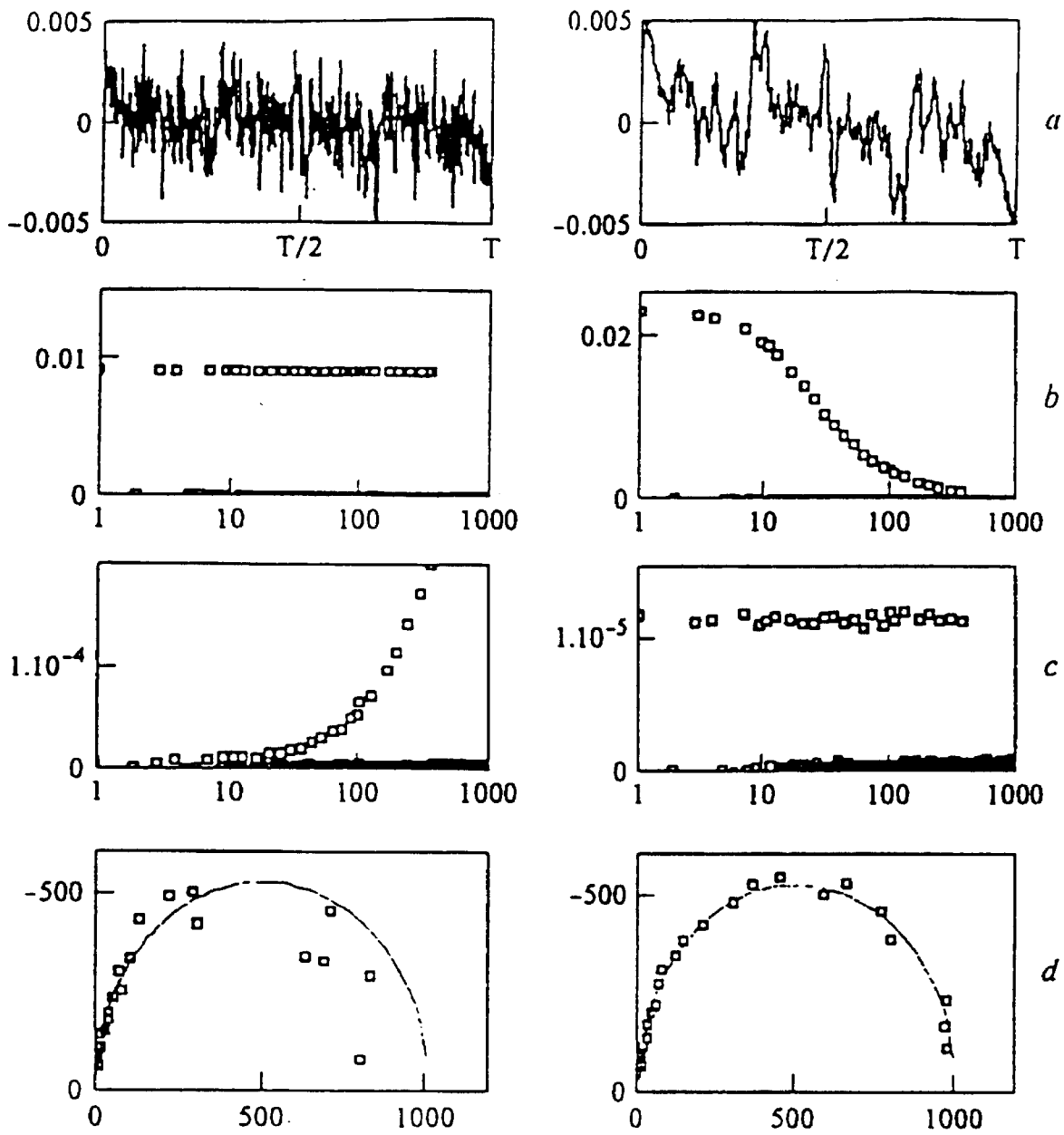
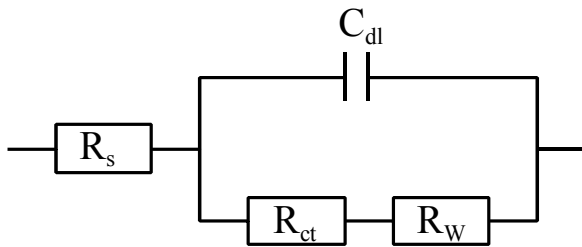
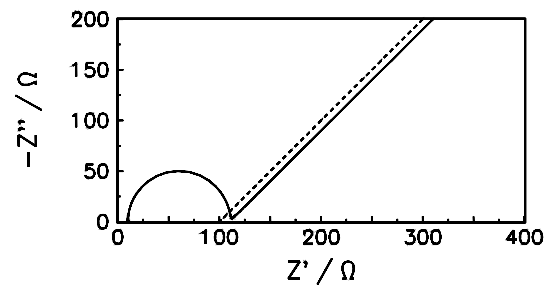


Figure 10. FFT analysis of the sum of sine waves perturbation; left - no optimization, right - optimization of amplitudes; a) perturbation voltage in the time domain, b) perturbation voltage in the frequency domain, c) current response with 10% noise added, presented in frequency domain, d) complex plane plots of simulated impedance spectra with 10% noise added to the current response. Solid lines show response without noise.⁵¹

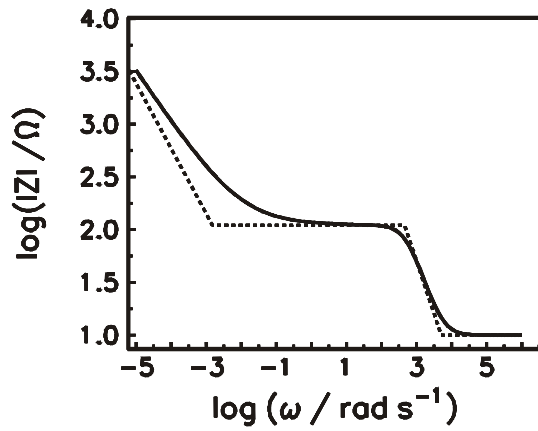
(a)



(b)



(c)



(d)

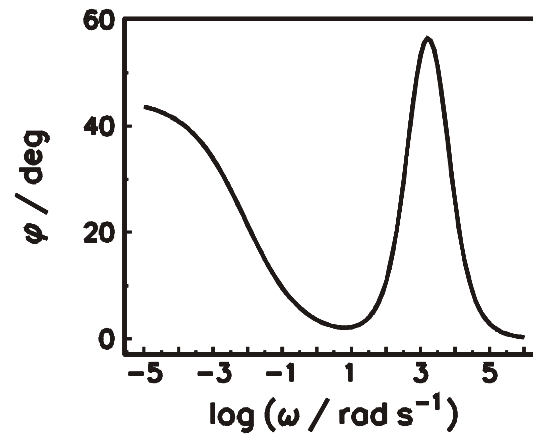


Figure 11. Complex plane (b) and Bode (c), (d), plots for the semi-infinite linear diffusion model (a); in (b) continuous line: total impedance, dashed line: faradaic impedance; $R_s = 10 \Omega$, $R_{ct} = 100 \Omega$, $C_{dl} = 20 \mu\text{F}$, $\sigma = 10 \Omega \text{ s}^{-1/2}$.

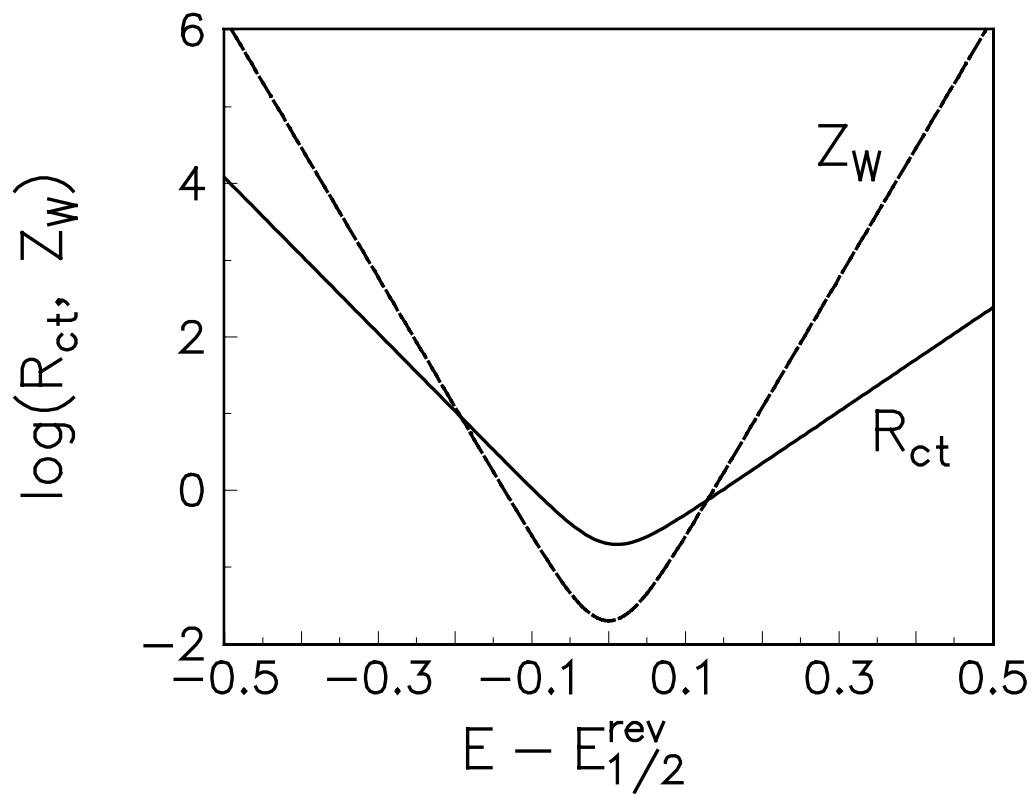


Figure 12. Dependence of logarithms of R_{ct} and $|Z_w|$ on potential for $\alpha = 0.4$.

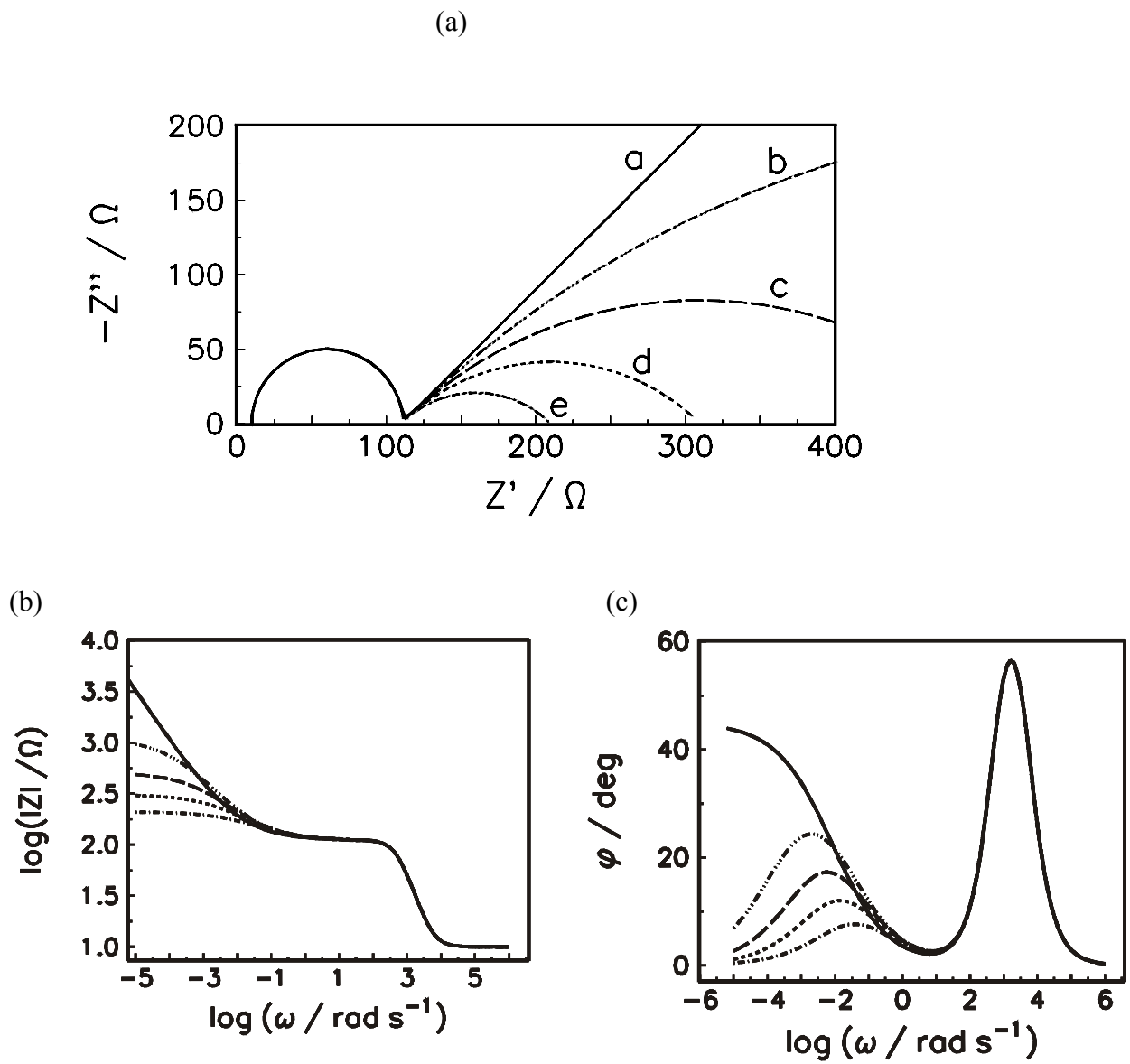


Figure 13. Complex plane (a) and Bode (b), (c) plots for semi-infinite spherical diffusion; sphericity parameter $\sqrt{2D_i}/r_0$: (a) ∞ - linear diffusion, (b) 0.02, (c) 0.05, (d) 0.1, (e) $0.2 \text{ s}^{-1/2}$; $R_s = 10 \Omega$, $R_{ct} = 100 \Omega$.

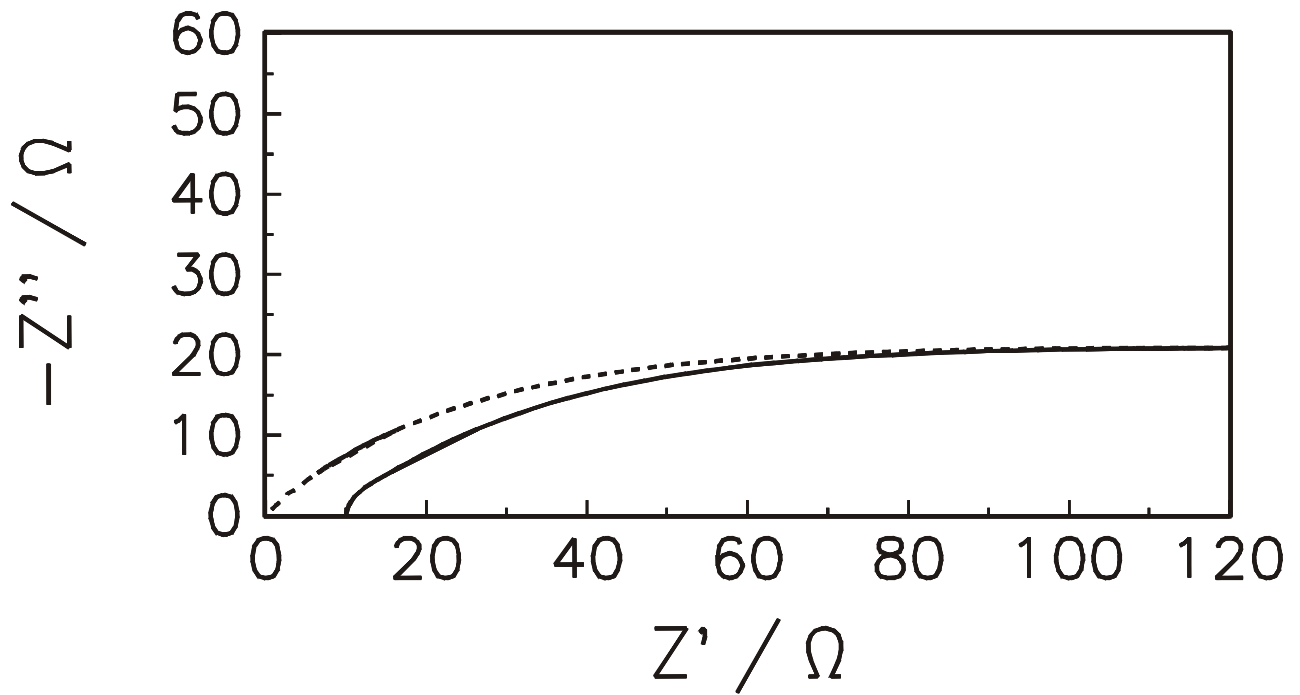


Figure 14. Faradaic (dashed line) and total (continuous line) impedance for a reversible reaction in the conditions of semi-infinite cylindrical diffusion, $R_s = 10 \Omega$.

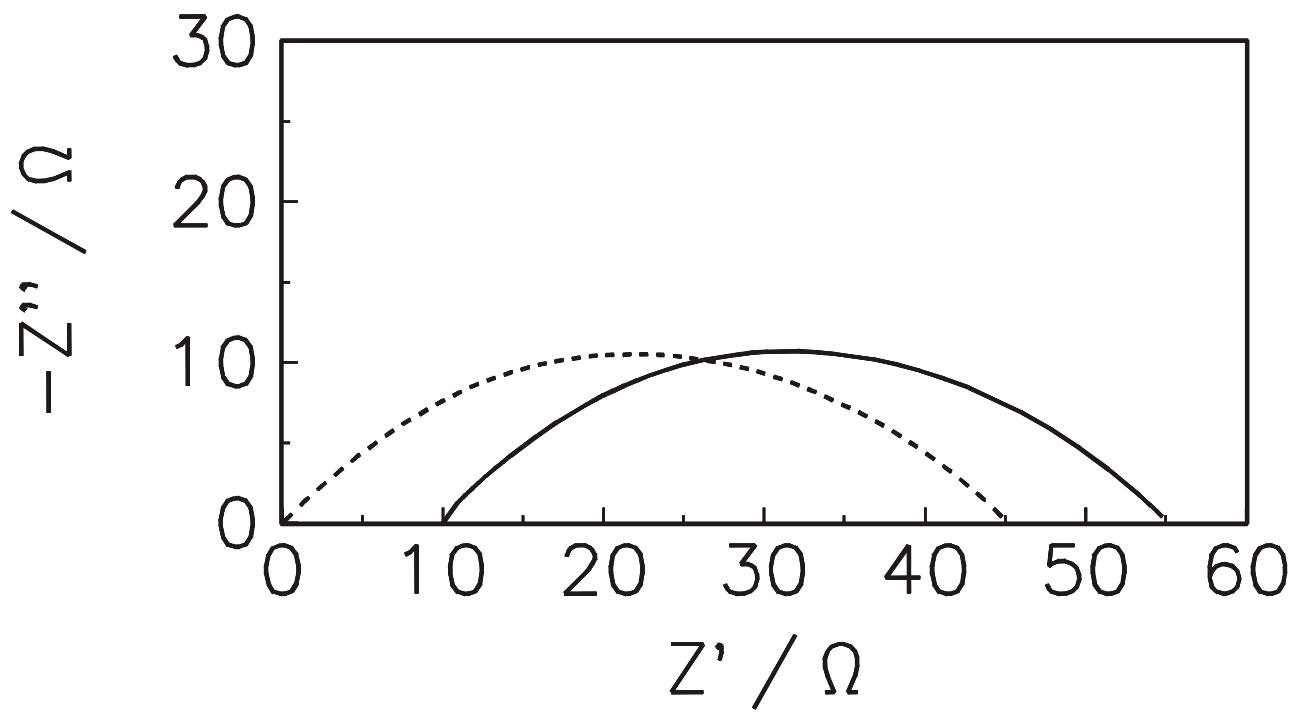


Figure 15. Faradaic (dashed line) and total (continuous line) impedances in the conditions of the diffusion to a disk and a reversible charge transfer.

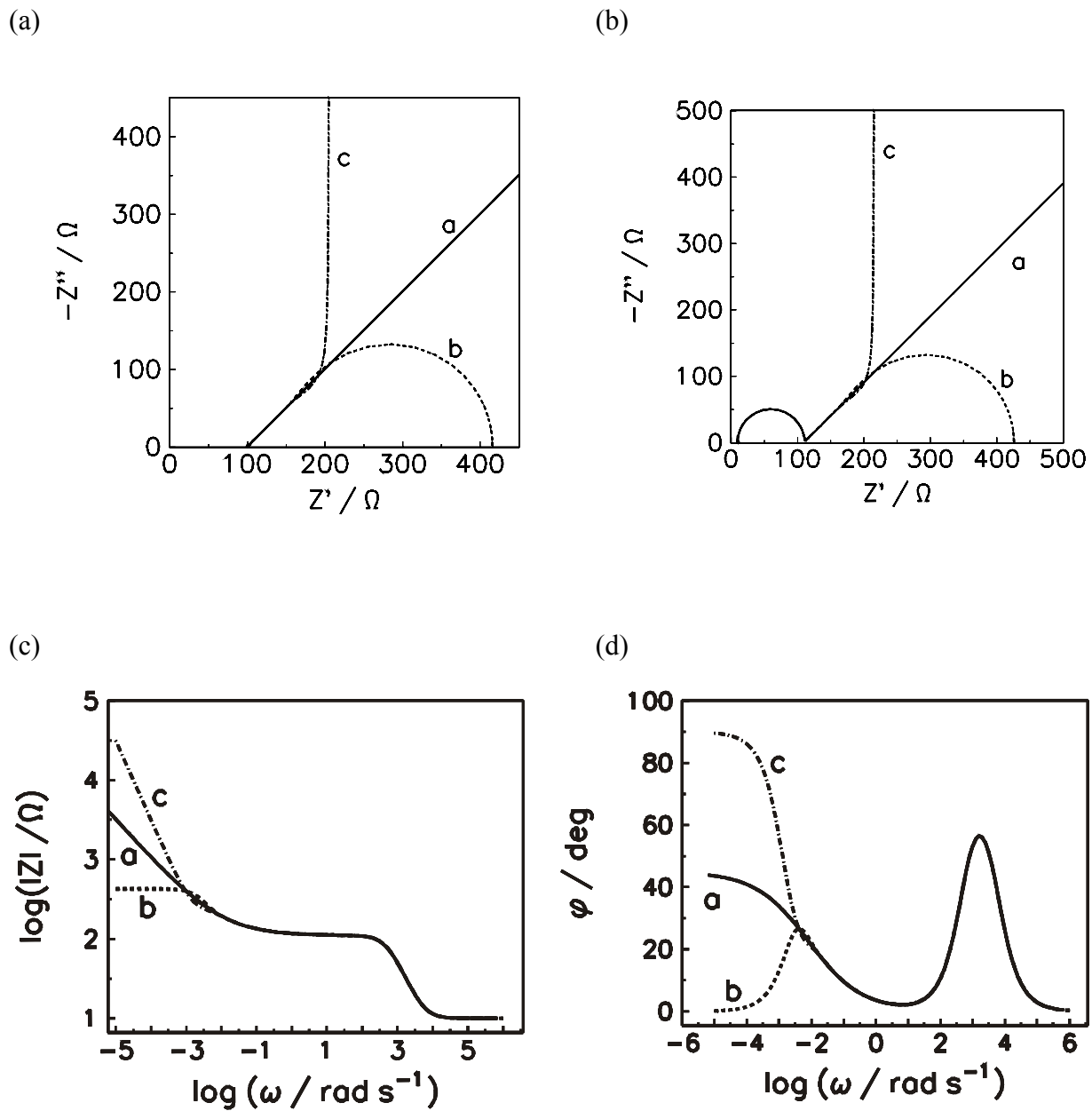


Figure 16. Faradaic (a) and total (b)-(d) impedances for: a) - linear semi-infinite, b) - finite transmissive, and c) - finite reflective boundaries, $R_s = 10 \Omega$, $R_{ct} = 100 \Omega$.

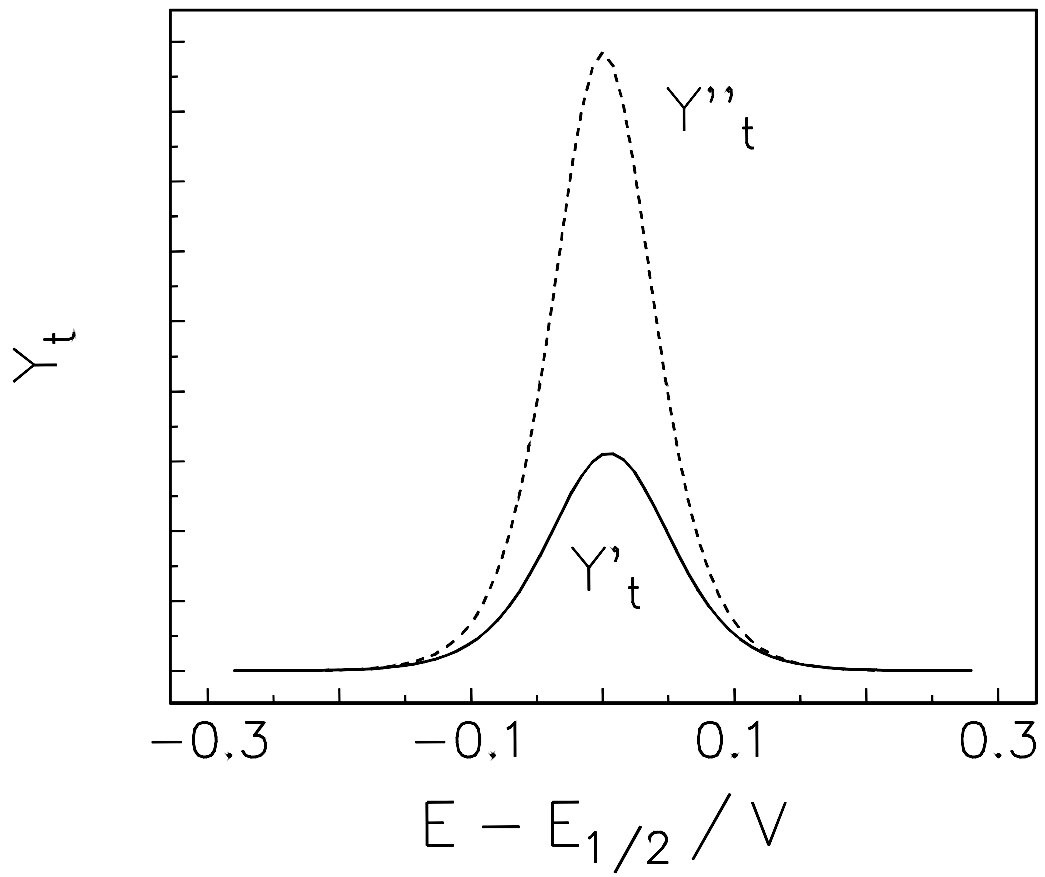


Figure 17. Dependence of the real and imaginary admittances for a diffusion-kinetic process on the electrode potential.

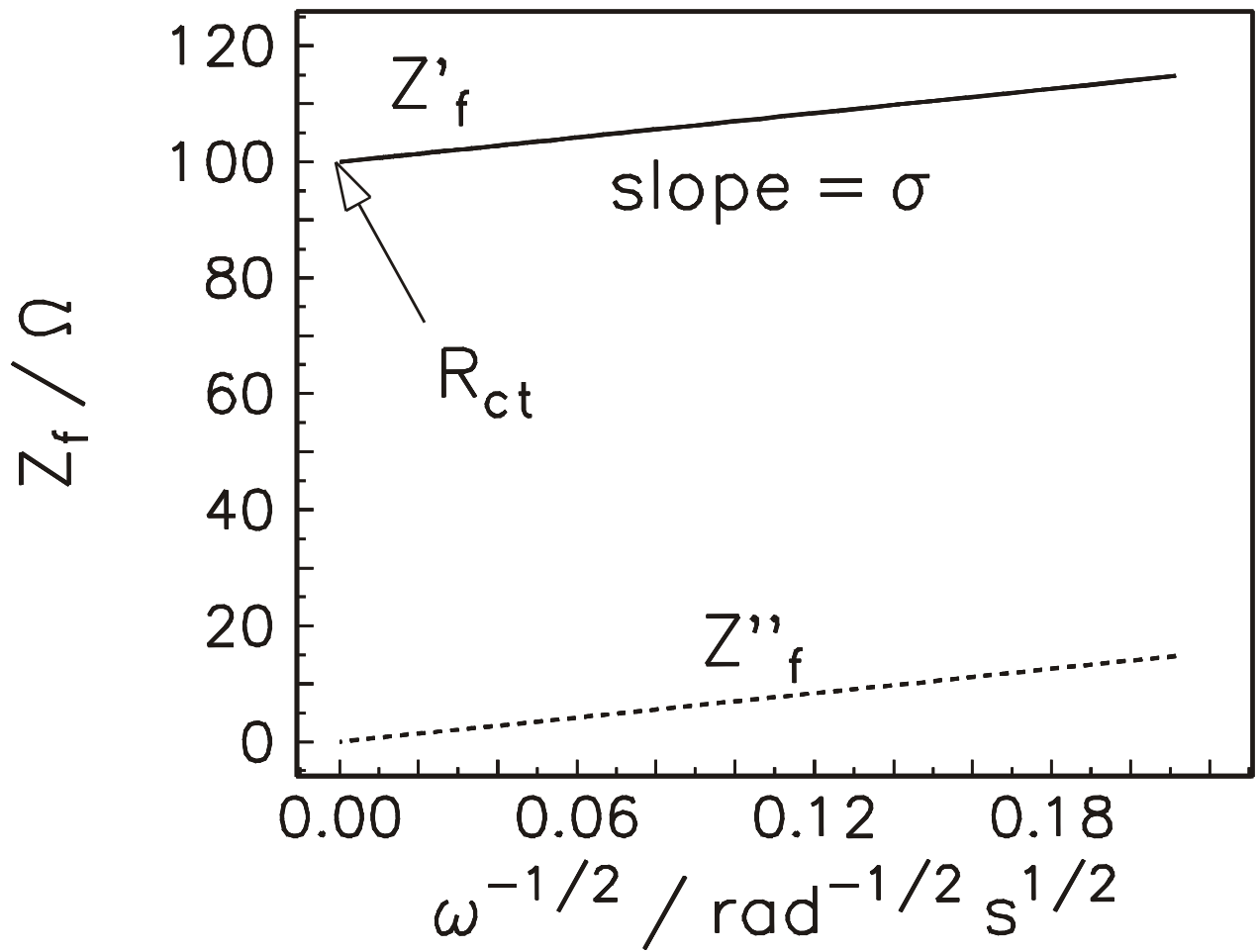


Figure 18. Dependence of real and imaginary parts of the faradaic impedance of a diffusion-kinetic process on $\omega^{-1/2}$ at constant potential.

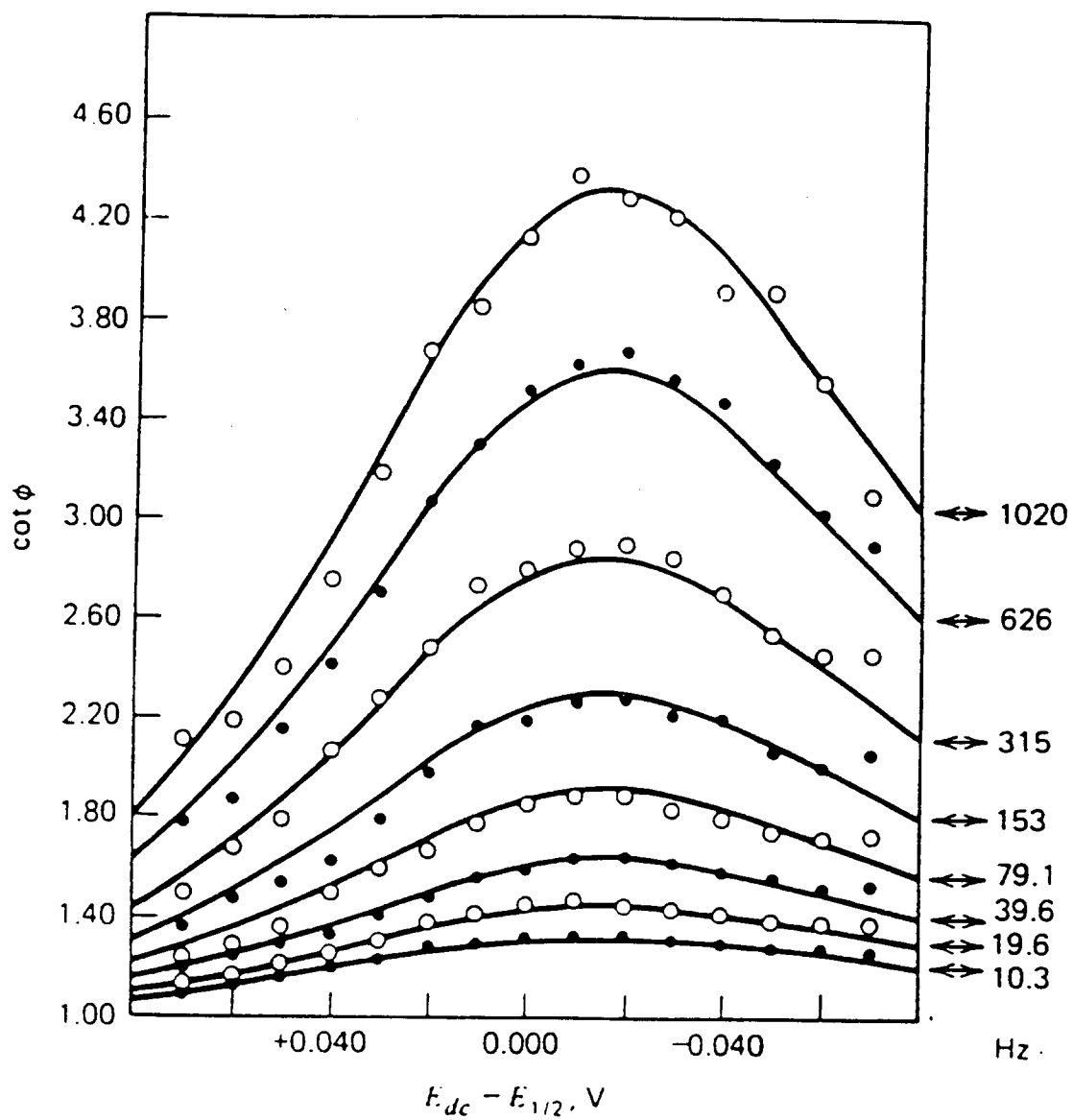


Figure 19. Dependence of $\cot \phi$ as a function of potential for TiCl_4 reduction in $\text{H}_2\text{C}_2\text{O}_4$ at various frequencies.⁷⁷

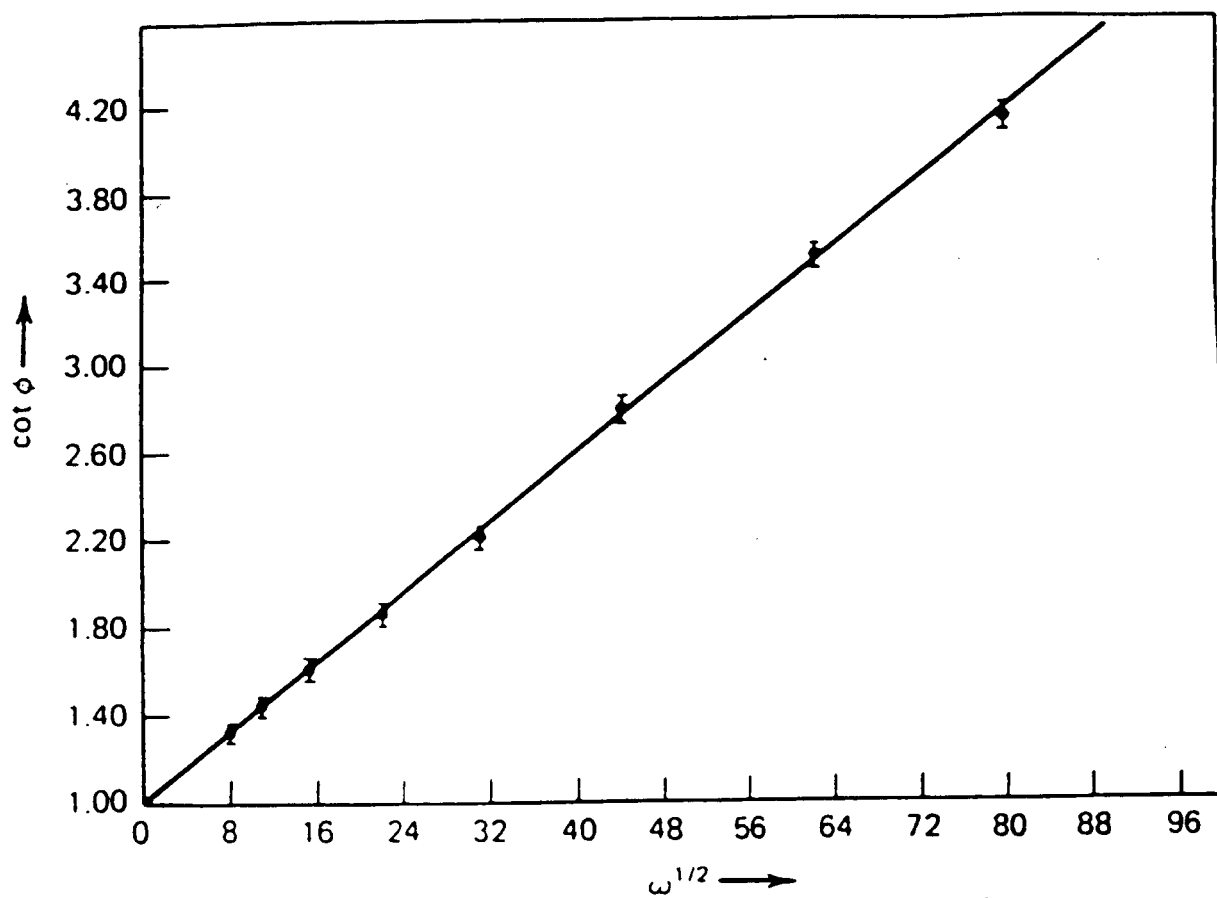


Figure 20. . Dependence of $\cot \phi$ vs. $\omega^{1/2}$ for TiCl_4 reduction in $\text{H}_2\text{C}_2\text{O}_4$. Data from ref. 77.

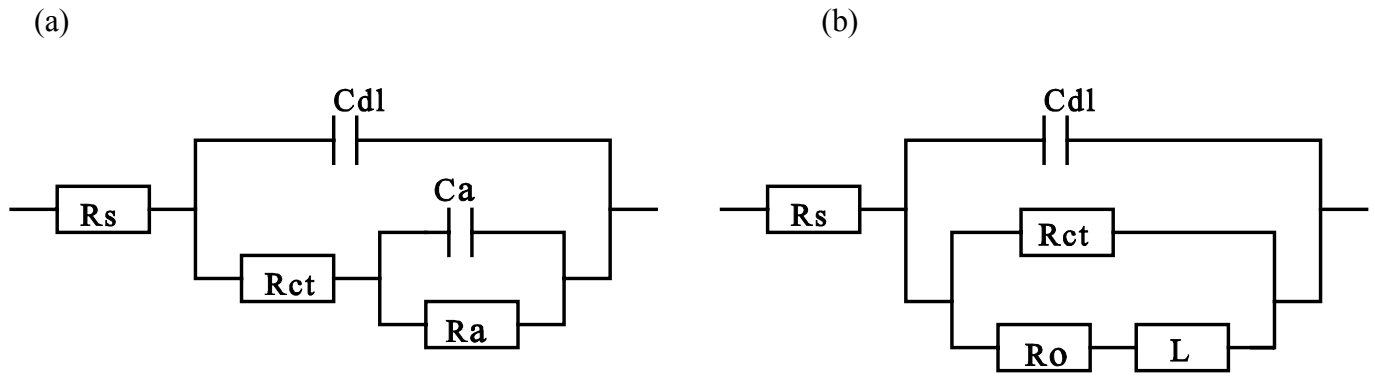


Figure 21. Equivalent circuit for the case of one adsorbed species: a) for $B < 0$, b) $B > 0$.

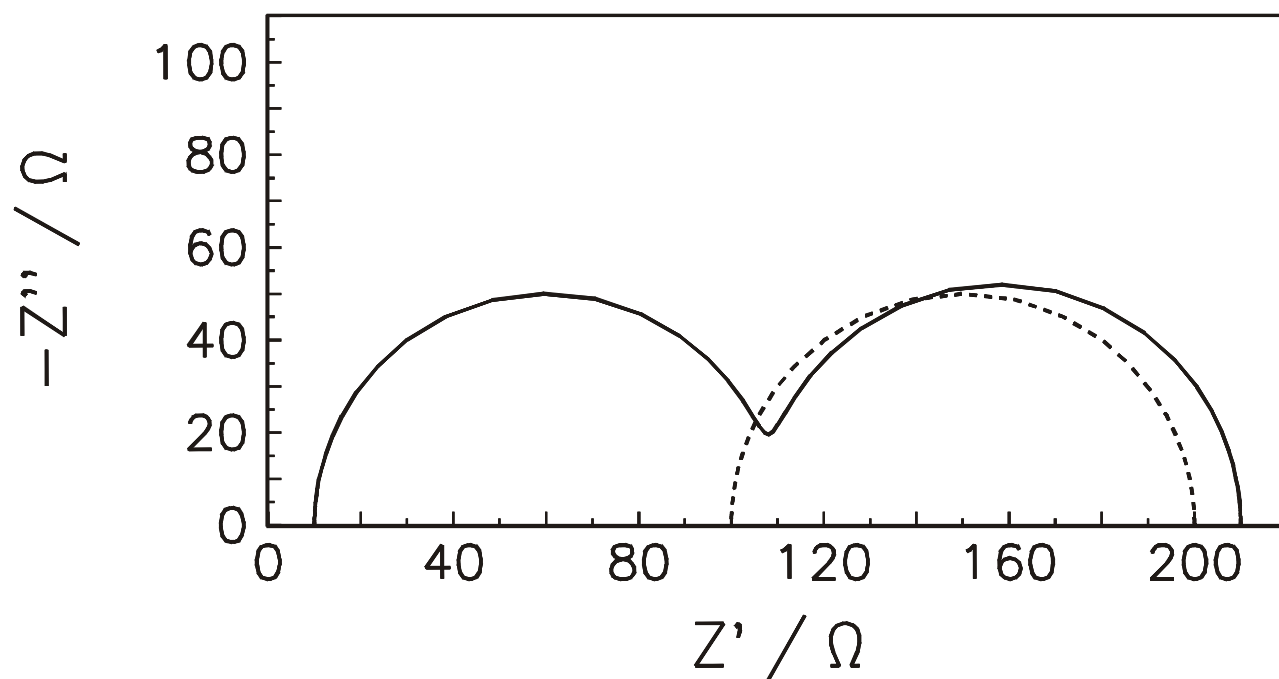


Figure 22. Complex plane plots for the case of one adsorbed species and $B < 0$, eqns. (139)-(140); continuous line - total impedance, dashed line - faradaic impedance; parameters used: $R_{ct} = 100 \Omega$, $R_a = 100 \Omega$, $C_a = 2 \times 10^{-3} \text{ F}$, $C_{dl} = 2 \times 10^{-5} \text{ F}$, $R_s = 10 \Omega$.

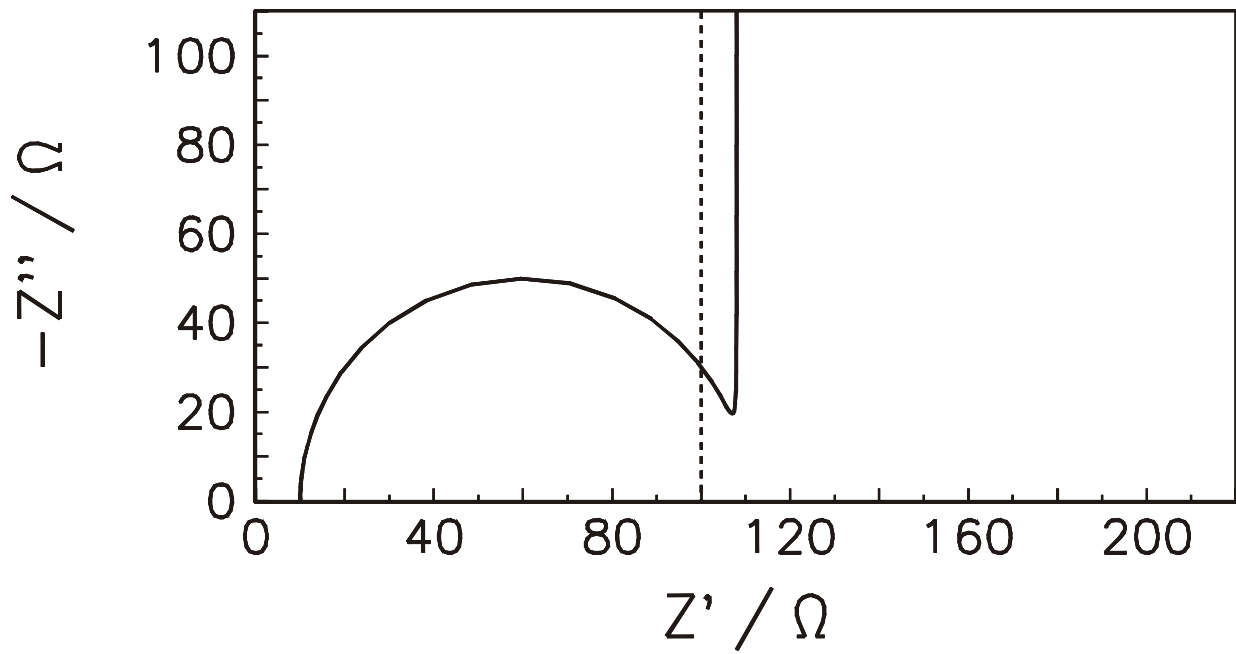


Figure 23. Complex plane plot for the case of one adsorbed species, $B < 0$ and $C - R_{ct} |B| = 0$; continuous line - total impedance, dashed line - faradaic impedance; parameters used: $R_{ct} = 100 \Omega$, $C_a = 2 \times 10^{-3} \text{ F}$, $C_{dl} = 2 \times 10^{-5} \text{ F}$, $R_s = 10 \Omega$.

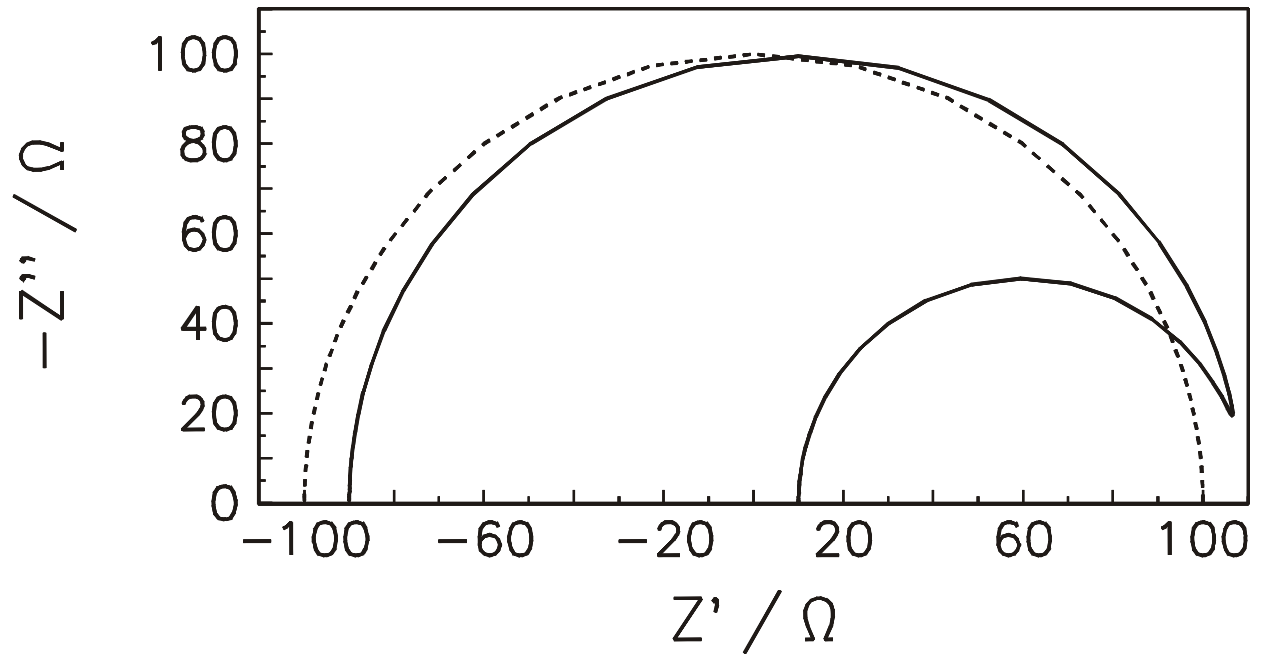


Figure 24. Complex plane plot for the case of one adsorbed species, $B < 0$ and $C - R_{ct} |B| < 0$; continuous line - total impedance, dashed line - faradaic impedance; parameters used: $R_{ct} = 100 \Omega$, $R_a = -200 \Omega$, $C_a = 2 \times 10^{-3} \text{ F}$, $C_{dl} = 2 \times 10^{-5} \text{ F}$, $R_s = 10 \Omega$.

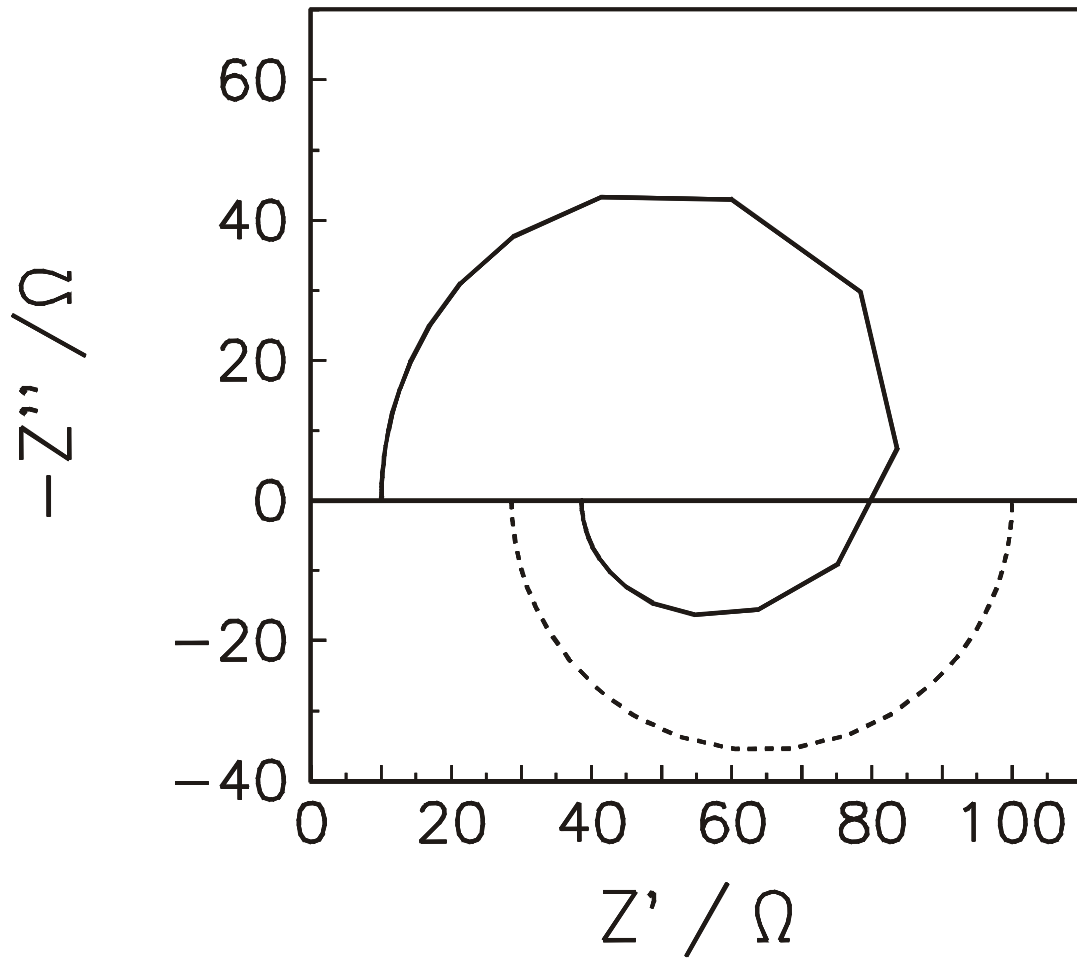


Figure 25. Complex plane plots for the case of one adsorbed species and $B > 0$, eqns. (144)-(146); continuous line - total impedance, dashed line - faradaic impedance; parameters used: $R_{ct} = 100 \Omega$, $R_o = 40 \Omega$, $L = 0.2 \text{ H}$, $C_{dl} = 2 \times 10^{-5} \text{ F}$, $R_s = 10 \Omega$.

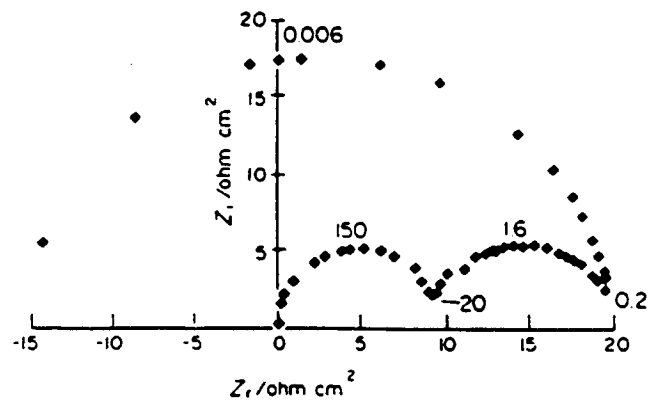
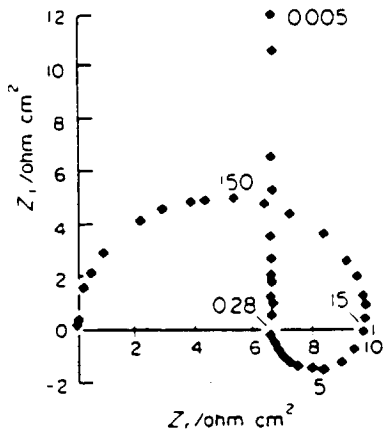
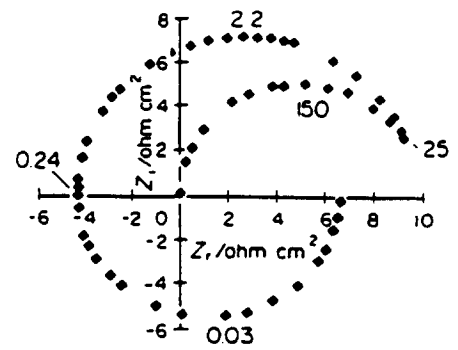
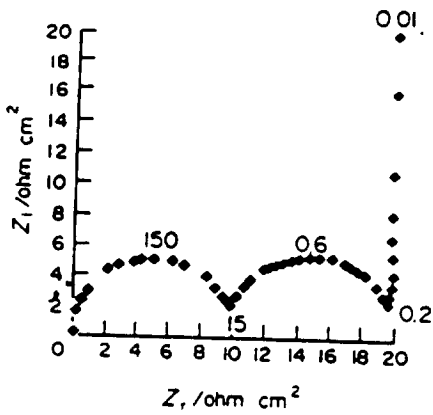
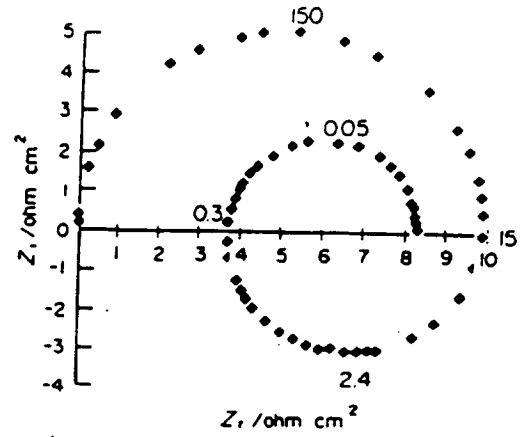
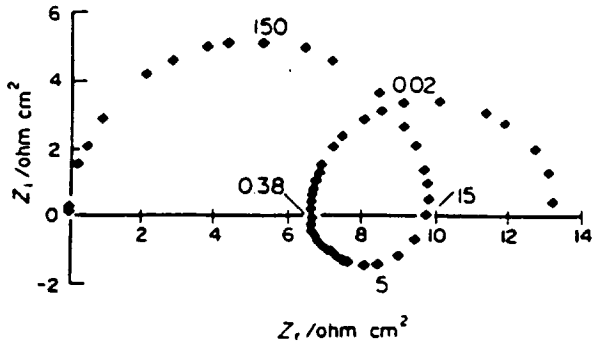


Figure 26. Some examples of the complex plane plots obtained for the case of two adsorbed species.⁹⁴

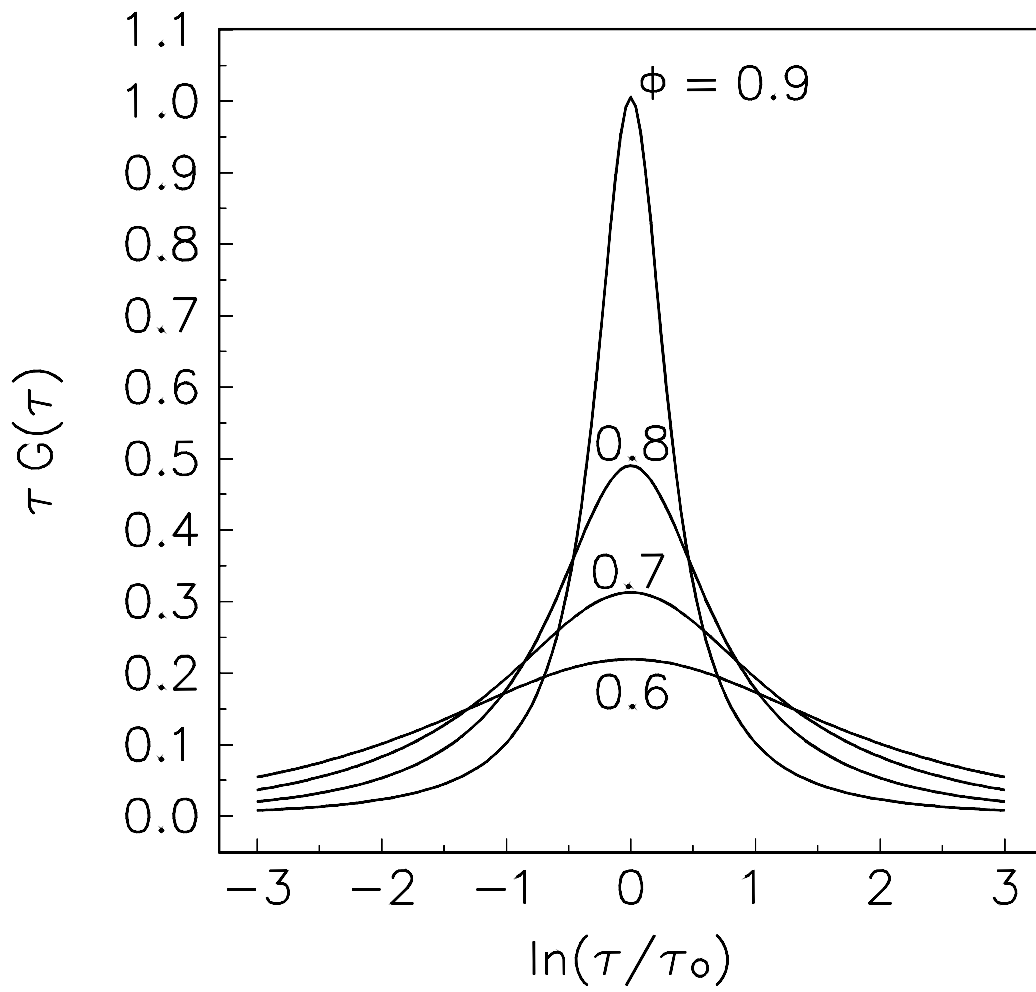
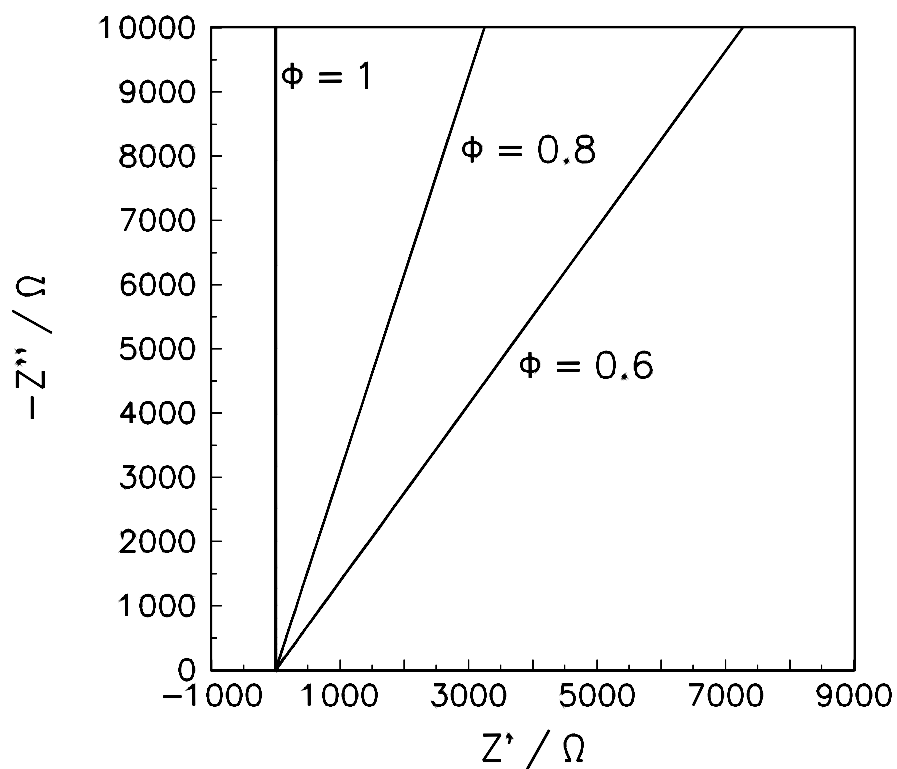


Figure 27. The distribution function $\tau G(\tau)$ versus $\ln(\tau/\tau_0)$ according to eqn. (176).

a)



b)

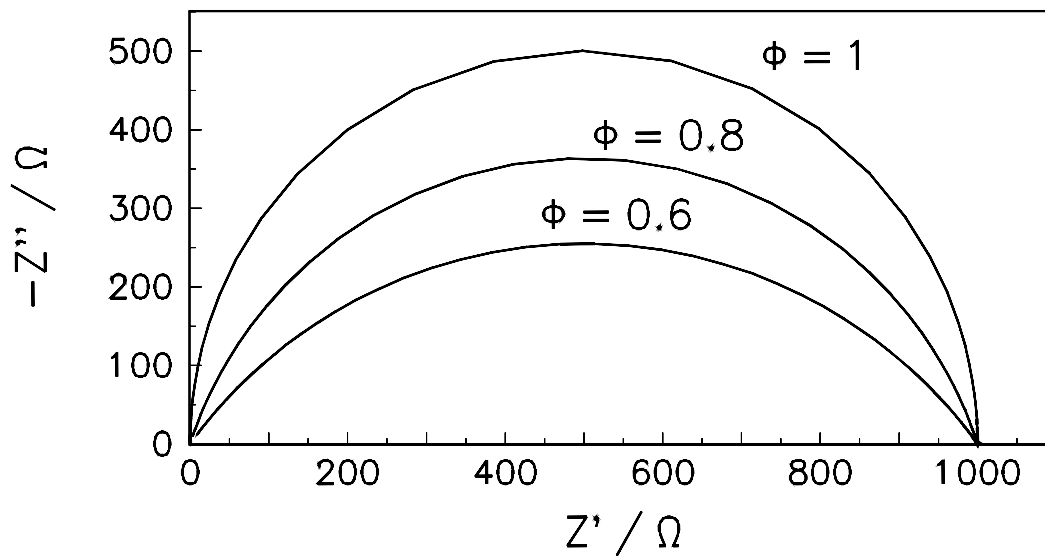


Figure 28. Complex plane plots in the presence of a CPE element: a) ideally polarizable electrode, b) in the presence of faradaic reaction.

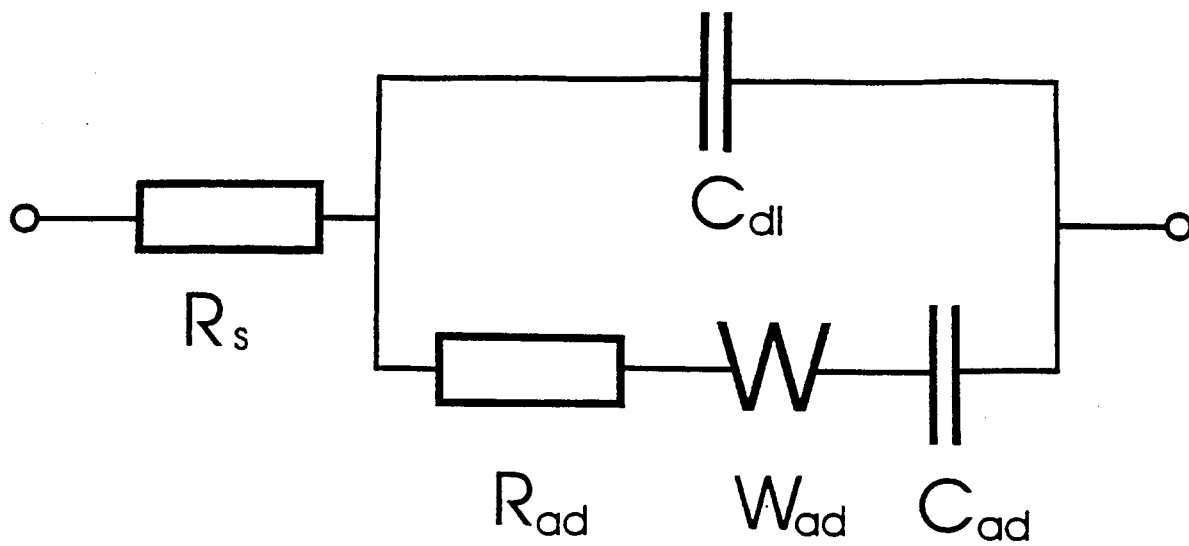


Figure 29. Equivalent-circuit model of the electrode in the presence of adsorption.¹⁰⁷

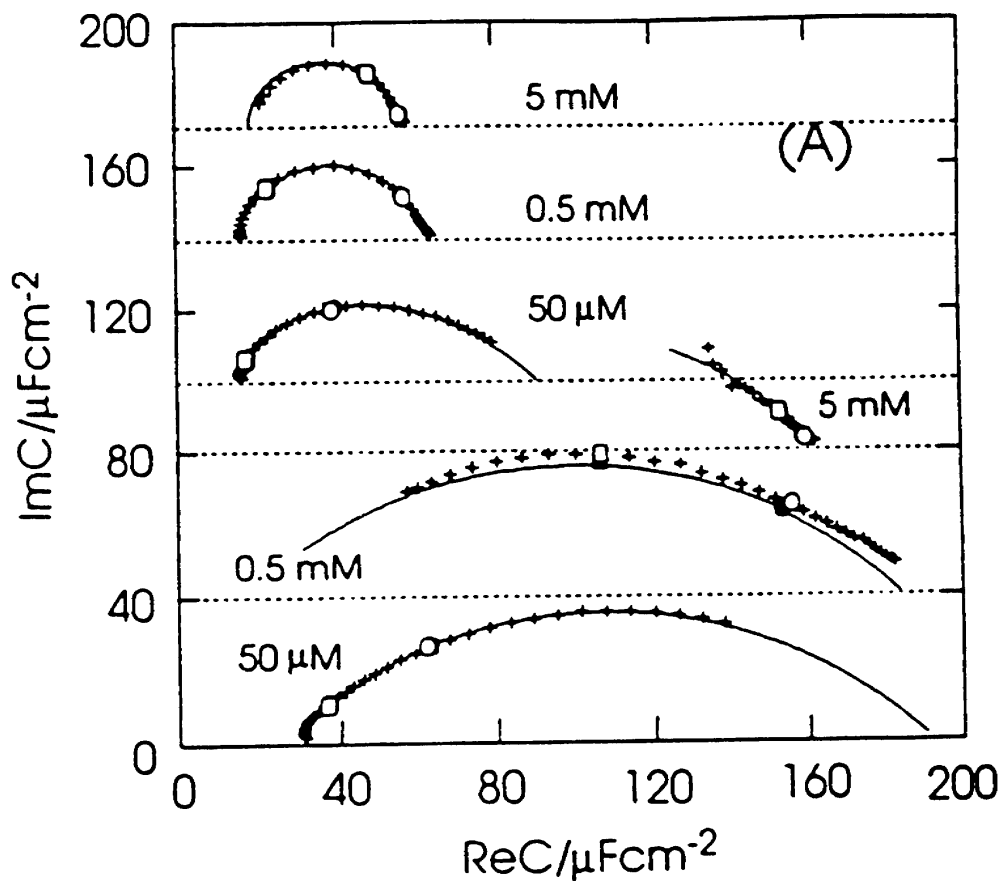


Figure 30. Nyquist plot of complex capacitances for Au(111) in 0.1 M HClO_4 in the presence of bromide ions; Br^- concentrations given in the figure, upper three curves at $E = 0.3$ V, lower three curves at $E = 0.1$ V vs. SCE.¹⁰⁷

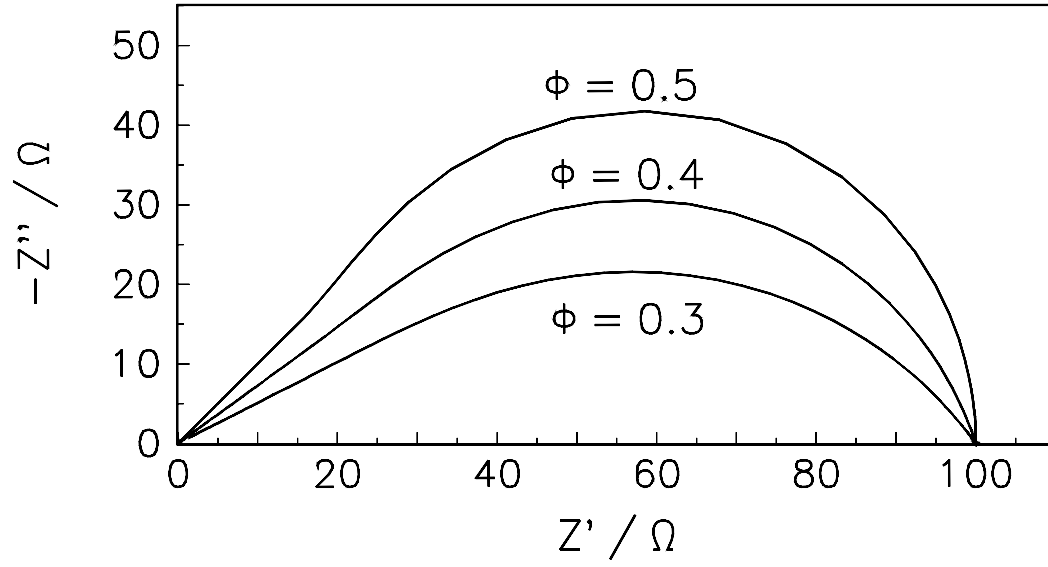


Figure 31. Complex plane plots for the bounded thickness impedance (BCP) for $R_s = 100 \Omega$, $T = 0.01 \text{ F cm}^{-2} \text{ s}^{\phi-1}$, and different values of parameter ϕ .

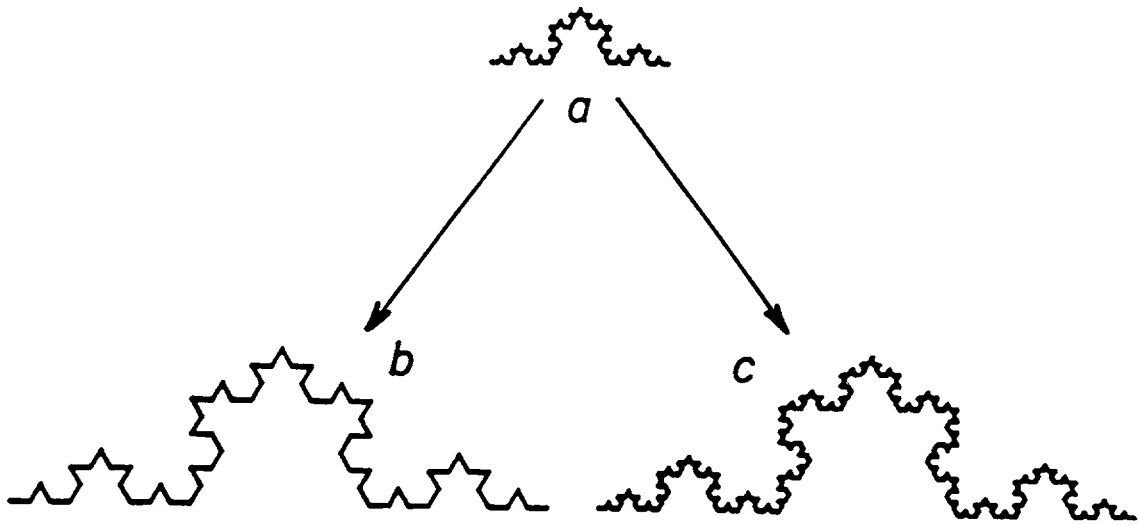


Figure 32. Comparison of a simple (b) and fractal (c) magnifications of the image (a).¹¹¹

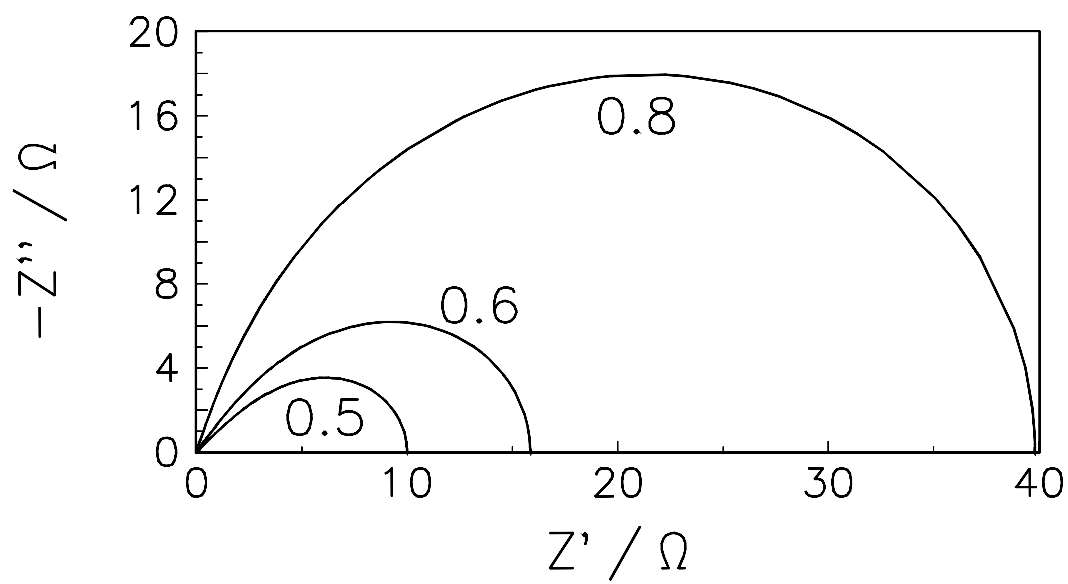


Figure 33. Complex plane plots on fractal electrodes for different values of parameter ϕ .

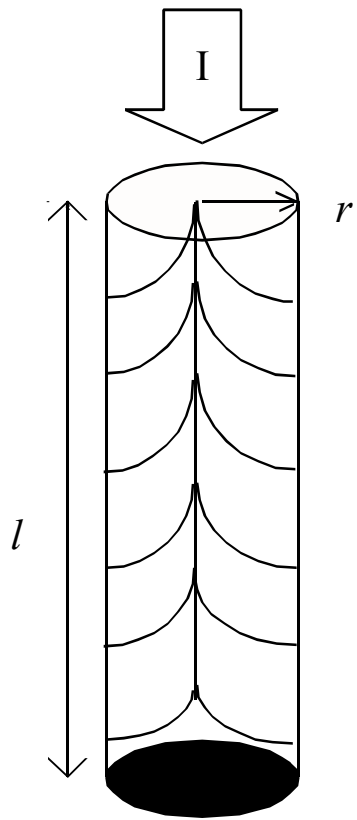


Figure 34. Pore model.

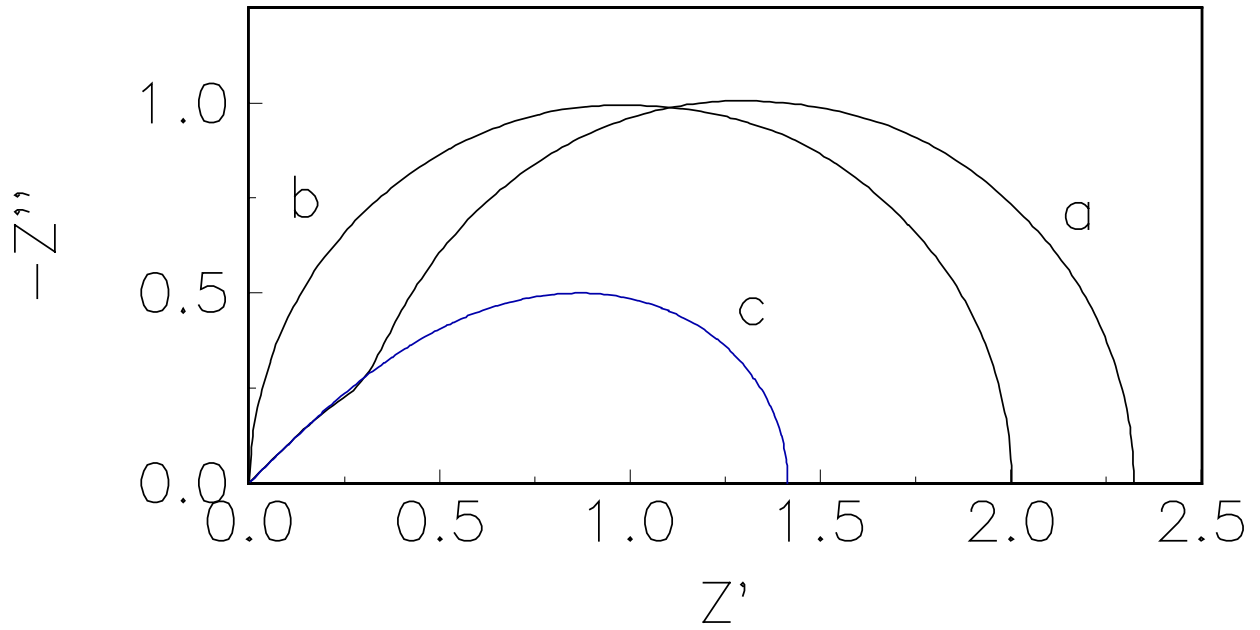


Figure 35. . Complex plane plots for a porous electrode according to de Levie's model, eqn. (195): (a) general case, eqn.(195); (b) limiting case for shallow pores, eqn. (199); (c) limiting case for very deep pores, eqn. (200).

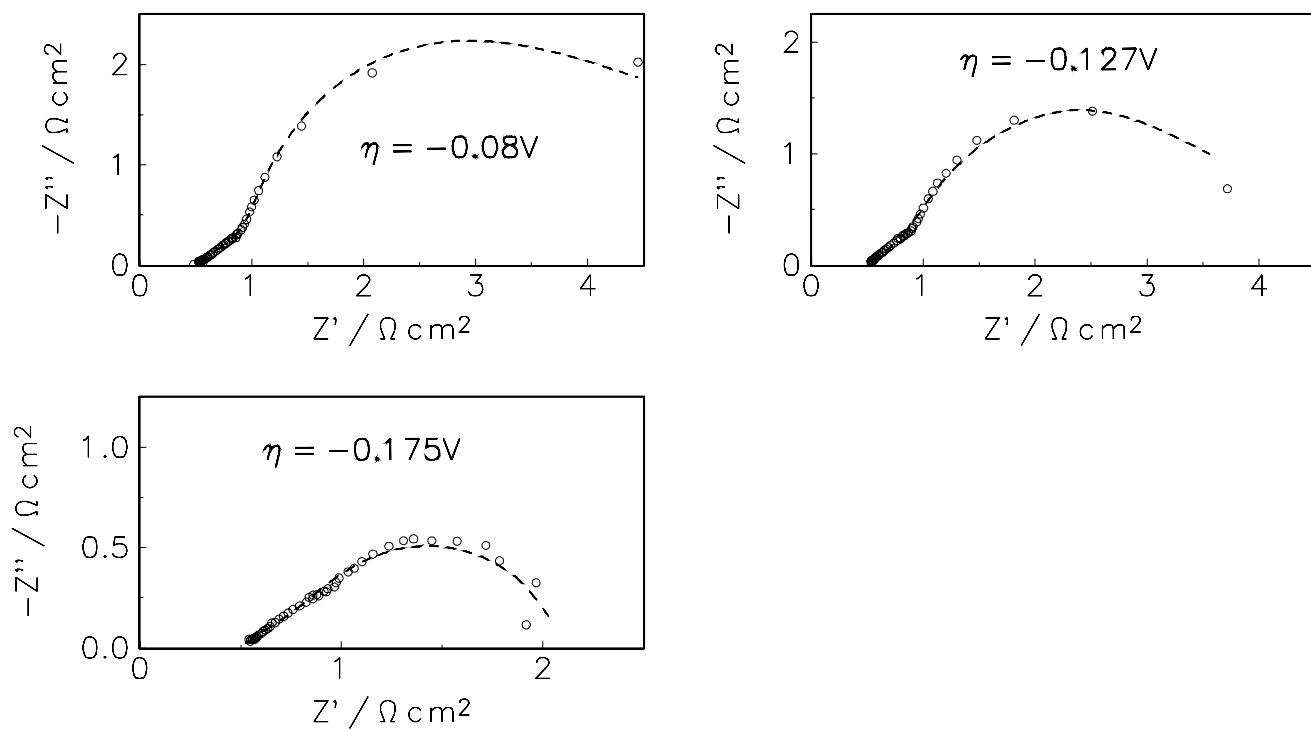


Figure 36. Complex plane plots for LaPO_4 -bonded Ni powder electrodes during hydrogen evolution in 30% NaOH at 70°C .¹⁴⁷

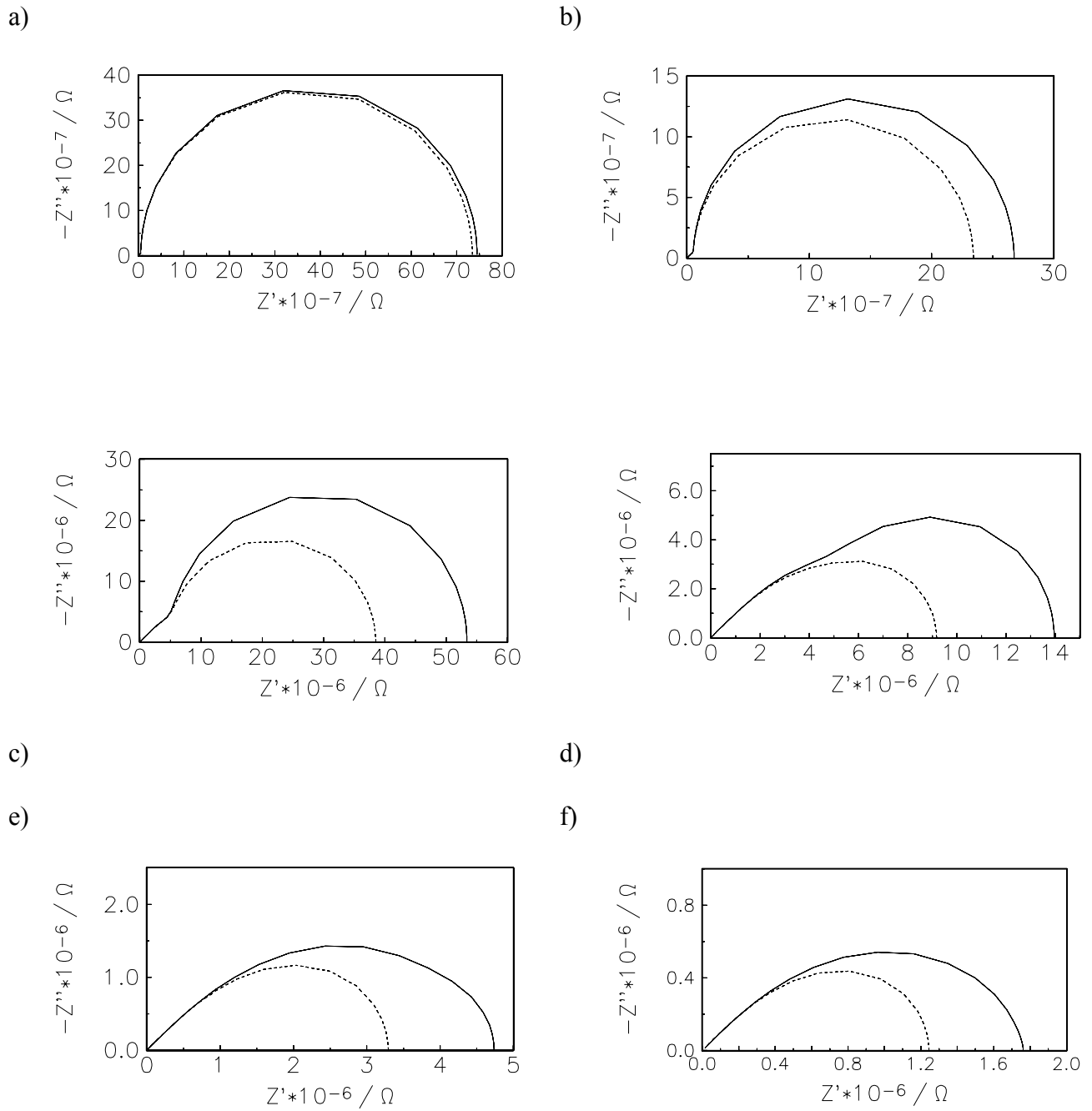


Figure 37. Complex plane plots for a porous electrode at different overpotentials ; pore parameters: $l = 0.05$ cm, $r = 10^{-4}$ cm, $\rho = 10 \Omega$ cm, $j_0 = 10^{-6}$ A cm $^{-2}$, η_0 : a) 0.025, b) 0.1, c) 0.2, d) 0.3, e) 0.4, and f) 0.5 V. Continuous lines - simulated, dashed lines - calculated using de Levie's model, eqn.(195).¹⁴⁹

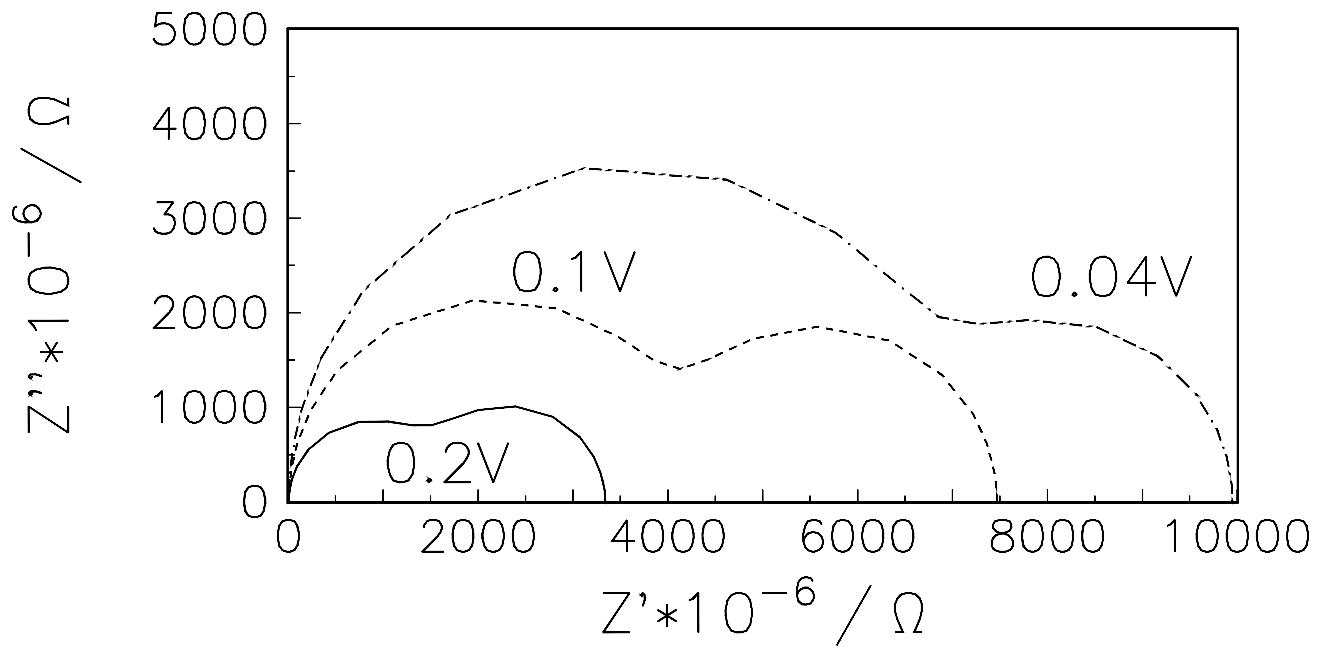


Figure 38. Complex plane plots for a porous electrode in the presence of a concentration gradient at different overpotentials; $l = 0.05$ cm, $r = 10^{-4}$ cm, $\rho = 10 \Omega$ cm, $D = 10^{-5}$ cm² s⁻¹, $m = 1$, $j_0 = 10^{-7}$ A cm⁻², $C_O^* = 0.01$ M.

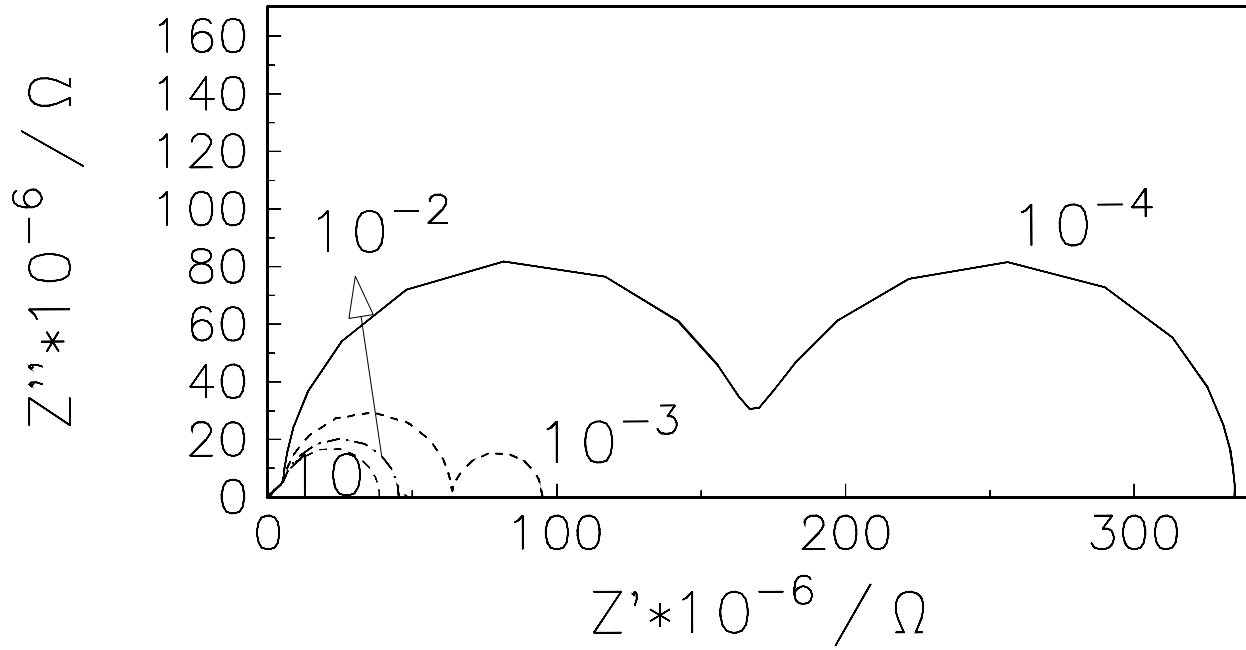


Figure 39. Influence of the depolarizer concentration on the complex plane plots for a porous electrode; $j_0 = 10^{-6} \text{ A cm}^{-2}$, $\eta = 0.2 \text{ V}$, concentrations in mol cm^{-3} are indicated in the figure, other parameters as in Figure 38.

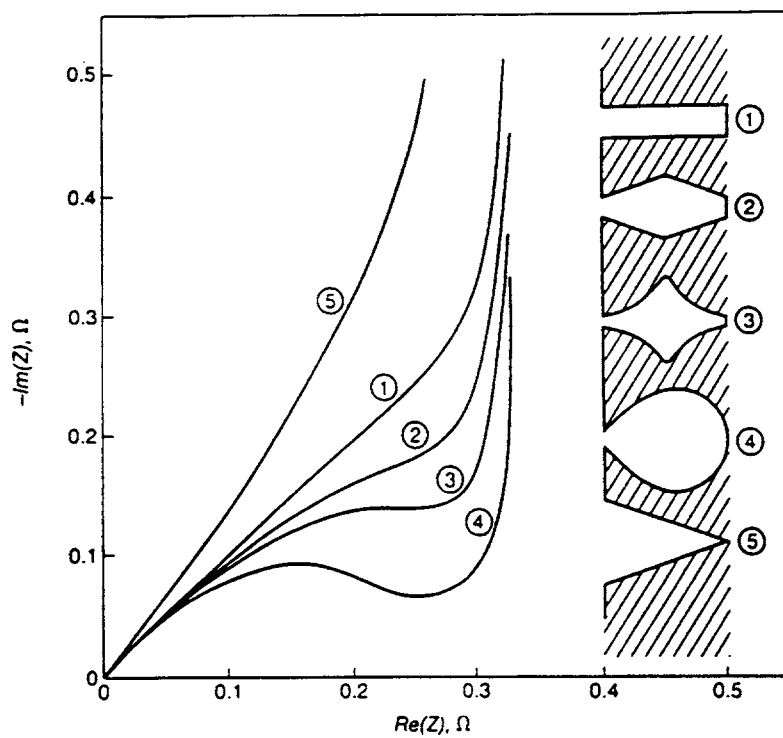
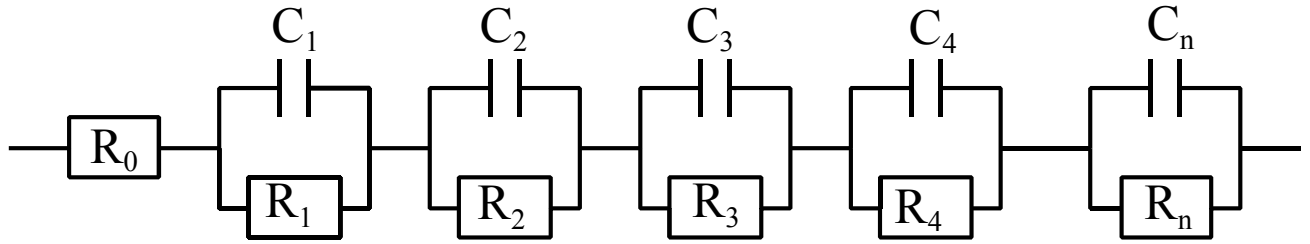


Figure 40. Calculated impedances for various shapes of a single pore blocking electrode.¹⁵⁹

(a)



(b)

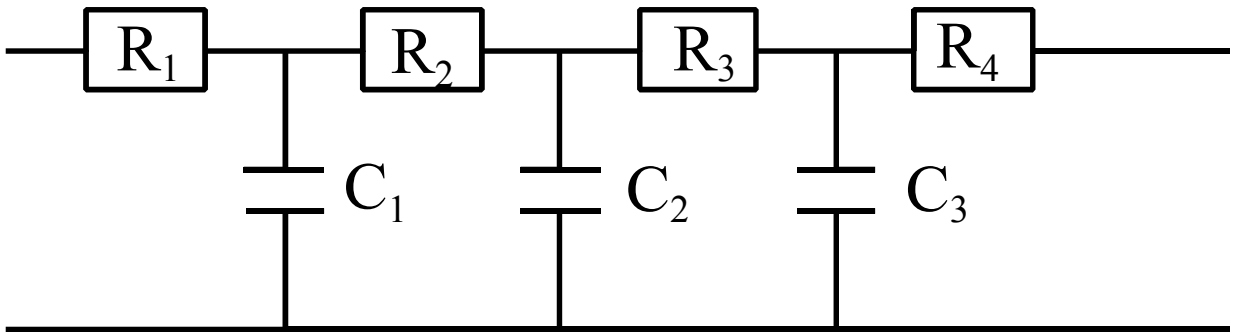
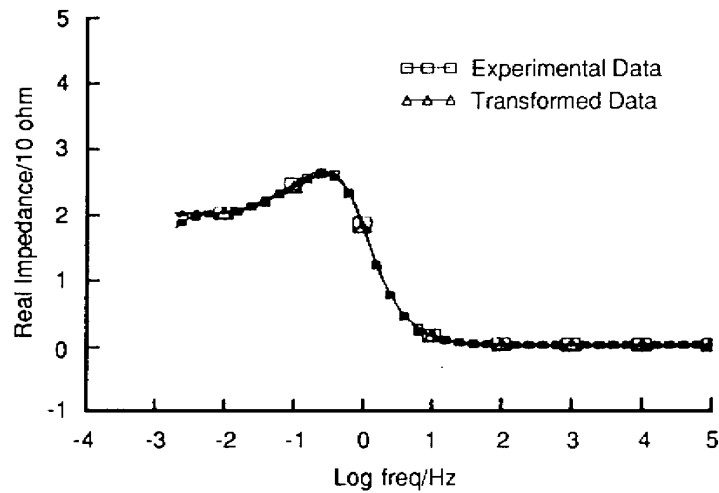
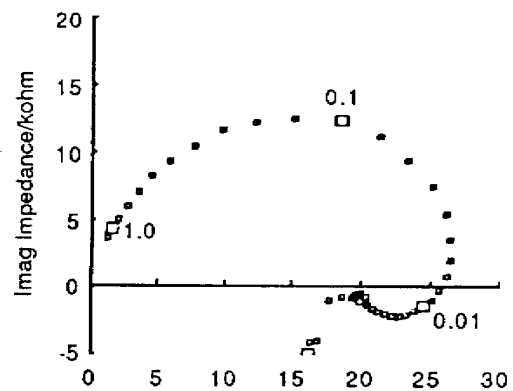


Figure 41. Voigt (a) and ladder (b) models.



(a) Imaginary-to-real transform

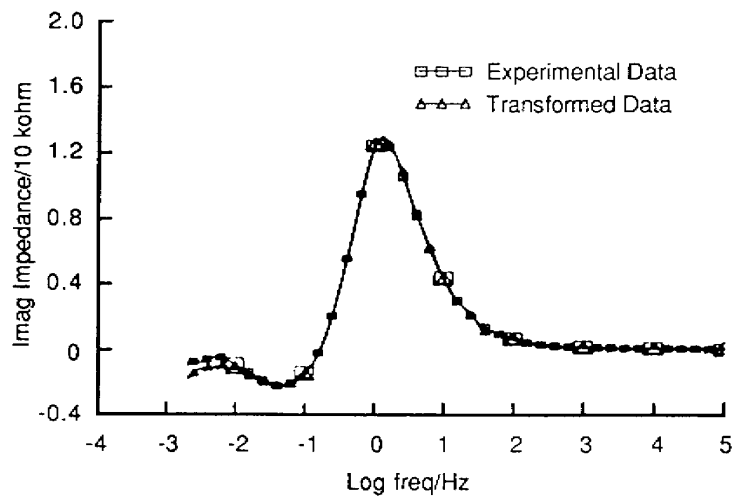


Figure 42. Impedance spectrum for an Al electrode in water (a) and its Kramers-Kronig transforms, (b) and (c).¹⁷⁷

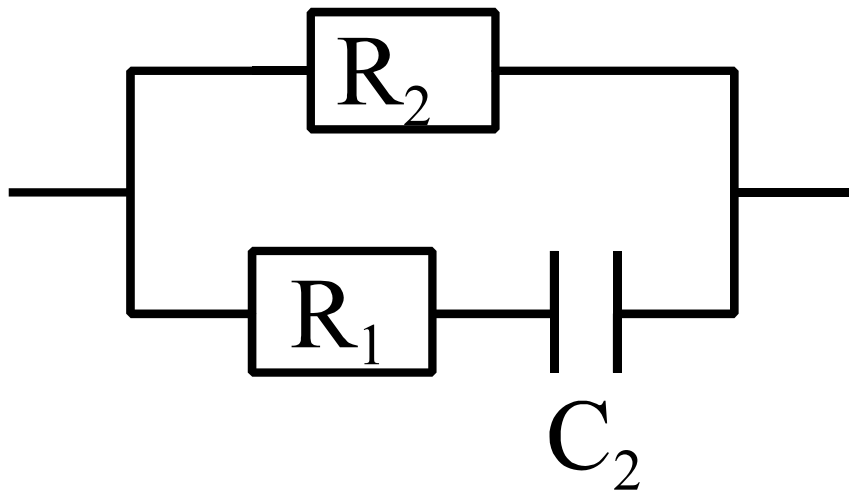
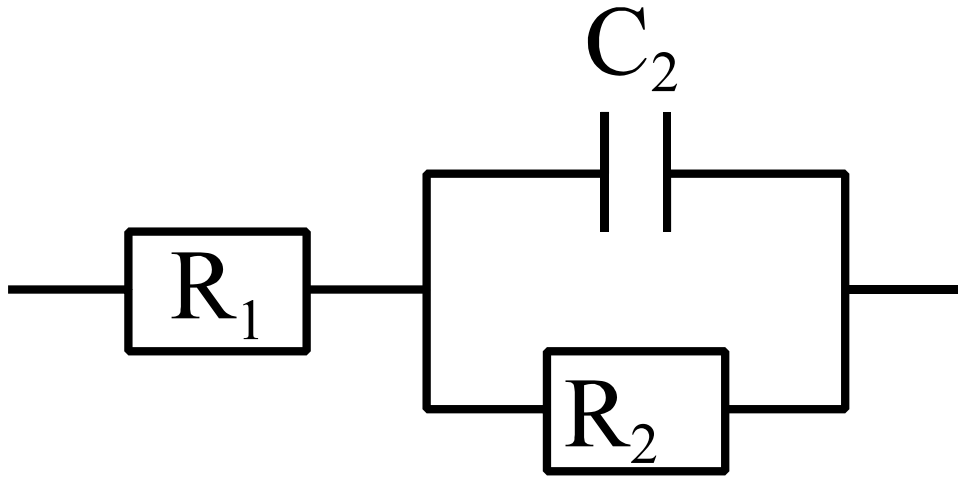
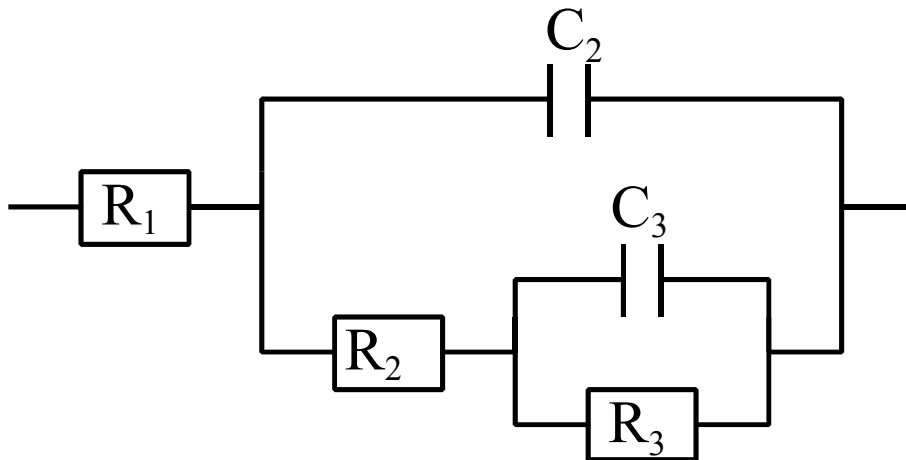
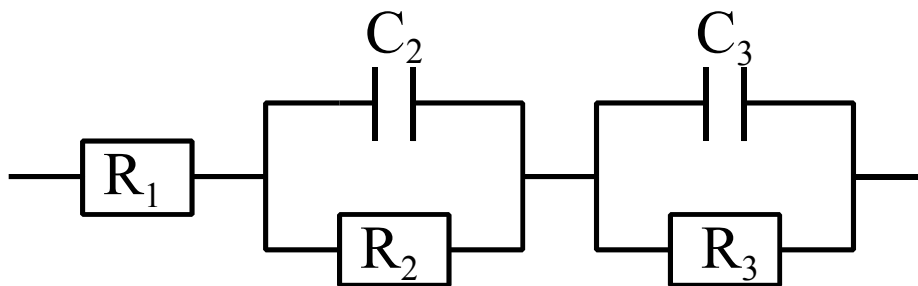


Figure 43. Alternative circuits for the impedance behavior of a system containing one capacitive loop.

(a)



(b)



(c)

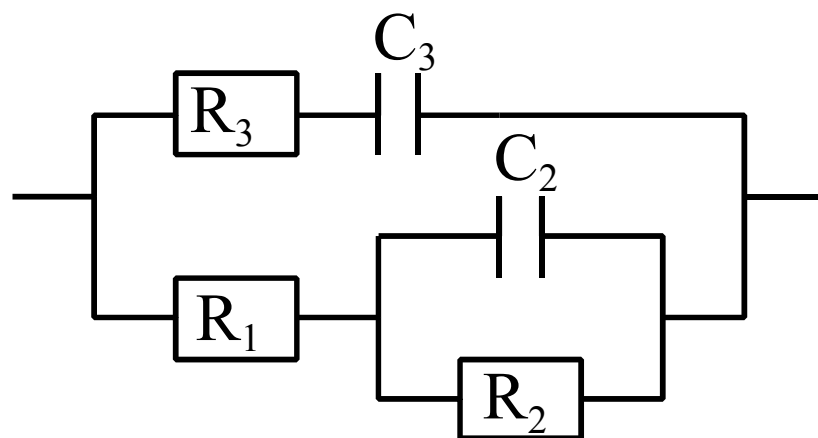


Figure 44. Three circuits describing a system displaying two capacitive loops: (a) ladder, (b) Voigt, (c) mixed.

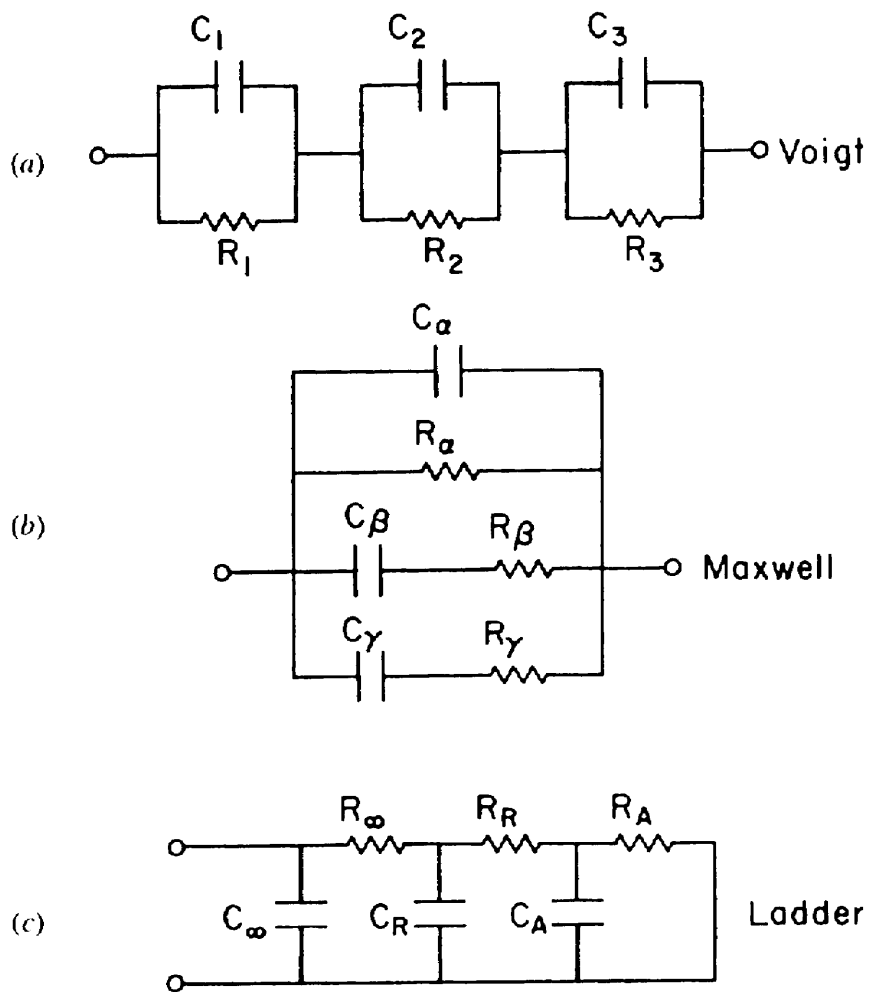


Figure 45. Typical circuits used in ac modeling; they are experimentally indistinguishable: (a) Voigt, (b) Maxwell, (c) ladder.¹⁸

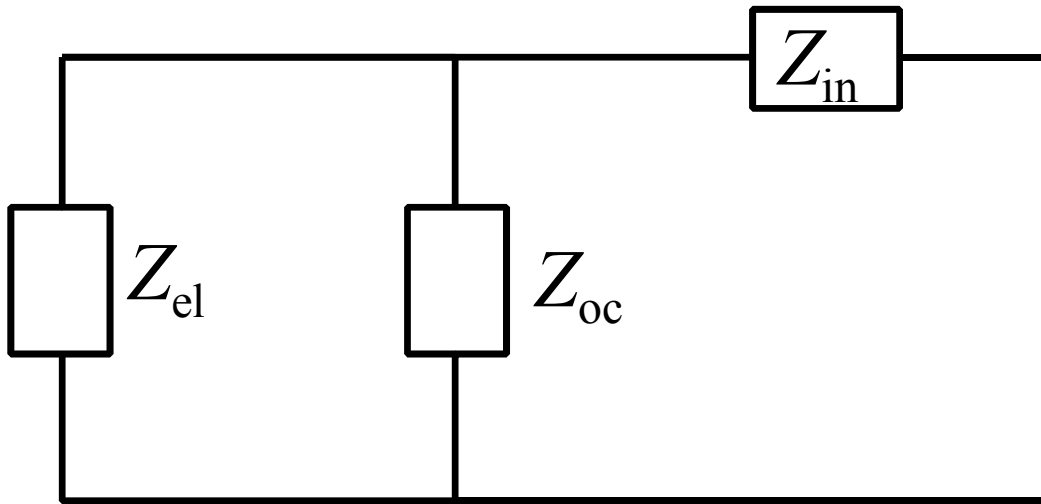


Figure 46. . Equivalent circuit for the case of a slow response of the potentiostat.

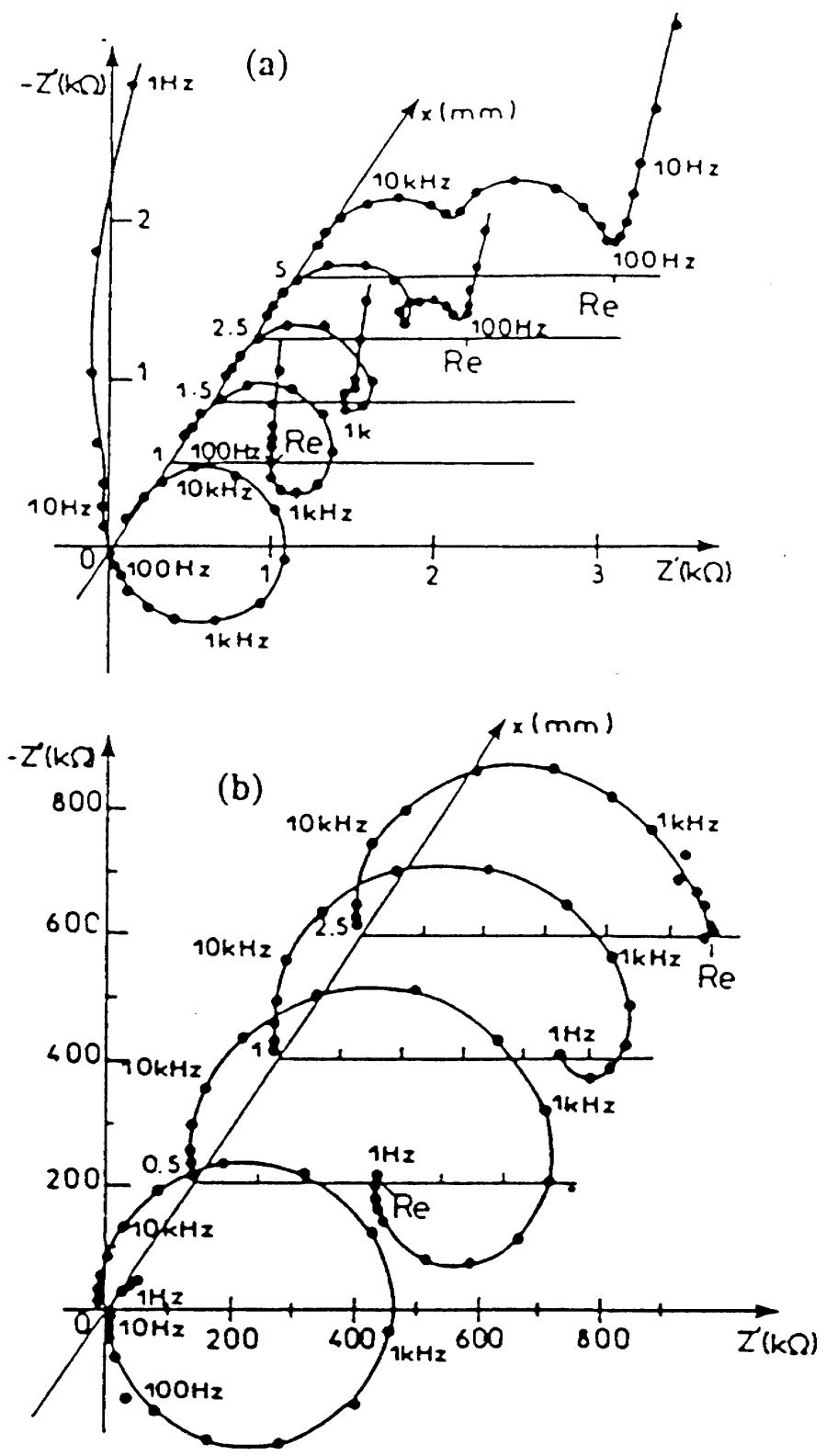


Figure 47. Impedance diagrams for different distances x between the working electrode and the Luggin capillary tip in: (a) 80% acetic acid; (b) 100% acetic acid.²²³